



EJBACS

**Eurasian Journal of
Biological and Chemical Sciences
(Eurasian J. Bio. Chem. Sci.)**

Cilt: 6 Volume: 1 Year: 2023

e-ISSN 2651-5237



EJBCS

Eurasian Journal of Biological and Chemical Sciences

Cilt: 6 Volume: 1 Year: 2023

Published Biannually

Corresponding Address

Gaziantep University, Faculty of Arts and Sciences, Department of Biology, Gaziantep, Turkey

E-mail: mtdogan1@gmail.com

Web: <http://www.dergipark.org.tr/ejbc>

Editor in Chief

Prof. Dr. Muhittin DOĞAN

Editor (Associate)

Assist. Prof. Dr. Muhammet DOĞAN

Editorial Board

Prof. Dr. Ali Tuncay ÖZYILMAZ	Hatay Mustafa Kemal University, Turkey
Prof. Dr. Anna PEKSA	Wrocław University, Poland
Prof. Dr. Elif LOLOĞLU	Gazi University, Turkey
Prof. Dr. Elif ÖZTETİK	Eskisehir Technical University, Turkey
Prof. Dr. Erol ATAY	Hatay Mustafa Kemal University, Turkey
Prof. Dr. Hikmet GEÇKİL	İnönü University, Turkey
Prof. Dr. Issa SHARİFPOUR	Iranian Fisheries Research Organization, Iran
Prof. Dr. İsmet YILMAZ	İnönü University, Turkey
Prof. Dr. Osman GÜLNAZ	Cukurova University, Turkey
Prof. Dr. Osman Selçuk ALDEMİR	Adnan Menderes University, Turkey
Prof. Dr. Vladimer TSITSISHVILI	Ivane Javakhishvili Tbilisi State University, Georgia
Prof. Dr. Zeliha SELAMOĞLU	Niğde Ömer Halisdemir University, Turkey
Assoc. Prof. Dr. Demet DOĞAN	Gaziantep University, Turkey
Assoc. Prof. Dr. Gökhan NUR	Gaziantep University, Turkey
Assoc. Prof. Dr. H. Ahmet DEVECİ	Gaziantep University, Turkey
Assoc. Prof. Dr. Şenay UĞUR	Niğde Ömer Halisdemir University, Turkey
Assoc. Prof. Dr. Utku AVCI	Recep Tayyip Erdoğan University, Turkey
Assoc. Prof. Dr. Mustafa PEHLİVAN	Gaziantep University, Turkey
Dr. Ardalan PASDARAN	Shiraz University, Iran.
Dr. Eva URGEOVÁ	The University of St. Cyril and Methodius of Trnava, Slovakia

Technical Editor

Assoc. Prof. Dr. Mustafa SEVİNDİK	Osmaniye Korkut Ata University, Turkey
-----------------------------------	--

Owner / Publisher
Muhammet DOĞAN

This journal is peer-reviewed and published twice (June, December) a year.

All responsibility of the articles belongs to the authors.

e-ISSN 2651-5237



EJBACS

Eurasian Journal of Biological and Chemical Sciences

Cilt: 6

Volume: 1

Year: 2023

Contents / İçindekiler

Research Articles / Araştırma Makeleleri

High Performance Liquid Chromatography with Size Exclusion Column (HPLC-SEC) Method for Identifying the Major Whey Proteins of Whey Protein Products..... 1 - 6
Lemuel DÍAMANTE

Electrosprayed WPC/PEO Mats Coated to Fresh Figs 7 - 11
Murad GULİYEV, Emine ŞEN, Boran ÇALIŞKAN, Gamze TETİK, Enver TARHAN, Özgür TARHAN

Malatya İli Sucul Böcek (Coleoptera) Faunası Bilgisine Katkılar 12 - 15
Gani Erhan TAŞAR

Metilal/metanol karışımlarının ZIF-8 katkılı PEI membran kullanarak pervaporasyon prosesi ile saflaştırılması 16 - 21
Derya ÜNLÜ

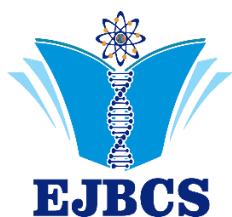
Moringa oleifera bitki yaprağının mineral ve yağ asidi bileşenlerinin belirlenmesi..... 22 - 25
Serpil KILIÇ, Murat KILIÇ

Morphological and molecular identification of fungi isolated from various habitat in Kirkuk city – Iraq 26 - 30
Yavuz MAHMUT, Abdul-Hameed M. HAMOODY, Rushdi Sabah ABDULQADER

Molecular modeling and thermodynamics of the interaction between DNA base pairs and radon originated ionizing alpha radiation 31 - 40
Çağlar ÇELİK BAYAR

Longevity toxicity after chronic α -endosulfan exposure in wild population of *Drosophila melanogaster* Oregon-R (Diptera: Drosophilidae) 41 - 47
Handan UYSAL

Computed tomography imaging, macroanatomical and morphometric analysis of os penis in brown bear (*Ursus arctos*) 48 - 51
Semine DALGA, Gülseren KIRBAŞ DOĞAN, Yalçın AKBULUT, Türkhun ÇETİN, Volkan KIZILGÖZ



High performance liquid chromatography with size exclusion column (HPLC-SEC) method for identifying the major whey proteins of whey protein products

Lemuel M. Diamante* 

*Seperex Nutritionals Ltd., Center for Innovation, University of Otago, Dunedin, New Zealand

*Corresponding author : lmdiamante2002@yahoo.com
Orcid No: <https://orcid.org/0000-0003-1203-7620>

Received : 11/07/2022
Accepted : 15/01/2023

Abstract: This study was carried-out: a) to develop a high-performance liquid chromatography with size exclusion column (HPLC-SEC) method for the identification of the major whey proteins from selected whey protein products; and b) use the method to estimate the relative composition of the major whey proteins in different whey protein products. An HPLC Shimadzu (LC-10AD VP liquid chromatograph) with system controller (SCL-10A VP) equipped with a pump and auto-injector (SIL-10AD VP) and UV-vis detector (SPD-10AV) was used in the identification of whey proteins in standards and whey protein products. The size exclusion column (SEC) was a Yarra 3 μm , SEC-3000 Column, 7.8 mm I.D. x 30 cm with a security guard. The HPLC-SEC method was successful in identifying the major whey proteins of the different whey protein products. The β -LG contents had the highest level among the whey proteins for all the whey protein products studied, followed by the α -LA and then IgG in both WPC products. However, the α -LA and IgG of the Procream product had almost the same level which was probably due to a different process used in WPC. All the major whey proteins with the highest pump flowrate had the shortest elution times while the whey proteins with the lowest pump flowrate had the longest elution times. The optimal pump flowrate was 0.75 mL/min since it gave a faster analysis but differentiate the peaks of the different major whey proteins.

Keywords: Whey Proteins; HPLC-SEC; β -lactoglobulin; α -lactalbumin; Immunoglobulin G

© EJBCS. All rights reserved.

1. Introduction

Whey is a co-product of cheese-making and casein manufacture in the dairy industry. After the casein curd separates from the milk, following coagulation of the casein proteins through the action of chymosin (rennet) or mineral/organic acid, the remaining watery and thin liquid is called whey (Zadow, 1994). Whey comprises 80-90% of the total volume of milk entering the process and contains about 50% of the nutrients in the original milk: soluble protein, lactose, vitamins, and minerals (Tetra Pak, 2015). Whey contains a multitude of biologically active proteins and peptides. Apart from the major whey proteins – β -lactoglobulin (β -LG), α -lactalbumin (α -LA) and glycomacropeptide – whey contains several proteins with potent bioactivity – immunoglobulins, lactoferrin, lactoperoxidase and growth factors (Smithers, 2008).

According to Huffman and Harper (1999), a wide range of whey protein products are available for a variety of application. The three major classes are the whey protein concentrate (WPC), whey protein isolate (WPI) and Lactalbumin. WPC involves clarification of the whey, followed by ultrafiltration and several stages of diafiltration and eventually spray drying of the concentrate. WPI

requires the microfiltration or ion exchange of whey, followed by similar operations as WPC. Lastly, Lactalbumin involves heat denaturation of whey, followed by precipitation/separation and several stages of washing and finally drying the washed material. Lactalbumin, not to be confused with α -LA, contains all the heat precipitable whey proteins, has a clean flavor, and is heat stable. WPC range in concentration from 34 to 85% proteins. The US produced the 34% WPC while the other dairy exporting countries developed the high protein products (75-85% WPC) with specific functionalities. Whey proteins of particular interest and currently commercially available include β -LG, α -LA, lactoferrin, lactoperoxidase, and immunoglobulins.

Modern membrane processing, including industrial applications of microfiltration, ultrafiltration/diafiltration, have helped to pioneer the development of high-protein and low-fat functional whey ingredients, such as whey protein concentrates (WPCs) (~35, 75 and 80% protein) and first-generation whey protein isolates (WPIs) (~85-90% protein), that have expanded the applications base for whey protein ingredients (Clark, 2005; Kelly et al., 2000; Saboya and Maubois, 2000). Microfiltration is a membrane separation process used for the reduction of bacteria in skim milk,

whey and brine, but also for defatting whey intended for WPC and for protein fractionation. Ultrafiltration is also a membrane separation process and typically used for concentration of milk proteins in milk and whey and for protein standardization of milk intended for cheese, yoghurt, and some other products. Diafiltration is a procedure in which water is added to the feed as filtration proceeds, to wash out low molecular components which will pass through the membranes, basically lactose and minerals. Procream or high fat retentate is obtained from microfiltration of whey retentate from the ultrafiltration of cheese whey which is a co-product obtained during the manufacture of WPI (Tetra Pak, 2015).

Whey proteins is of high nutritional value and has become an important source of functional ingredients in various health-promoting foods. For value-added industrial applications of whey proteins, the composition, and the changes in both the physicochemical and functional properties need to be accurately analyzed. Because whey proteins are a mixture of proteins, accurate analysis of whey proteins requires separation of the whey proteins (Kang et al., 2011). These include gel electrophoresis (Kinghorn et al., 1995; Bouaouina et al., 2006), capillary zone electrophoresis (Kinghorn et al., 1995; Liang et al., 2006) and various forms of high-performance liquid chromatography (HPLC) (Geberding and Byers, 1998; Elgar et al., 2000). The HPLC methods include reversed-phase (Garcia et al., 1998; Elgar et al., 2000), ion-exchange (Geberding and Byers, 1998; El-Sayed and Chase, 2010) and size-exclusion chromatography (SEC) (Bouaouina et al., 2006; El-Sayed and Chase., 2010).

Diosady et al. (1980) used a high-performance liquid chromatography size exclusion chromatography (HPLC SEC) method to determine the whey proteins using 2 Syncropak GPC columns in series. Gupta (1983) also used the HPLC SEC method to determine the native and denatured milk proteins but used a TSK 3000 SW column only. Downes and Silcock (2014) also reported the use of HPLC SEC method to analyze a range of whey proteins from pilot ultrafiltered dairy products using a Yarra 3 μm 2000 and Yarra 3 μm 4000 columns in series.

This study was carried-out: a) to develop a high-performance liquid chromatography with size exclusion column (HPLC-SEC) method for the identification of the major whey proteins from selected whey protein products; and b) use the method to estimate the relative composition of the major whey proteins in different whey protein products.

2. Materials and Methods

2.1. Materials

The Sodium Phosphate Dibasic Dodecahydrate was from Sigma Aldrich (St. Louis, MI, USA), Sodium Chloride from Fisher Chemical (Loughborough, UK) and Hydrochloric Acid (36%) from Ajax Finechem (Taren Point, Australia). The Bovine Whey Proteins standards such as β -lactoglobulin, α -lactalbumin, and Immunoglobulin G were procured from Sigma Aldrich (St. Louis, MI, USA). The Whey Protein Concentrate powders were procured from Westland Milk Products (JZ19) and Fonterra (CW29), New

Zealand while the Procream powder was obtained from Mullins Whey (Mosinee, WI, USA).

2.2. Reconstitution of Whey Protein Powders

All the whey protein powders (WPC and Procream) were reconstituted to 5% solids by dissolving the powders in a lukewarm purified water ($\sim 40^\circ\text{C}$) by stirring until all the powder particles were dissolved. The reconstituted products were left overnight in the chiller at 4°C to fully hydrate and then stored until use. All the reconstituted products were used within one week.

2.3. Whey Proteins Detection Method

A high-performance liquid chromatography (HPLC) Shimadzu (LC-10AD VP liquid chromatograph) with system controller (SCL-10A VP) equipped with a pump and auto-injector (SIL-10AD VP) and UV-vis detector (SPD-10AV) was used in the detection of whey proteins in standards and whey products (permeate and retentate from ultrafiltration). The chromatographic column was a Yarra 3 μm , SEC-3000 Column, 7.8 mm I.D. x 30 cm with a security guard. The detector signal was analysed using the LC Solution software to obtain the integrated area of the peaks from the chromatogram. The mobile phase was a 50 mM sodium phosphate buffer containing 150 mM sodium chloride and buffered to $\text{pH} = 7.0$ using 1 M HCl solution and using an isocratic pump mode with a flowrate of 0.50 mL/min. HPLC measurements were done at room temperature of about 25°C using a column heater (Thermasphere TS-130). The UV-vis detector was set with a wavelength of 280 nm for Channel 1 and 220 nm for Channel 2. The whey protein standards samples were prepared by dissolving various amounts of whey protein powders in 5-10 mL purified water. Then about 2 mL of sample was then filtered thru a 0.45 μm PTFE filter into glass vials for HPLC-SEC detection of the elution time for each whey protein standard. In the case of the whey products, about 13 mL of the sample was first centrifuged at 6500 rpm for 5 minutes (Eppendorf), then 2 mL of the supernatant liquid was obtained and centrifuged at 13,000 rpm for 5 minutes (Heraeus). Another supernatant liquid from this sample was obtained and then filtered thru a 0.45 μm PTFE filter into glass vials for HPLC detection of the elution time for each whey protein. A 50 μL of the filtered sample was automatically injected into the system for measurement. The running time for the HPLC detection was for 30 minutes. The elution time of the whey proteins were obtained from the print-out of the run.

2.4. Analysis of IgG from Whey Protein Products

The IgG contents of the reconstituted whey protein products were analyzed at Cawthron Institute, Nelson, New Zealand using the method of Holland et al. (2011).

3. Results and Discussion

3.1. Detection of Whey Proteins Standards

The top 3 major whey proteins standards used in the analysis have the following approximate molecular weights as shown in Table 1.

The SEC used in the HPLC serves solely as a fractionation step to separate the various whey proteins based on its molecular weight with the heavier protein being eluted first and the lightest protein eluted last. Hence, it will be expected that the IgG will have the shortest retention time and the α lactalbumin will have the longest retention time.

Table 1. Approximate molecular weights of the major whey proteins

Whey Protein	Molecular Weight (Da)
Alpha Lactalbumin (α -LA)	14,175 ^a – 16,250 ^b
Beta Lactoglobulin (β -LG)	18,277 ^a – 19,800 ^b
Immunoglobulin G (IgG)	146,000 ^a - >150,000 ^b

^aMadureira et al., (2007); ^bOstertag et al. (2021)

Table 2 shows the results for the elution time of the 3 whey proteins dairy standards at the conditions specified in the previous section. As expected, IgG had the shortest elution time of about 16 minutes and the α Lactalbumin had the longest elution time of about 20 minutes. Figures 1, 2 and 3 are the chromatograms of IgG, β -LG and α -LA standards, respectively. There were 2 distinct peaks in the IgG chromatogram indicating that the whey standard was not very pure as compared with the β -LG and α -LA standards.

Table 2. Elution times of major whey proteins standards

Whey Protein Standard	Elution Time (minutes)
IgG	15.88-15.91
β -LG	18.49-18.51
α -LA	19.76-19.78

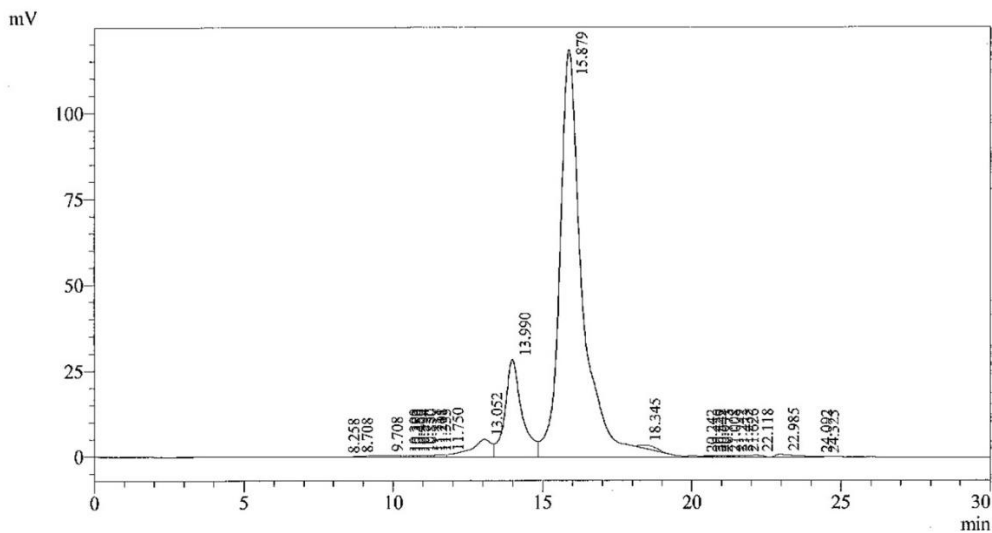


Fig 1. Chromatogram of the IgG standard

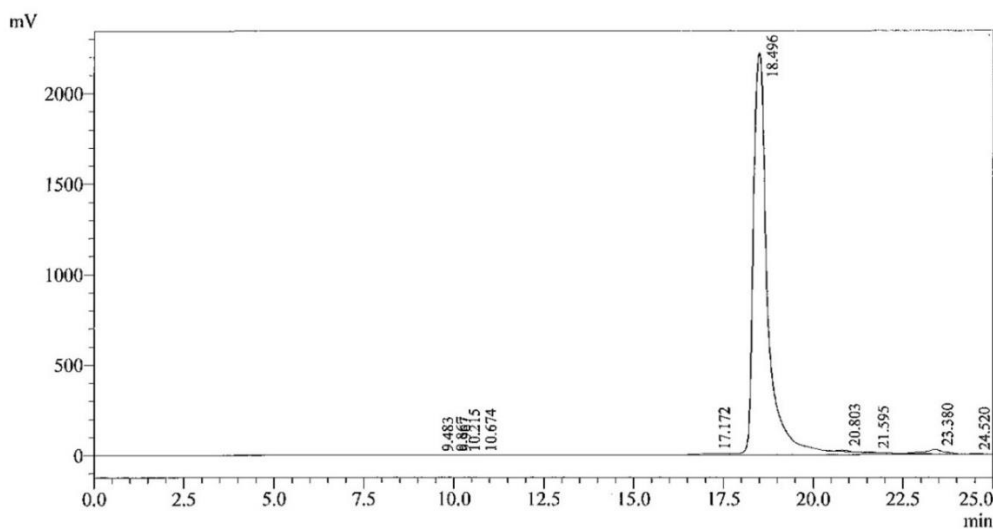


Fig 2. Chromatogram of the β -LG standard

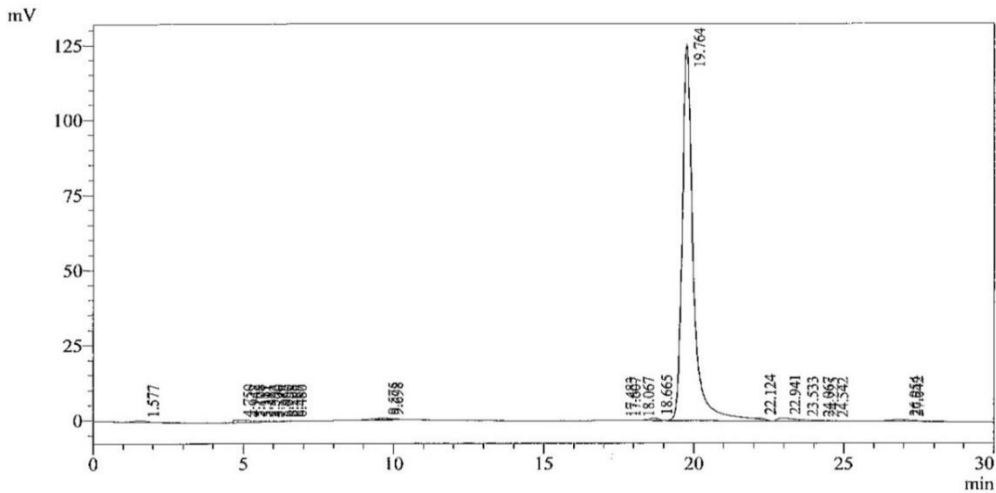


Fig 3. Chromatogram of the α -LA standard

3.2. Elution Times for the Whey Proteins in Various Whey Products

Table 3 shows the elution times of the various whey proteins found in the various whey protein products studied. There were some variations from the elution times of whey protein standards probably due to the impurities in the whey protein products. Figures 4, 5 and 6 are the chromatograms of WPC JZ19, WPC CW29 and Procream products, respectively. The other peaks in the chromatograms were not identified since these were not part of the objective of the study. Table 4 presents the percentage of the total area of the chromatogram for the major whey proteins in the various whey protein products. The percentage of the total area can be used as an estimate of the relative composition of the major whey proteins in the various whey protein products. The results showed that the β -LG contents were the highest among the whey proteins, followed by α -LA and then IgG in both WPC products. De Wit (1998) and Pires et al. (2021) reported that β -LG was the highest, followed by α -LA and then IgG in bovine whey proteins. However, the α -LA and

IgG of the Procream product was almost the same which was probably due to a different process used in WPC. Procream was from a high fat retentate obtained from microfiltration of the whey retentate from the ultrafiltration of cheese whey, which is co-product obtained during the manufacture of WPI (Tetra Pak, 2015). The Procream gave the highest IgG content, followed by WPC JZ19 and then WPC CW29. This is the same order also of IgG contents of 221, 67 and 18 mg/g for Procream, WPC JZ19 and WPC CW29, respectively from the analysis using the Protein G Affinity Chromatography method (Holland et al., 2011).

Table 3. Elution times of whey proteins from whey products

Whey Protein	Elution Time (minutes)		
	WPC JZ19	WPC CW29	Procream
IgG	15.75	15.80	15.75
β LG	18.45	18.44	18.51
α LA	19.75	19.70	19.73

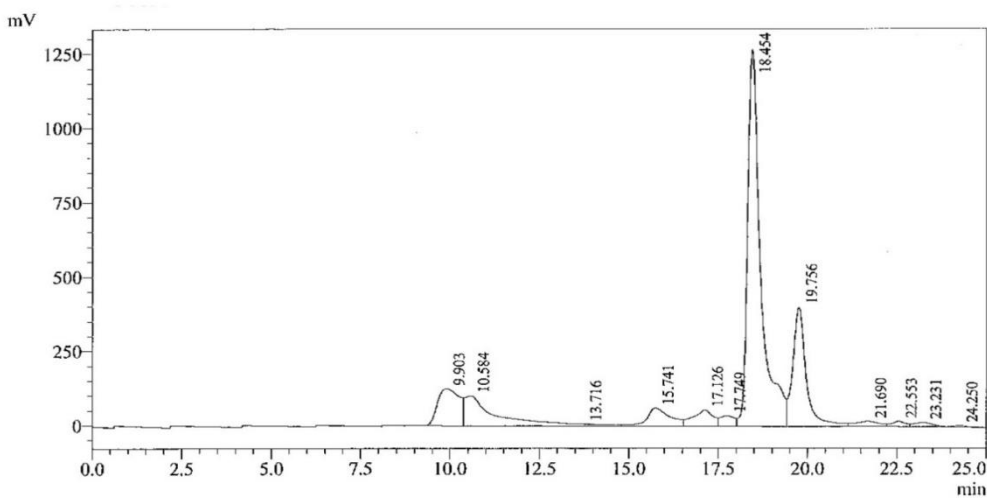


Fig 4. Chromatogram of the WPC JZ19 product

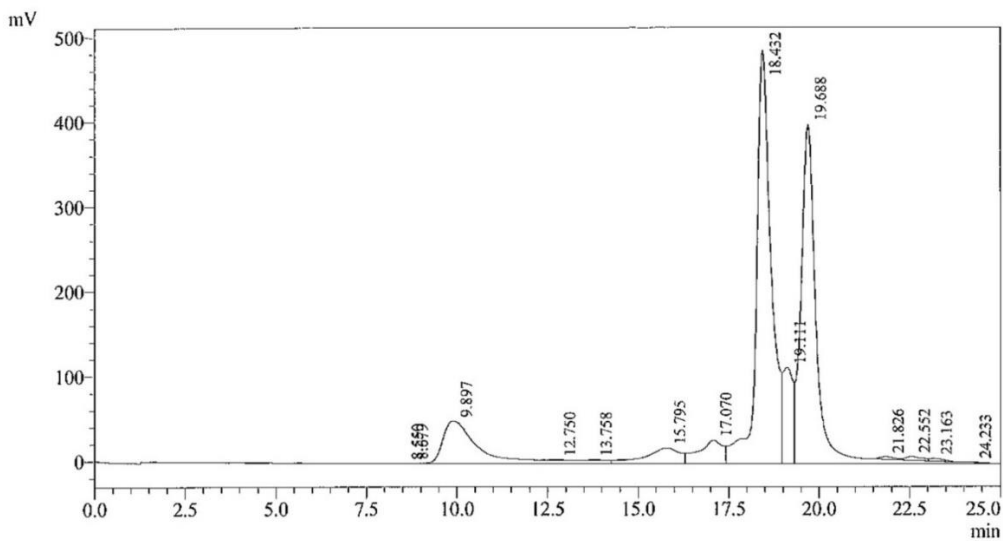


Fig 5. Chromatogram of the WPC CW29 product

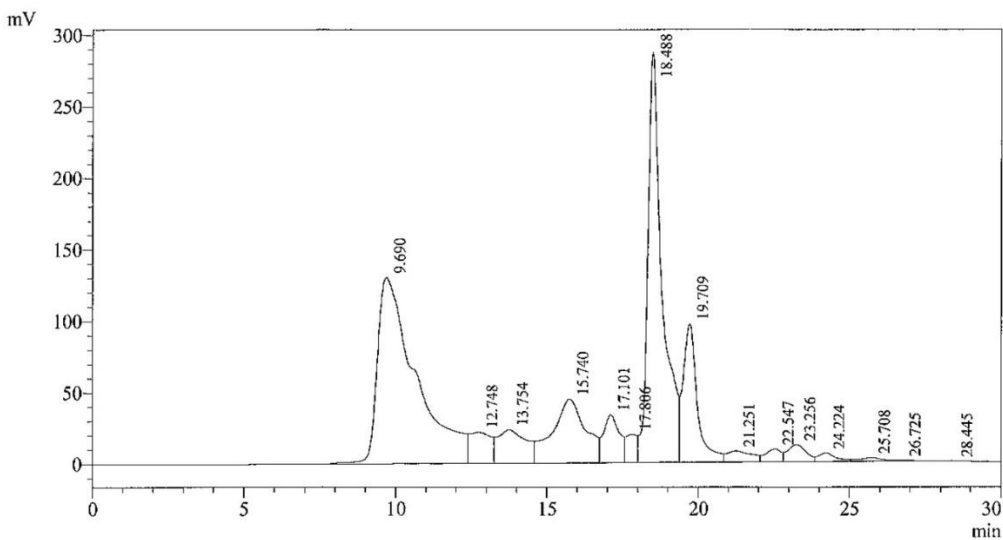


Fig 6. Chromatogram of the Procream product.

Table 4. Percentages of the total area of the chromatogram for the top 3 major whey proteins in various whey protein products

Sample	α -LA(%)	β -LG(%)	IgG(%)
WPC JZ19	17.0	52.1	4.3
WPC CW29	34.7	40.2	3.6
Procream	11.1	33.0	11.3

3.3. Effect of HPLC Pump Flowrate on the Elution Times for the Selected Whey Proteins Standards

Table 5 shows the elution time of the major whey proteins standards at the conditions specified earlier but with different HPLC pump flowrates. As expected, all the whey proteins with the highest pump flowrate had the shortest elution times while the whey proteins with the lowest pump flowrate had the longest elution times. At higher pump flowrate, the speed of whey proteins elution will be faster, hence shorter elution time.

Table 5. Elution times of major whey protein standards with different pump flowrates

Whey Protein	Pump Flowrate (mL/min)/Elution Time (minutes)		
	0.50	0.75	1.00
IgG	15.90	10.63	7.80
β -LG	18.50	12.34	9.29
α -LA	19.77	13.20	9.93

3.4. Effect of HPLC Pump Flowrate on the Elution Times for the Selected Whey Proteins from WPC Products

Table 6 shows the elution times of the major whey proteins from two WPC products. There were minimal variations from the elution times of the major whey proteins from each other at the same pump flowrates. Again, the whey proteins with the highest pump flowrate had the shortest elution times while the whey proteins with the lowest pump flowrate had the longest elution times. The purpose of this

investigation was to determine the optimum pump flowrate that would give faster analysis but would still differentiate the peaks of the different whey proteins for each product. The results show that a pump flowrate of 0.75 mL/min would be the optimum.

Table 6. Elution times of major whey proteins from WPC products with different pump flowrates

Sample/Whey Protein	Pump Flowrate (mL/min) / Elution Time (minutes)		
	0.50	0.75	1.00
WPC JZ19			
IgG	15.75	10.55	7.80
β -LG	18.45	12.32	9.27
α -LA	19.75	13.19	9.92
WPC CW29			
IgG	15.80	10.57	7.95
β -LG	18.44	12.33	9.27
α -LA	19.70	13.17	9.90

4. Conclusion

The HPLC-SEC method was successful in identifying the major whey proteins of the different whey protein products. The β -LG contents had the highest level among the whey proteins for all the whey protein products studied, followed by the α -LA and then IgG in both WPC products. However, the α -LA and IgG of the Procream product had almost the same level which was probably due to a different process used in WPC.

All the major whey proteins with the highest pump flowrate had the shortest elution times while the whey proteins with the lowest pump flowrate had the longest elution times. The optimal pump flowrate was 0.75 mL/min since it gave a faster analysis but differentiate the peaks of the different major whey proteins.

Acknowledgments

The author would like to thank Seperex Nutritionals Ltd. for providing the research funds and facilities.

Conflict of interest disclosure:

The author declares no conflict of interest on the written article.

References

Anonymous 2001. Reference Manual for US Whey Products. US Dairy Export Council, Arlington, VA, USA.

Bicah, P, Blanc B 1982. Milk protein analysis – a high-performance chromatography study. *Milchwissenschaft*. 37: 592-593.

Bouaouina H, Desrumaux A, Loisel C, Legrand J 2006. Functional properties of whey proteins as affected by dynamic high-pressure treatment. *International Dairy Journal*. 16: 275-284.

Clark PJ 2005. Concentrating proteins from milk and meat. *Food Technol*. 59: 80-83.

De Wit JN 1998. Nutritional and functional characteristics of whey proteins in food products. *J Dairy Sci*. 81: 597-608.

Diosady LL, Bergen I, Harwalkar VR 1980. High performance liquid chromatography of whey proteins. *Milchwissenschaft*. 35: 671-674.

Downes N, Silcock P 2014. HPLC method development for quantification of proteins from UF pilot scale-up. Seperex Nutritionals Ltd., Dunedin, New Zealand Internal Report. 4 pp.

Elgar DF, Norris CS, Ayers JS, Oritchard M, Otter DE, Palmano KP 2000. Simultaneous separation and quantitation of the major bovine whey proteins including proteose peptone and caseinomacropeptide by reversed-phase high-performance liquid chromatography on polystyrene-divinylbenzene. *J Chromatogr A*. 878: 183-196.

El-Sayed MMH, Chase HA 2010. Purification of the two major proteins from whey concentrate using a cation-exchange selective adsorption process. *Biotechnol Prog*. 26: 192-199.

Garcia MC, Marina ML, Torre M 1998. Ultrarapid detection of bovine whey proteins in powdered soybean milk by perfusion reversed-phase high-performance liquid chromatography. *Journal of Chromatography A*. 822: 225-232.

Geberding SJ, Byers CH 1998. Preparative ion-exchange chromatography of proteins from dairy whey. *J Chromatogr A*. 808: 141-151.

Gupta BB 1983. Determination of native and denatured milk proteins by high-performance size exclusion chromatography. *J Chromatogr A*. 282: 463-475.

Holland PT, Cargill A, Selwood AI, Arnold K, Krammer JL, Pearce KN 2011. Determination of soluble immunoglobulin G in bovine colostrum products by protein G affinity chromatography – Turbidity correction and method validation. *J Agric Food Chem*. 59: 5248-5256.

Huffman LM, Harper JW 1999. Maximizing the value of milk through separation technologies. *J Dairy Sci*. 82: 2238-2244.

Kang DY, Moon JM, Lee S 2011. Comparison of size-exclusion chromatography and flow field-flow fractionation for separation of whey proteins. *Bull Korean Chem Soc*. 32: 1315.

Kelly PM, Kelly J, Mehra R, Oldfield DJ, Raggett E, O'Kennedy BT 2000. Implementation of integrated membrane processes for pilot scale development of fractionated milk components. *Lait*. 80: 139-153.

Kinghorn NM, Norris CS, Paterson GR, Otter DE 1995. Comparison of capillary electrophoresis with traditional methods to analyse bovine whey proteins. *J Chromatogr A*. 700: 111-123.

Liang M, Chen V Y, Chen HL, Chen W 2006. A simple and direct isolation of whey components from raw milk by gel filtration chromatography and structural characterization by Fourier transform Raman spectroscopy. *Talanta*. 69: 1269-1277.

Madureira AR, Pereira CI, Gomes AMP, Pintado ME, Malcata FX 2007. Bovine whey proteins – Overview on their main biological properties. *Food Res Int*. 40: 1197-1211.

Ostertag F, Schmidt CM, Berensmeier S, Hinrichs J 2021. Development and validation of an RP-HPLC DAD method for the simultaneous quantification of minor and major whey proteins. *Food Chemistry*. 342: 18176 (8 pp.).

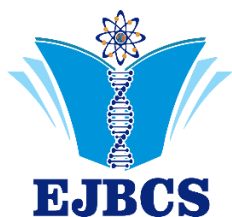
Pires AF, Marnotes NG, Rubio OD, Garcia AC, Pereira CD 2021. Dairy by-products: A review on the valorization of whey and second cheese whey. *Foods*. 10: 1067 (24 pp.).

Saboya LV, Maubois JL 2000. Current development of microfiltration technology in the dairy industry. *Lait*. 80: 541-553.

Smithers GW 2008. Review - Whey and whey proteins – from 'gutter-to-gold'. *International Dairy Journal*. 18: 695-704.

Tetra Pak. 2015. Dairy Processing Handbook. Tetra Pak Processing Systems AB, Lund, Sweden. 480 pp.

Zadow JG 1994. Utilization of milk components: Whey. In *Modern Dairy Technology, Advances in Milk Processing*, Vol. 1 (2nd Edition) (R.K. Robinson, ed.). Chapman and Hall, London, UK. pp. 313-373.



Electrosprayed WPC/PEO Mats Coated to Fresh Figs

Murad Guliyev¹, Emine Şen², Boran Çalışkan², Gamze D. Tetik², Enver Tarhan³, Özgür Tarhan^{1*}

¹Uşak University, Engineering Faculty, Food Engineering Dept., 64100, Uşak, Türkiye

²Uşak University, Engineering Faculty, Materials Science and Nanotechnology Engineering Dept., 64100, Uşak, Türkiye.

³İzmir Institute of Technology, Faculty of Science, Physics Dept, 34360, İzmir, Türkiye.

*Corresponding author : ozguratarhan@gmail.com
Orcid No: <https://orcid.org/0000-0001-7084-6253>

Received : 05/12/2022
Accepted : 15/01/2023

Abstract: Electrohydrodynamic atomization that is also defined as electrospraying is a method of producing mats that are composed of nano- or micro-scaled droplets. Unlike nanofibers that are obtained by electrospinning, the droplets are in spherical forms, and this is the result of the struggle between the applied electrostatic forces and the surface tension of the liquid (meaning polymer solution). This study aims to prepare and characterize electrosprayed biopolymer mats. The 1:2 blend of HWPC (hydrolyzed whey protein concentrate): PEO (poly (ethylene oxide)) is the polymer solution prepared in 2.5% aqueous acetic acid solvent. Physicochemical, morphological and structural analysis are applied to both solution and the electrosprayed mat. Increased viscosity in the protein solution by the addition of PEO enhanced the formation of regular beads observed through SEM images. Image J Visualization and Measurement Software was occupied to determine the diameter distributions of the droplets forming the mat. The mean diameter was found as $1.02 \pm 0.55 \mu\text{m}$. ATR-FTIR spectroscopy analyses revealed remarkable structural changes in protein and interaction between protein and PEO in the electrosprayed mats. The HWPC/ PEO electrosprayed mat coating revealed one log decrease in the microbial load of fresh figs at the end of fourteen-day storage (4°C). The findings of the presented research are promising for the application of this electrosprayed biopolymer mat for food coating purposes.

Keywords: electrospraying, nanoparticle, WPC, PEO

© EJBCS. All rights reserved.

1. Introduction

To increase both the stability and the shelf life of foods by nano-scaled materials has been in the focus of researchers from various disciplines for years. In this search, it was revealed that nanomaterials are designed as systems that give good responses to prolong the shelf life of foods. Improvement of surface area, permeability, and some other abilities of food packages are actualized by the usage of nanofibrous or nanodroplet mats. Electrospinning or electrospraying were two similar methods used for this purpose. Electrohydrodynamic atomization or electrospraying is a method of producing ultra-fine droplets from a polymer solution with the help of electrostatic forces (Gómez-Mascaraque and Lopez-Rubio 2019). The continuity of the jet is disturbed in electrospraying to form nano-scaled droplets. The method's theoretical foundations were laid by Gilbert, and Rayleigh, Zeleny, and Taylor were the ones explaining the method mathematically and experimentally (Jingwei et al. 2015). From the 2000s that experimental studies have been accelerated, spraying has continued to maintain its importance in diversified fields such as textiles (Jadhaw et al. 2011), cosmetics (Bae et al.

2019), biomedical (Wang et al. 2019) and food applications (Lim et al. 2019). Method is based on the principle of formation of droplets by instability of the polymer solution desired to be sprayed in an equipment equipped with a high voltage power supply, syringe pump and collector under the influence of electrostatic field, surface tension, viscoelastic and even negligible air drag and gravity forces. High surface tension and low viscosity are the key factors for the formation of spraying (Lim et al. 2019).

Surfaces with nano-scale unit structure (droplet) have one or more of the very critical features for food packaging such as exhibiting a higher surface area, effectively protecting food from dirt and dust, creating a stable barrier against the passage of oxygen, light, and microorganisms, and maintaining moisture balance (Vasile 2018). In addition, due to the flexibility provided by the electrospraying, multifunctional structures can be obtained by a wide variety of polymers.

Polyethylene oxide (PEO) is a synthetic polymer that is biocompatible, nontoxic, water-soluble, and it tends to form H bonds with the materials used together (Reneker and Chun 2003). Whey protein concentrate (WPC) is a well-

recognized natural biopolymer used for carrying and delivery purposes of bioactives. Whey based proteins are also used to fabricate both electrospun and electrospayed micro-/ nano-particles especially with the help of carrier polymers (Soleimanifar et al. 2021).

Whey-based films and coatings in different formulations have been reported to be successfully used for coating of fruits and vegetables (Kandasamy et al. 2021). Various bioactives were encapsulated and protected within whey electrospayed nanospheres as well (Lopez-Rubio and Lagaron 2012). Perishable nature of some fruits, eg. figs requires preservation after harvesting to maintain it in the market. Thus, nanoscale coating matrices can promise for longer post-harvest storage opportunity for this kind of fruits (Moccia et al. 2021).

This study aims to investigate the formation of nano- and micro-scaled droplets from WPC and PEO for food application. Within the scope of the presented study, the morphological and structural features of electrospayed droplets were analyzed through scanning electron microscopy (SEM) and Fourier transform infrared spectrometer (FT-IR). Some physical properties of spraying solution and sprayed mats such as viscosity, electrical conductivity, thickness, and weight per unit area were also determined. Finally, the effectiveness of the obtained mats coated over fresh figs were evaluated.

2. Materials and Method

2.1. Materials

WPC/PEO electrospayed mats were prepared using PEO (MW of 100,000, Sigma-Aldrich, USA), and WPC (80 %, Alfamol, Kimbiatek, Turkey). All the reagents were used without further purification. Alcalase enzyme (2.4 AU-A/g) was kindly supplied by Novozymes A/S (Bagsvaerd, Denmark).

2.2. Preparation of Electrospaying Solution

The 20 wt% WPC was dissolved in ultra-pure water by mechanical stirring for 1h at RT and stored at 4 °C for an overnight to achieve complete dissolution. WPC solution was then subjected to enzymatic hydrolysis by mixing 5 v/w% (enzyme/protein) alcalase at 50 °C for an overnight. The 10 wt% PEO was dissolved in ultra-pure water via magnetic stirring for an overnight at room temperature (RT). To obtain a homogeneous solution, one-part WPC and two parts PEO solutions (1:2) were stirred for another overnight at 1000 rpm (RT).

2.3. Viscosity and Electrical Conductivity Measurements of Electrospaying Solution

Prior to electrospaying, viscosity and electrical conductivity of the solutions were determined. Viscosity measurements were performed using a rotational viscometer (Brookfield DV2T, MA, USA) with the spindle RV-5 rotating at a rate of 100 and 200 rpm. Each measurement was made in duplicate and average viscosities were calculated.

Electrical conductivities of WPC, PEO and WPC/PEO solutions were measured through an electrical conductometer (HACH, HQ440d multi, USA).

2.4. Electrospaying

The WPC/PEO solutions were filled into a 20 ml syringe with a 21 G needle connected to a high voltage power supply for electrospaying. The voltage applied was 8 kV and flow rate of the solution was 0.24 ml/min. The distance between the syringe and collector was kept as 21 cm and the electrospayed (ES) nanobeads were collected on a grounded plate coated with Al foil.

2.5. SEM Analysis

The morphology of WPC/PEO based mats were characterized by SEM ((FEI QUANTA 250 FEG) with an acceleration voltage of 10 kV and a secondary-electron detector. For this purpose, the samples were coated with gold and fixed onto metallic stubs with double-sided carbon tape.

2.6. Thickness and weight of ES mats

The thickness of ES mats was measured using a digital micrometer (Mitutoyo, Japan) with the sensitivity of 0.001, at ten different points and the average thickness was recorded. Ten pieces of the 2x2 cm² cuts of the mats were weighed and the average weight of the ES mats were recorded using an analytical balance (Radwag, Poland) with a sensitivity of 0.1 mg.

2.7. FT-IR Analysis

FTIR characterizations of WPC/PEO samples were carried out between 400 and 4000 cm⁻¹ wavenumbers with Perkin Elmer UATR Spectrum Two FTIR. The resolution was 4 cm⁻¹ and the number of scans collected was 32.

2.8. Coating of Fresh Figs by Electrospayed WPC/PEO Mats

The fresh figs were tied to an apparatus with a strand and hanged up in front of the stable collector. The electrospaying was continued for 4 hours to coat all surfaces with sprayed nano droplets. Then, the coated and uncoated fresh figs were stored at +4°C for 14 days. Besides visual evaluation, microbial load of the coated and uncoated figs was investigated at the end of this period. Samples prepared in peptone water (0.1%) from both coated and uncoated figs were inoculated on the plate count agar (PCA) and the colony forming units per ml (CFU/ml) were determined after 48 h incubation at 35 °C.

3. Results

3.1. Properties of Electrospaying Solutions

Viscosity and electrical conductivity measurements of the HWPC, PEO and HWPC/PEO solutions were presented in Table 1. Except for pure HWPC, viscosity values were recorded at 100 rpm with torque varying between 65% and 95%. Since it was not achieved at 100 rpm, viscosity measurement for HWPC was performed at 200 rpm.

Unprocessed WPC had very low viscosity (data not shown). Viscosity of WPC protein was increased in case of enzymatic hydrolysis. However, it was not enough to prepare electro sprayed mats having uniformly distributed droplets. Although low viscosity is a prerequisite for electro spraying, the ~1500 cP of viscosity seemed still too low to spray droplets. Thus, it was aimed to blend with an auxiliary polymer, PEO to enhance viscosity, facilitating a desirable electro spraying process. The final viscosity of the electro spraying solution was measured as 3701 cP. Although viscosity values in the range of 800-4000 cP are required for the electro spinning process and fiber formation (Chakraborty et al. 2009), lower viscosities are enough to produce droplets by electrohydrodynamic atomization. Since there is a requisite for long polymer chain entanglements that contribute to the viscosity to ensure the continuity of the fiber structure and high aspect ratio, the viscosity limit is a more crucial parameter for the electro spinning of nanofibers than the electro spraying of droplets.

Due to its high mineral content, the conductivity of HWPC (20%) was remarkably high when compared to the PEO solution. Most probably, this prevents its spraying ability alone. Morota et al. (2004) were not able to electro spray the PEO aqueous solutions whose conductivities were changed with CaCl₂ at an electrical conductivity value above 5 mS/cm. The blended solution exhibited an electrical conductivity of 3.41 mS/cm value which is in the sprayable range.

Table 1 Viscosity and electrical conductivity of biopolymer solutions

Sample solutions	Viscosity (cP)	Electrical conductivity (mS/cm)
HWPC	1491 ± 173	6.520 ± 0.339
PEO	3419 ± 43	0.371 ± 0.010
HWPC/ PEO	3701 ± 101	3.410 ± 0.021

3.2. Thickness, Weight, and Morphology of Electro sprayed Mats

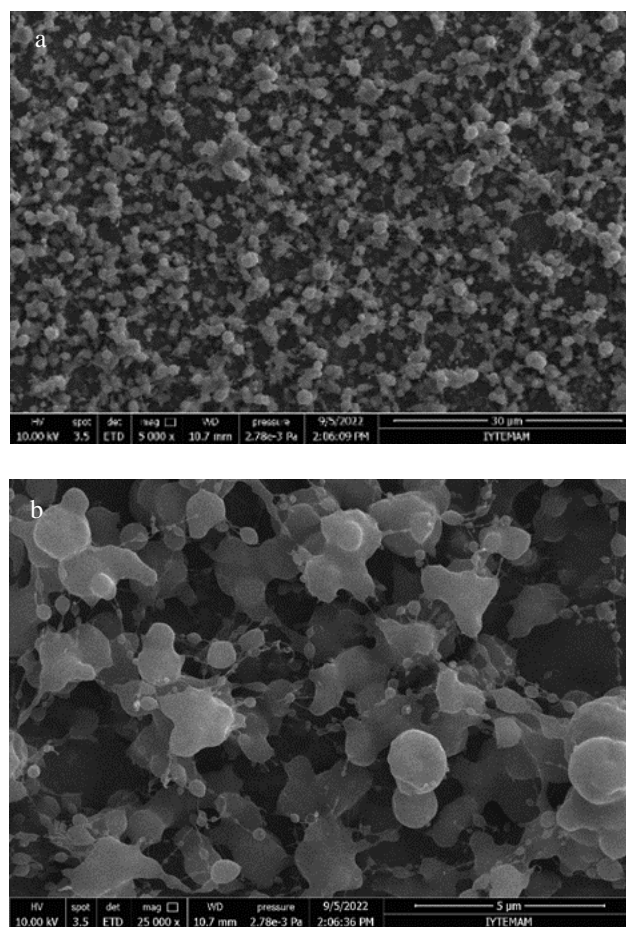
Physical parameters, thickness and weight per unit area of electro sprayed mats produced with an electro spraying of about 4 hours were given in Table 2. As known, the thickness and the weight per unit area of the electro sprayed mats are directly affected by the spraying duration. The results show that a very thin mat structure can be produced in about four hours. Moreover, it can be coated on food without almost any change on the weight of the food which is important in terms of transportation.

Table 2 Thickness and weight per unit area of ES mats

Sample	Thickness (µm)	Weight per unit area (g/m ²)
HWPC/ PEO ES mat	1.8 ± 0.7	0.040 ± 0.009

SEM images of HWPC/PEO mats were given in Figure 1. Increased viscosity in the protein solution by the addition of PEO enhanced the formation of regular beads observed through SEM images. Image J Visualization and Measurement Software was occupied to determine the diameter distributions of the droplets forming the mat. The mean diameter was found as 1.02±0.55 µm. Similar diameters have been obtained with aqueous solutions of different polymers in the literature (Ambrus et al. 2013; Suksamran et al. 2013; Tian et al. 2013).

Fig. 1 SEM images of HWPC/PEO mats (a) X5K (b) X25K



As a result of the interactions between the viscous, surface tension, and electrostatic forces, nanoscaled droplets were obtained as seen in the SEM images. As droplets having diameters of 1 µm or less are considered as nanoscaled 0D structures, it can be concluded that droplets having an average diameter of 1 µm was achieved in this study.

3.3. Structure of Electro sprayed Mats

FTIR spectra of Al foil and electro sprayed HWPC/PEO mats on Al foil were given in figure 2. ATR-FTIR spectroscopy analyses revealed remarkable structural changes in protein and interaction between protein and PEO in the electro sprayed mats. The peaks at ~2882, 1467, 1360 and 699 cm⁻¹ were assigned to PEO. The signals at ~1632 and 1547 cm⁻¹ were attributed to amide I and amide II vibrations.

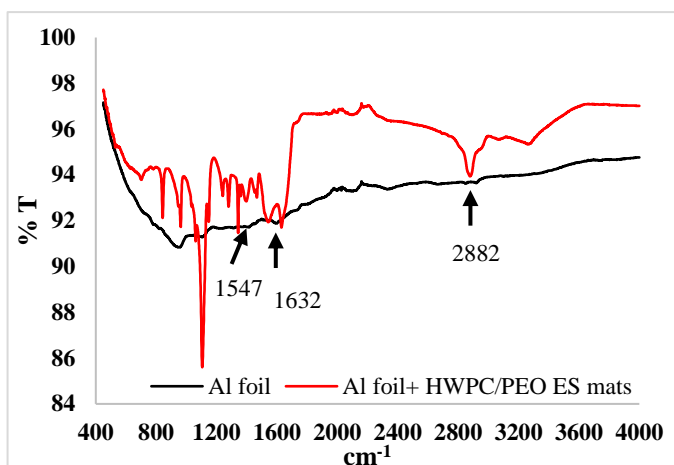


Fig. 2 FT-IR Spectra of naked Al foil and Al foil +HWPC/PEO electrosprayed mats

3.4. Evaluation of Fresh Figs Coated by Electrospayed WPC/PEO Mats

The four-hour coating provided a thin shield over fresh figs (Figure 3a) partially protecting them from moisture loss (data not shown). Visual evaluation during storage showed that microbial decay in uncoated figs was started earlier than the coated ones. Based on plate counts, electrospayed HWPC/PEO mat coating alone exhibited almost one log decrease in microbial load (Figure 3b). Besides, it is expected to reach more reduction in case of including antimicrobial agents within mat matrix. Microbial safety of fresh figs was assessed when coated with edible polysaccharide films as well (Paolucci et al. 2020). Although it is not our scope in this study, it was reported that nutraceutical characteristic of fresh figs was preserved while coated with an edible film ((Moccia et al. 2021).

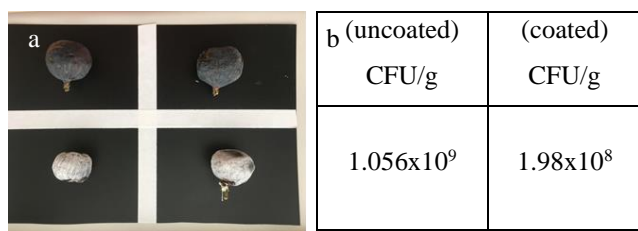


Fig. 3 Fresh figs a) uncoated (upper) and coated (lower) by HWPC/PEO mats (1st day); b) with CFU/g in uncoated and coated cases.

5. Conclusion

With the given formulation of hydrolyzed WPC and PEO, electrospayed mat consisting well-distributed nanoparticles were successfully formed. Viscosity and conductivity of the polymer blend solutions critically affect their electrospaying ability. Coating application of electrospayed HWPC/PEO mats over fresh figs was desirably achieved. Nanodroplets accumulating within the matrix through a certain thickness is promising for making this electrospayed mat an eligible candidate for food

coating purposes. Relevant research work is currently ongoing with the other applications.

Acknowledgements

This research work has been financially supported by Uşak University Scientific Research Projects (BAP) Department with the project 2022/MF001. The authors are very thankful to UBATAM/ Uşak University and IYTE-MAM.

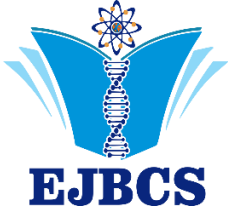
Authors' contributions: MG, obtaining data; EŞ, obtaining data; BÇ, obtaining data; GDT, principle investigation & editing & writing; ET, editing; ÖT, principle investigation & editing & writing.

There is no conflict of interest.

References

- Ambrus R, Radacsi N, Szunyogh T, van der Heijden AE, Ter Horst JH, Szabó-Révész P. 2013. Analysis of submicron-sized niflumic acid crystals prepared by electro spray crystallization. *J Pharm Biomed Anal*, 76:1-7
- Bae SB, Nam HC, Park WH 2019. Electro spraying of environmentally sustainable alginate microbeads for cosmetic additives. *Int J Biol Macromol*, 133:278-283
- Chakraborty S, Liao IC, Adler A, Leong KW. 2009. Electrohydrodynamics: A facile technique to fabricate drug delivery systems. *Adv. Drug Deliv. Rev*, 61:1043-1054
- Gómez-Masaraque LG, Lopez-Rubio A. 2019. Chapter Three - Production of food bioactive-loaded nanoparticles by electro spraying. In: Jafari SM (Ed), *Nanoencapsulation in the Food Industry*. Academic Press, 107-149
- Jadhav A, Wang LJ, Lawrence C, Padhye R 2011. Study of Electro spraying Characteristics of Polymer Solution Coating on Textile Substrate. *AMR* 332-334, 710-715
- Jingwei X, Jiang J, Davoodi P, Srinivasan MP, Wang C-H. 2015. Electrohydrodynamic atomization: A two-decade effort to produce and process micro-/nanoparticulate materials. *Chem Eng Sci*, 125: 32-57
- Kandasamy S, Yoo J, Yun J, Kang HB, Seol KH, Kim HW, Ham JS. 2021. Application of whey protein-based edible films and coatings in food industries: An updated overview. *Coatings*, 11(9): 1056
- Lim L-T, Mendes AC, Chronakis IS 2019. Chapter Five - Electro spinning and electro spraying technologies for food applications, In: Lim L-T, Rogers M (Eds.) *Advances in Food and Nutrition Research*, Academic Press, 88, 167-234
- Moccia S, La Cara F, Cervellera C, Russo GL, Volpe MG. 2021. Active Edible Coating to Preserve Fresh Figs. *Chemical Engineering Transactions*, 87: 181-186
- Morota K, Matsumoto H, Mizukoshi T, Konosu Y, Minagawa M, Tanioka A, Yamagata Y, Inoue K. 2004. Poly(ethylene oxide) thin films produced by electro spray deposition: morphology control and additive effects of alcohols on nanostructure. *J Colloid Interface Sci*, 279 (2): 484-492
- Paolucci M, Di Stasio M, Sorrentino A, La Cara F, Volpe MG. 2020. Active edible polysaccharide-based coating for preservation of fresh figs (*Ficus carica* L.). *Foods*, 9(12): 1793.
- Reneker DH, Chun I 1996. Nanometer Diameter Fibers of Polymer, Produced by Electro spinning, *Nanotechnology*, 7: 216-223.

- López-Rubio A, Lagaron JM. 2012. Whey protein capsules obtained through electrospraying for the encapsulation of bioactives. *Innovative Food Science & Emerging Technologies*, 13: 200-206
- Soleimanifar, M., Jafari, S. M., Assadpour, E., & Mirarab, A. (2021). Electrosprayed whey protein nanocarriers containing natural phenolics; thermal and antioxidant properties, release behavior and stability. *J Food Eng*, 307, 110644.
- Suksamran T, Ngawhirunpat T, Rojanarata T, Sajomsang W, Pitaksuteepong T, Opanasopit P. 2013. Methylated N-(4-N,N-dimethylaminocinnamyl) chitosan-coated electrospray OVA-loaded microparticles for oral vaccination. *Int J Pharm*, 1;448(1):19-27
- Tian Y, Wu G, Tian X, Tao X, Chen W. 2013. Novel erythrocyte-like graphene microspheres with high quality and mass production capability via electrospray assisted self-assembly. *Sci Rep*, 25; 3:3327
- Vasile C 2018. Polymeric Nanocomposites and Nanocoatings for Food Packaging: A Review. *Materials (Basel)*, 11(10):1834
- Wang J, Jansen JA, Yang F 2019. Electrospraying: Possibilities and Challenges of Engineering Carriers for Biomedical Applications—A Mini Review. *Front. Chem*, 7:258



Malatya ili sucul böcek (Coleoptera) faunasına katkılar

Gani Erhan Taşar^{1*}

¹Adıyaman University, Kahta Vocational High School, Adıyaman, Türkiye

*Corresponding author: erhantasar@gmail.com
Orcid No: <https://orcid.org/0000-0002-9217-0706>

Received : 07/12/2022
Accepted : 31/01/2023

Özet: Bu çalışmada, 2019-2020 yılları arasında Malatya ilinden toplanan sucul kınkanatlı türleri değerlendirilmiştir. Araştırma bölgesinde, yedi familyaya (Dryopidae, Dytiscidae, Helophoridae, Hydrophilidae, Hydrochidae, Haliplidae ve Noteridae) ait 21 tür tespit edilmiştir. Tespit edilen türlerin 14 tanesi Malatya ili için yeni kayıttır.

Anahtar Kelimeler: Sucul Kınkanatlılar, Hydrophiloidea, Dryopidae, Dytiscidae.

Contributions to the knowledge of aquatic insect (Coleoptera) fauna in malatya province

Abstract: In this study, aquatic Coleoptera species collected from the province of Malatya between 2019-2020 were evaluated. In the study area, 21 species belonging to seven families (Dryopidae, Dytiscidae, Helophoridae, Hydrophilidae, Hydrochidae, Haliplidae and Noteridae) were identified. 14 of the identified species are new records for Malatya province.

Keywords: Aquatic Coleoptera, Hydrophiloidea, Dryopidae, Dytiscidae.

© EJBCS. All rights reserved.

1. Giriş

Yaklaşık 380000 türü bilinen Kınkanatlılar takımının (Beutel ve ark. 2019), küçük bir kısmı sucul/yarı sucul türlere sahiptir (Jäch 1998). Sucul kınkanatlıların ülkemizde 597 türe sahip olduğu belirtilmektedir (Özdamar 2022). Bu çalışma ile Malatya ilinden Dryopidae, Dytiscidae, Helophoridae, Hydrophilidae, Hydrochidae, Haliplidae ve Noteridae familyalarına ait türler tespit edilmiştir.

Dryopidae familyası dünya genelinde yaklaşık 34 cinsle bağlı 281 türe sahiptir (Bilton ve Shepard 2022). Ülkemizden ise üç cinsle bağlı 11 türü bilinmektedir (Taşar 2018a). Erginlerinin sucul/yarı sucul olduğu bilinen bu familyanın larva ve pupaları karasal olup, bazen kum ve toprakların derinlerinde de bulunmaktadırlar (Bilton ve Shepard 2022). Dytiscidae familyasının dünya genelinde bilinen 182 cinsle bağlı yaklaşık 4600 türü bulunmaktadır (Nilsson ve Hájek 2022). Ülkemizden 28 cinsle ait 165 türü kaydedilmiştir (Aykut ve Fery 2017; Aykut 2018; Aykut ve ark. 2018; Aykut ve Taşar 2018; Erman ve ark. 2018; Aykut ve ark. 2019; Aykut ve ark. 2021). Helophoridae familyası dünya genelinde 192 türe sahip olup (Archangelsky ve ark. 2016), ülkemizden 52 türü bilinmektedir (Taşar 2018b). Birçok Helophoridae türü gerçek sucul böcekler olarak sınıflandırılmaktadır. Erginler vakitlerinin çoğunu su altında geçirirler. Bilinen tüm larva ve pupalar karasaldır

(Stals 2008). Hydrochidae familyası dünya genelinde 182 türe sahiptir. Ülkemizden sekiz türü bilinmektedir (Taşar 2017a). Hem larva hem de erginleri suculdur (Archangelsky et al. 2016). Hydrophilidae familyasının dünya genelinde tanımlanmış yaklaşık 2932 türü bulunmaktadır. Ülkemizden 103 türü bilinmektedir (Taşar 2017b; Polat ve ark. 2021). Büyük bir çoğunluğu sucul olup, yarı sucul, karasal ve kıyı seven türleri de bulunmaktadır (Archangelsky ve ark. 2016). Haliplidae familyasının dünya genelinde bilinen beş cinsle bağlı yaklaşık 200 türü bulunmaktadır. Hem ergin hem de larvaları çok çeşitli sucul habitatlarda yaşamaktadırlar (Garrido ve ark. 2011). Türkiye'den 16 türü bilinmektedir (Darılmaz ve Kıyak 2009). Noteridae familyası dünya genelinde 14 cinsle bağlı 250 türe temsil edilmektedir. Hem ergin hem de larvaları suculdur (Garrido ve ark. 2011). Türkiye'den üç türü bilinmektedir (Darılmaz ve Kıyak 2009).

Bu çalışmanın amacı Malatya ilinin sucul kınkanatlı varlığına katkı sağlamaktır. Yapılan bu çalışma ile Malatya ilinden bilinen sucul kınkanatlı varlığı daha da artmıştır.

2. Materyal ve Metot

2.1. Araştırma Alanı

Malatya ili Türkiye'nin Doğu Anadolu Bölgesi'nde yer almaktadır. Karasal iklime sahip olan ilin merkezi 960

metre rakıma sahiptir. %10'u ormanlık alanlarla, %54'ü çayır ve meralarla kaplıdır. Etrafı dağlarla çevrilidir. Başlıca akarsuları: Söğütlü Çayı, Morhamam Çayı, Kuruçay, Tohma Suyu, Sultan Suyu, Sürgü Suyu, Beyler Deresi, Mamihan ve Şiro Çayı'dır (Anonim 1 2022).

Araştırma alanının haritası Şekil 1'de sunulmuştur.

Şekil 1 Malatya il haritası (Anonim 2 2022).



2.2. Örnekleme Metodu

Örneklerin toplanmasında 3,15x1 mm çapında gözeneklere sahip olan elekler kullanılmıştır. Elekler ile sucul habitatlardan toplanan örnekler, aspiratör yardımıyla küçük şişelere aktarılmıştır. Şişelerin içerisine %70'lik etil alkol dökülerek örneklerin ölmesi sağlanmıştır. GPS (Küresel Konumlandırma Servisi) cihazı (Garmin etrex 30) yardımı ile lokalitelere ait koordinat ve yükseklik verileri tespit edilmiştir. Bu veriler etiketlere yazılarak şişelere yapılandırılmıştır. Daha sonra kapakları kapatılan şişeler muhafaza altına alınmıştır. Tür teşhisi için laboratuvara getirilen örnekler, şişelerden çıkarılarak petri kaplarına aktarılmıştır. Burada, üzerlerindeki çamur ve benzeri artıklardan temizlenen örnekler, Soif Szm-45 marka mikroskop altında incelenerek, tür seviyesinde teşhisleri yapılmıştır.

Araştırma alanında 26 lokaliteden örnekler toplanmıştır. Bu örnekler içerisinde yedi familyaya ait toplam 21 tür teşhis edilmiştir. Toplanan örnekler yazarın kişisel koleksiyonunda muhafaza edilmektedir. Örneklerin toplandığı lokalitelere ait bilgiler Tablo 1'de sunulmuştur.

Tablo 1 Araştırma alanına ait lokalite bilgileri

Kısaltma	Örnek Toplanan Lokalite	Koordinat	Yükseklik (m)
M1	Akçadağ/Görgü	38°18.235'K 38°6.787'D	1015
M2	Doğuşehir	38°21.501'K 38°11.987'D	867
M3	Doğuşehir	38°19.399'K 38°9.351'D	940
M4	Doğuşehir	38°6.068'K 37°53.985'D	1215
M5	Doğuşehir	38°4.997'K 37°55.002'D	1285
M6	Darende/Güdü	38°30.216'K 37°32.091'D	995
M7	Darende/ Akçatoprak	38°30.552'K 37°33.570'D	978
M8	Darende/Akova	38°30.700'K 37°33.551'D	973
M9	Darende	38°30.833'K 37°35.051'D	962
M10	Darende	38°30.934'K 37°36.685'D	951
M11	Darende/ İrmaklı	38°32.668'K 37°36.269'D	959
M12	Erkenek/ Reşadiye	37°58.118'K 38°2.754'D	1390
M13	Kurucaova/ Kalecik	37°59.367'K 38°4.136'D	1405
M14	Kurucaova	37°58.903'K 38°5.168'D	1450
M15	Pütürge/ Yandere	38°2.317'K 38°46.651'D	1045
M16	Pütürge/ Yeşildere	38°3.819'K 38°46.201'D	1150
M17	Pütürge/ Mollahan Çayı	38°11.520'K 38°44.600'D	800
M18	Pütürge/ Çayköy	38°14.300'K 38°41.583'D	1258
M19	Pütürge	38°14.653'K 38°32.520'D	1610
M20	Sürgü	38°0.934'K 37°55.750'D	1322
M21	Sürgü	38°0.632'K 37°58.017'D	1332
M22	Sürgü/Takas	38°0.503'K 37°59.377'D	1341
M23	Yeşilyurt/ Gündüzbey	38°15.272'K 38°16.321'D	1166
M24	Yeşilyurt	38°18.015'K 38°14.429'D	980
M25	Yeşilyurt	38°18.327'K 38°13.843'D	950
M26	Yeşilyurt	38°22.586'K 38°11.821'D	827

3. Bulgular ve Tartışma

Familya Helophoridae

Helophorus brevipalpis Bedel, 1881

Toplanan örneklerin lokaliteleri: M1, 2 örnek; M2, 2 örn.; M12, 3 örn.; M14, 2 örn.

Not: Araştırma alanı için yeni kayıttır.

Helophorus micans (Faldermann, 1835)

Toplanan örneklerin lokaliteleri: M3, 5 örn.; M24, 2 örn.; M25, 2 örn.

Helophorus aquaticus (Linnaeus, 1758)

Toplanan örneklerin lokaliteleri: M12, 2 örn.; M21, 2 örn.

Not: Araştırma alanı için yeni kayıttır.

Helophorus hilaris Sharp, 1916

Toplanan örneklerin lokaliteleri: M2, 2 örn.; M12, 10 örn.; M20, 2 örn.; M21, 2 örn.; M23, 2 örn.

Not: Araştırma alanı için yeni kayıttır.

Helophorus nubilis Fabricius, 1776

Toplanan örneklerin lokaliteleri: M16, 2 örn.

Not: Araştırma alanı için yeni kayıttır.

Helophorus pallidipennis Mulsant & Wachanru, 1852

Toplanan örneklerin lokaliteleri: M17, 1 örn.

Not: Araştırma alanı için yeni kayıttır.

Helophorus syriacus Kuwert, 1885

Toplanan örneklerin lokaliteleri: M12, 2 örn., M20, 1 örn.; M21, 3 örn.

Not: Araştırma alanı için yeni kayıttır.

Familya Hydrochidae

Hydrochus flavipennis Kuster, 1852

Toplanan örneklerin lokaliteleri: M12, 2 örn.

Not: Araştırma alanı için yeni kayıttır.

Familya Hydrophilidae

Enochrus politus (Küster, 1849)

Toplanan örneklerin lokaliteleri: M24, 2 örn.; M25, 2 örn.

Enochrus quadripunctatus (Herbst, 1797)

Toplanan örneklerin lokaliteleri: M7, 2 örn.; M22, 2 örn.

Enochrus fuscipennis (Thomson, 1884)

Toplanan örneklerin lokaliteleri: M4, 1 örn.; M26, 2 örn.

Helochares lividus (Forster, 1771)

Toplanan örneklerin lokaliteleri: M15, 3 örn.; M18, 2 örn.

Not: Araştırma alanı için yeni kayıttır.

Hydrochara dichroma (Fairmaire, 1892)

Toplanan örneklerin lokaliteleri: M5, 1 örn.

Not: Araştırma alanı için yeni kayıttır.

Laccobius hindukuschi Chiesa, 1966

Toplanan örneklerin lokaliteleri: M6, 1 örn.; M8, 2 örn.; M11, 2 örn.

Not: Araştırma alanı için yeni kayıttır.

Laccobius simulatrix d'Orchymont, 1932

Toplanan örneklerin lokaliteleri: M26, 2 örn.

Laccobius syriacus Guillebeau, 1896

Toplanan örneklerin lokaliteleri: M22, 2 örn.

Laccobius gracilis Motschulsky, 1855

Toplanan örneklerin lokaliteleri: M13, 1 örn.; M15, 5 örn.; M16, 2 örn.

Not: Araştırma alanı için yeni kayıttır.

Familya Noteridae

Noterus clavicornis (De Geer, 1774)

Toplanan örneklerin lokaliteleri: M15, 5 örn.

Not: Araştırma alanı için yeni kayıttır.

Familya Haliplidae

Pelodytes caesus (Duftschmid, 1805)

Toplanan örneklerin lokaliteleri: M9, 2 örn.; M10, 1 örn.

Not: Araştırma alanı için yeni kayıttır.

Familiya Dryopidae*Dryops rufipes* (Krynicky, 1832)

Toplanan örneklerin lokaliteleri: M19, 3 örn.

Not: Araştırma alanı için yeni kayıttır.

Familiya Dytiscidae*Dytiscus marginalis* (Linnaeus, 1758)

Toplanan örneklerin lokaliteleri: M1, 1 örn.

Not: Araştırma alanı için yeni kayıttır.

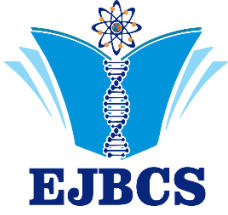
4. Sonuç

Bu çalışmada Malatya ilinden toplanan sucul/yarı sucul kınkanatlı türleri değerlendirilmiştir. Yedi familyaya bağlı toplamda 21 tür teşhis edilmiştir. Bu türlerden 14'ü araştırma alanı için yeni kayıt özelliğindedir. Yapılan bu çalışma Malatya ili sucul kınkanatlı varlığının bilinirliğine önemli katkılar sunmuştur. Ülkemizin sucul kınkanatlı varlığının tam olarak tespit edilebilmesi için bu tarz faunistik çalışmaların tüm illeri kapsayacak şekilde artarak devam etmesi gerekmektedir.

Kaynaklar

- Anonim 1. 2022. <https://tr.wikipedia.org/wiki/Malatya>. Erişim tarihi 01.12.2022.
- Anonim 2. 2022. cografyaharita.com. Erişim tarihi 01.12.2022.
- Archangelsky M, Beutel RG, Komarek A. 2016. Morphology and Systematics (Archostemata, Adephaga, Myxophaga, Polyphaga partim) 2nd edition, Chapter 12, Hydrophiloidea Latreille, 1802. Coleoptera Beetles, vol 1. Walter de Gruyter GMBH, Germany, pp 231-272.
- Aykut M, Fery H. 2017. *Scarodytes costatus* nov. sp. from the Bingöl Province in Turkey, the first species of the genus with costate elytra (Insecta: Coleoptera: Dytiscidae: Deronectina). Linz Biol Beitr. 49:395-414.
- Aykut M. 2018. The Diving Beetle Fauna of Diyarbakır and Bingöl Provinces, Turkey (Coleoptera: Dytiscidae) with a New Record. Pak J Zool. 50(1):65-74.
- Aykut M, Taşar GE, Fery H. 2018. *Deronectes taron* sp. n. from the eastern Anatolian region of Turkey (Coleoptera, Dytiscidae, Hydrophorinae). Zootaxa. 4422(2):403-410.
- Aykut M, Taşar GE. 2018. Contributions to the knowledge of Adephagan fauna in Adıyaman Province, Turkey (Coleoptera: Dytiscidae, Gyrinidae, Haliplidae and Noteridae). Mun Ent Zool. 13:249-255.
- Aykut M, Yıldırım İH, Tusun S, Fery H. 2019. *Deronectes kabilcevz* sp. n. and *D. propedoriae* sp. n. from south-eastern Anatolia (Turkey) (Coleoptera, Dytiscidae, Hydrophorinae). Zootaxa. 4691(1):5-10.
- Aykut M, Taşar GE, Fery H. 2021. *Bidessus anatolicus adıyaman* ssp. n. from Adıyaman province, southern Turkey (Coleoptera, Dytiscidae, Bidessini). Zootaxa. 5027(4):563-575.
- Beutel RG, Pohl H, Yan EV, Anton E, Liu SP, Slipinski SA. 2019. The phylogeny of Coleoptera (Hexapoda) morphological characters and molecular phylogenies. Syst Entomol. 74:75-102.

- Bilton DT, Shepard WD. 2022. *Rhithrops capensis* gen. et sp. nov., a new aquatic dryopid beetle from the Western Cape of South Africa (Coleoptera: Dryopoidea: Dryopidae). Zootaxa. 5195(6):539-553.
- Darılmaz MC, Kiyak S. 2009. Checklist of Gyrinidae, Haliplidae, Noteridae and Dytiscidae of Turkey (Coleoptera: Adephaga). J Nat Hist. 43:1585-1636.
- Erman ÖK, Taşar GE, Aykut M, Kurt K. 2018. First record of *Hydaticus histrio* Clark, 1864 (Coleoptera, Dytiscidae) from Turkey. Acta Biologica Turcica, 31(4): 174-177.
- Garrido J, Benetti JC, Bilbao AP. 2011. Identification Guide of Freshwater Macroinvertebrates of Spain (Chrysomelidae, Curculionidae, Dryopidae, Dytiscidae, Elmidae, Gyrinidae, Helophoridae, Haliplidae, Hydraenidae, Hydrochidae, Hydrophilidae, Hydroscaphidae, Hygrobiidae, Noteridae, Psephenidae, Scirtidae). Springer, London, pp 21-25, 102-111.
- Jäch MA. 1998. Annotated check list of aquatic and riparian/littoral beetle families of the world (Coleoptera). M.A. Jäch & L. Ji (eds.): Water Beetles of China Vol. II, pp 25-42.
- Nilsson AN, Hájek J. 2022. A world catalogue of the family Dytiscidae (Coleoptera, Adephaga). World Wide Web Electronic Publication. <http://www.waterbeetles.eu>. Erişim tarihi 10.08.2022.
- Özdamar H. 2022. Muğla İli Gyrinidae (Coleoptera) Faunası İçin Yeni Kayıt: *Aulonogyrus concinnus* (Klug, 1834). Gazi Üniv Fen Bilim Derg. 3(1):54-57.
- Polat A, Darılmaz MC, İncikara Ü. 2021. An annotated checklist of the Hydrophiloidea (Coleoptera) of Turkey. Mun Ent Zool. 16(1):151-178.
- Stals R. 2008. Guides to the Freshwater Invertebrates of Southern Africa, Volume 10: Coleoptera (Ed: R. Stals & IJ de Moor) Chapter 12: Helophoridae. Republic of South Africa, pp 113-116.
- Taşar GE. 2018a. Checklist of Dryopidae and Elmidae (Coleoptera: Byrrhoidea) of Turkey. Biharian Biol. 12(1):1-6.
- Taşar GE. 2018b. Investigations on the Hydrophiloidea (Coleoptera: Helophoridae, Hydrochidae and Hydrophilidae) Fauna of Şanlıurfa Province. KSU J Agric Nat. 21(2):111-118.
- Taşar GE. 2017a. *Hydrochus adıyamanensis* sp. n. from Adıyaman Province in South-Eastern Turkey (Coleoptera: Hydrochidae). Zool Middle East. 63(4):356-361.
- Taşar GE. 2017b. Contributions to the knowledge of Aquatic Coleoptera Fauna (Dryopidae, Helophoridae, Heteroceridae, Hydrochidae, Hydrophilidae, Gyrinidae, Haliplidae and Noteridae) of Diyarbakır, Mardin and Batman Provinces (Turkey). Turkish J Fish Aquat Sci. 18:927-936.



Metilal/metanol karışımlarının ZIF-8 katkılı PEI membran kullanarak pervaporasyon prosesi ile saflaştırılması

Derya Ünlü^{1*} 

¹Bursa Teknik Üniversitesi, Mühendislik ve Doğa Bilimleri Fakültesi, Kimya Mühendisliği Bölümü, Bursa, Türkiye.

*Corresponding author : derya.unlu@btu.edu.tr
Orcid No: <https://orcid.org/0000-0001-5240-5876>

Received : 29/12/2022
Accepted : 19/03/2023

Özet: Bu çalışmada, metilal/metanol karışımlarının ayrılması için pervaporasyon işlemi kullanılmıştır. Metanole afinitesinden dolayı membran hazırlamak için polieterimid (PEI) polimeri seçilmiştir. ZIF-8, membran için katkı maddesi olarak kullanılmıştır. ZIF-8 katkılı PEI membranı sentezlenmiş ve karakterize edilmiştir. Membranların kimyasal bağ yapısı, termal dayanımı ve morfolojisi sırasıyla Fourier dönüşümü kızılötesi spektroskopisi (FTIR), Termogravimetrik Analiz (TGA) ve Taramalı elektron mikroskobu (SEM) ile analiz edilmiştir. Membranların ayırma performansı farklı çalışma sıcaklıklarında, farklı besleme metanol konsantrasyonlarında ve farklı ZIF-8 yükleme oranlarında incelenmiştir. Optimum proses koşulları, 20°C operasyon sıcaklığı, ağırlıkça %6 besleme metanol konsantrasyonu ve ağırlıkça %0.5 ZIF-8 yükleme oranı olarak belirlenmiştir. Akı ve metanol seçicilik değerleri bu koşullar altında sırasıyla 0.57 kg/m²h akı ve 8169 metanol seçiciliği olarak belirlenmiştir.

Anahtar Kelimeler: Membran, Metilal, Pervaporasyon, Polieterimid

Purification of methylal/methanol mixtures by pervaporation process using ZIF-8 doped PEI membrane

Abstract: In this study, pervaporation process is evaluated for the separation of methylal/methanol mixtures. Polyetherimide (PEI) polymer was chosen for the membrane preparation due to the affinity of the methanol. ZIF-8 was used as additive for the membrane. ZIF-8 doped PEI membrane was synthesized and characterized. The chemical bond structure, thermal strength and morphology of the membranes were analyzed by Fourier transform infrared spectroscopy (FTIR), Thermogravimetric Analysis (TGA) and Scanning Electron Microscopy (SEM), respectively. Separation performance of membranes were investigated in different operation temperatures, different feed methanol concentrations and different ZIF-8 loading ratios. Optimum operation conditions were determined as 20 °C of operation temperature and 6 wt. % of feed methanol concentration and 0.5 wt.% ZIF-8 loading ratio. Flux and methanol selectivity values were 0.57 kg/m²h and 8169, respectively.

Keywords: Membrane, Methylal, Pervaporation, Polyetherimide

1. Giriş

Çeşitli dezavantajlarına rağmen, küresel enerji ihtiyacının yaklaşık %84'ü fosil yakıtlardan karşılanmaktadır. Biyoyakıtlar daha yaygın olarak kullanılmaya başlandığında fosil yakıtlara olan bağımlılık azaltılabilir. Fosil yakıtların, sera gazlarının emisyonu da dahil olmak üzere birçok nedenden dolayı çevre üzerinde olumsuz etkileri olduğu bilinmektedir. Fosil yakıtların sınırlı mevcudiyeti, yenilenebilir enerji kaynaklarına acil ve sürdürülebilir bir geçişi zorunlu kılmaktadır. Yenilenebilir kaynaklardan elde edilen biyoyakıtlar ve yakıt biyokatki maddeleri, potansiyel enerji kaynakları olarak araştırılmıştır

(Ahmed ve ark., 2008). Son yıllarda yapılan çalışmalar, yeni alternatif biyoyakıtların üretimine ve benzin, dizel ve biyodizelin yakıt özelliklerini geliştirmek ve daha iyi performans elde etmek için eklenecek yakıt katkı maddelerinin sentezi üzerine yoğunlaşmaktadır (Gonçalves ve ark., 2008).

Metilal, dizel ve biyodizel yakıtları ile karışabilen önemli bir yakıt katkı maddesidir. Dimetoksümetan olarak da adlandırılan metilal, toksik olmayan biyobozunur bir yakıt biyokatki maddesidir. Metilal, dizel ve biyodizel ile %100 karışabilme özelliğine sahiptir. Ağırlıkça %42 oranında oksijen içeren bir oksijenattır, yüksek hidrojen/karbon

oranına sahiptir. Düşük setan sayısına ve kendiliğinden tutuşma sıcaklığına sahiptir. Aynı zamanda yakıtın yanma performansını ve emisyon salımlarını iyileştirmektedir. Metilal, dizel yakıtın enerji yoğunluğunun %55'ine sahiptir. Geleneksel dizel yakıtı ile %20 oranında karıştırıldığında yakıtın enerji yoğunluğunu yaklaşık olarak %10 kadar azaltmaktadır (Dong ve ark., 2018; Lu ve ark., 2007). Tüm bunların yanında metilal olağan üstü bir çözücü gücü, amfilik karakteri, oldukça düşük viskozitesi ve yüksek buharlaşma hızı sayesinde kozmetik sektöründe, boya ve vernik üretiminde, yağ çözücülerinde, tıbbi ilaçlarda, polimerlerde, reçinelerde ve yapıştırıcılarda olmak üzere pek çok endüstriyel uygulamada yeşil solvent olarak kullanılmaktadır. Kullanım alanındaki bu çeşitlilik, metilalin küresel talebinin artmasına neden olmaktadır (Carretier ve ark., 2003).

Metilal, formaldehit ile metanolün sentezi ile üretilir. Metilal sentezi sonucunda reaksiyon karışımı içerisinde reaksiyona girmemiş metanol bulunmaktadır. Ağırlıkça %94.06 metilal içeren metilal/metanol karışımı atmosfer basıncı altında azeotrop özellik göstermektedir. Azeotrop karışımları, klasik ayırma prosesleri ile ayırmak oldukça güçtür. Bu çalışmada geleneksel ayırma proseslerine alternatif olarak, metilal sentez reaksiyonu sonucunda elde edilen metilal/metanol karışımlarının membran destekli ayırma prosesi olan pervaporasyon prosesi ile ayrılması hedeflenmiştir.

Pervaporasyon, sıvı-sıvı karışımları ayırmak için kullanılan, karışım içerisindeki bileşenlerden birinin membrandan seçici geçtiği, itici gücün kimyasal potansiyel olduğu membran destekli bir ayırma prosesidir. Membranda kütle transferi çözünme difüzyon mekanizması ile ifade edilir. Bu süreç düşük maliyetli, enerji tüketimi az ve çevreci bir prosesdir (Baker, 2000; Basile ve ark., 2016). Pervaporasyonda taşınım, beslemedeki bileşenler ve membran arasındaki etkileşim ile ilgilidir. Bu sebeple membran sentezinde kullanılacak malzemenin özellikleri membranın ayırma performansında önemli bir etkidir (Basile ve ark., 2015). Polimerik membranlarda iyi bir ayırma performansı, kullanılacak olan polimerik malzemenin kimyasal, termal ve mekanik dayanımı ve sorpsiyon kapasitesi ile ilişkilidir (Das ve ark., 2007). Bu çalışmada metilalin saf olarak eldesi amaçlandığından, metanole ilgisi olan Polieterimid (PEI) polimeri kullanılarak membranlar hazırlanmış ve karışımdan metanolün uzaklaştırılması sağlanmıştır. Polieterimid (PEI) yüksek termal, kimyasal ve mekanik dayanımı ve düşük maliyeti nedeniyle polimerik membran hazırlamada sık kullanılan polimerlerden biridir (Mensitieri ve ark., 2019). Ayrıca katkı maddesi olarak kullanılacak olan malzeme olan ZIF-8'de metanole seçici özellikte seçilmiştir. PEI membranının metanole olan ilgisini artırarak ayırma performanslarının gelişmesini sağlamıştır (Wasewar ve ark., 2007).

Zeolitik imidazolat yapılar (ZIF), metal organik yapıların bir alt sınıfıdır. ZIF'lerin bağlayıcı kısmı imidazollerken, metalik kısmı ise Zn, Co veya In gibi geçiş metallere aittir. Zeolitik denmesinin sebebi ise zeolitlere oldukça yakın

yapıya sahip olmalarıdır (Park ve ark., 2006). ZIF-8 homojen gözenek boyutu, yüksek termal ve kimyasal dayanımı nedeniyle ilgi çekici bir zeolitik imidazolat yapısıdır. ZIF-8 pervaporasyon uygulaması için uygun bir dolgu maddesidir. Delik açıklığı 3.4°A ve büyük boşluk ebadı 11.6° olması dolayısıyla alkoller ve suyu ayırma için kullanımı uygundur (Shi ve ark., 2012).

Bu çalışmada operasyon sıcaklığının, besleme metanol konsantrasyonunun ve ZIF-8 yükleme oranının metilal/metanol karışımının ayırma performansına etkisi incelenmiştir.

2. Malzeme ve Yöntem

2.1. Malzemeler

Membran sentezinde kullanılan polimer PEI (Eriyik Akış İndisi: 9 g/10 dak, 337°C/6.6 kg) Sigma Aldrich firmasından tedarik edilmiştir. PEI çözücüsü olarak kullanılan N-Metil-2-Pirolidon Carlo Erba'dan alınmıştır. ZIF-8 sentezinde kullanılan 2-Metilimidazol (99%) Sigma Aldrich'ten, çinko nitrat heksahidrat (98%) ABCR'den satın alınmıştır.

2.2. ZIF-8 Sentezi

10 mmol çinko nitrat heksahidrat, ve 80 mmol 2-metil imidazol ayrı ayrı metanolde çözülmüştür. Her iki çözelti homojen oluncaya kadar karıştırılmıştır. Daha sonra hazırlanan bu iki çözelti bir araya getirilerek oda sıcaklığında karıştırılmıştır. Elde edilen karışımın bir müddet sonra bulanıklaştığı görülmüştür. 1 saat karıştırıldıktan sonra çözelti santrifüj edilerek ZIF-8 partikülleri çöktürülmüştür. Santrifüj sonrası elde edilen ZIF-8 partikülleri metanol ve kloroform ile yıkanarak saflaştırılmıştır. Ardından 80°C'de 24 saatte kurutulmuştur. (Amirilargani ve Sadatnia, 2014; Song ve ark., 2012).

2.3. ZIF-8 Katkılı PEI Membranın Hazırlanması

Ağırlıkça %10 PEI, N-Metil-2-Pirolidon (NMP) içerisinde 90°C'de çözülmüştür. Daha sonra içerisine belirli oranlarda ZIF-8 eklenerek manyetik karıştırıcıda karıştırılmıştır. Membran çözeltisi içerisinde ZIF-8 katkı maddelerinin uniform dağılımını sağlamak için belirli bir sürede ultrasonik banyoda da karıştırılmıştır. Ardından çözelti cam yüzeye dökülerek oda sıcaklığında kurumaya bırakılmıştır. Kuruyan membran cam yüzeyden dikkatlice çıkarılarak kullanıma hazır hale getirilmiştir (Li ve ark., 2018, Gao ve ark., 2017).

2.4. Membranların Karakterizasyonu

Sentezlenen membranlar SEM, FTIR ve TGA kullanılarak karakterize edilmiştir. Saf ve ZIF-8 katkılı PEI membranların morfolojik yapı analizinde Carl Zeiss/Gemini 300 model SEM cihazı kullanılmıştır. ZIF-8 ilavesi ile membranların kimyasal bağ yapılarındaki değişim PerkinElmer, Spectrum Two model FTIR cihazı ile belirlenmiştir. Membranların termal dayanımları TA Instruments, SDT650 model termogravimetrik analiz cihazı kullanılarak incelenmiştir.

2.5. Pervaporasyon Prosesi ile Metilal/Metanol Karışımının Saflaştırılması

Metilal/metanol karışımlarının saflaştırılması pervaporasyon prosesi ile gerçekleştirilmiştir. Pervaporasyon prosesinde membranın üst yüzeyi besleme karışımı ile temas ederken, hücrenin alt tarafında vakum bulunmaktadır. PEI membran hidrofilik özellikte olduğu için metanole yüksek ilgi göstermekte, metanol membrandan difüze olmakta ve geçen akım tarafında vakumdan dolayı oluşan düşük basınçta buhar faza geçmektedir. Buhar fazdaki metanol, sıvı azot ile dolu tuzaklarda toplanarak, yoğunlaştırılmakta ve tekrar sıvı fazda elde edilmektedir. Akı ve seçicilik değerleri saat başı numune alınarak GC ile analiz edilerek hesaplanmıştır. Akı değeri Eşitlik 1, seçicilik ise Eşitlik 2'deki formül kullanılarak hesaplanmıştır.

$$J = \frac{m}{S.t} \quad (1)$$

$$\alpha = \frac{P_a/P_b}{F_a/F_b} \quad (2)$$

Eşitlik 1'de m soğutucu kapanlarda toplanan numune miktarının ağırlığını, S membranın etkin kullanım yüzey alanını, t ise deney süresini ifade etmektedir. Eşitlik 2'de ise α , seçicilik değerini, P geçen akım konsantrasyonunu, F besleme konsantrasyonunu ifade ederken, a ve b karışımdaki bileşenleri ifade etmektedir. Bu çalışma kapsamında a metanolü, b metilali ifade etmektedir.

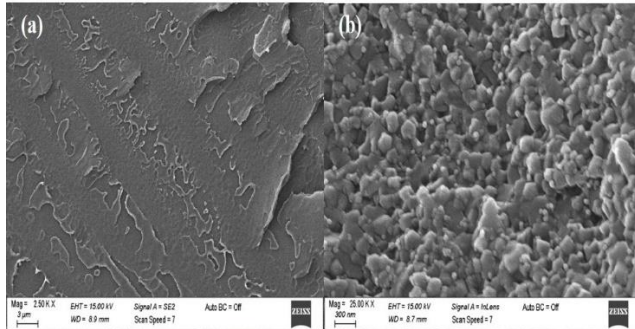
Membranın ayırma performansı farklı ZIF-8 yükleme oranlarında (ağırlıkça %0.25, %0.5, %0.75 ve %1), farklı operasyon sıcaklıklarında (20 °C, 30 °C, 40°C) ve farklı besleme konsantrasyonlarında (ağırlıkça %6, %10, %15 ve %20 metanol) incelenmiş ve akı ve seçicilik değerleri hesaplanmıştır.

3. Bulgular ve tartışma

3.1. Membran Karakterizasyon Sonuçları

3.1.1. SEM

SEM analizi, saf PEI ve ZIF-8 katkılı PEI membranlardan alınan örnekler ile yapılmıştır. Şekil 1'de membranların kesit görüntüleri görülmektedir.

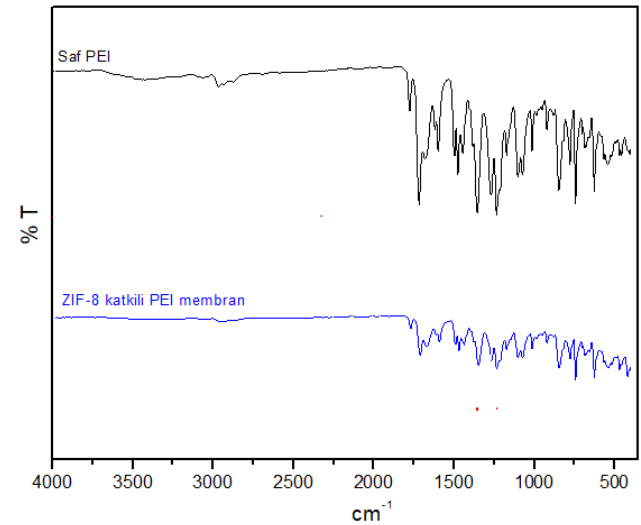


Şekil 1. SEM kesit görüntüleri (a) Saf PEI (b) ZIF-8 katkılı PEI membran

Saf PEI membranın Şekil 1.(a)'daki kesit görüntüsü; tek bir polimer tabakasından oluştuğunu, yapının yoğun, homojen bir görüntü sergilediğini göstermektedir. ZIF-8 katkılı PEI membranın Şekil 1.(b)'deki kesit görüntüsü ise ZIF-8'in membran içerisinde homojen bir şekilde dağıldığını, polimer ile ZIF-8 arasında boşluk oluşturmadığını, uyumlu bir yapı sergilediğini göstermektedir. Elde edilen SEM görüntüleri membranların başarı ile sentezlendiğini göstermektedir.

3.1.2. FTIR

Şekil 2'de hazırlanan membranların FTIR spektrumları verilmiştir.

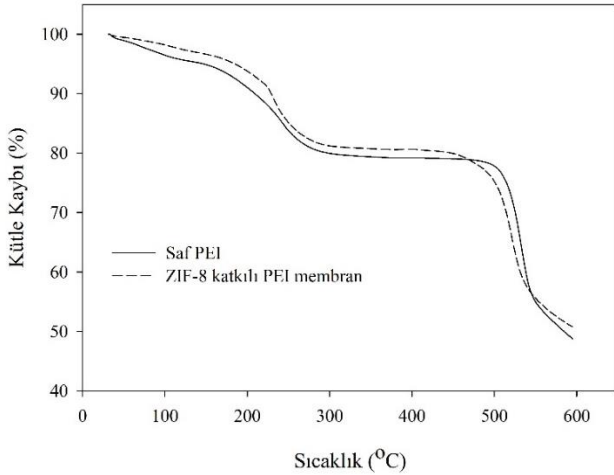


Şekil 2. Sentezlenen membranların FTIR analizi

FTIR spektrumunda saf PEI membrana ait imid karbonil asimetrik ve simetrik grupları 1777 ve 1717 cm^{-1} 'de, C-N gerilim ve eğilme pikleri 1352 ve 742 cm^{-1} 'de, aromatik eter C-O-C grupları 1234 cm^{-1} 'de görülmektedir (Chen, ve ark., 2006). Membranın yapısındaki -OH ve ikincil amin grupları 3000-3500 cm^{-1} aralığındaki geniş pike karşılık gelmektedir. -CH₂ gruplarının gerilim pikleri 2962 cm^{-1} 'de gözlenmiştir. C=O (amid I) ve N-H (amid II) gerilme titreşimi pikleri, sırasıyla 1643 ve 1570 cm^{-1} 'de görülmüştür. Bununla birlikte, imidazol kısımlarının C=N ve N-H grupları için karakteristik tepe noktaları, PEI membranında bulunan diğer fonksiyonel grupların benzer germe titreşimi nedeniyle örtüşmektedir. Sadece bağların yoğunluğu değişim göstermiştir (Barankova, 2017). Metal ve organik ligand arasındaki bağ (Zn-N) 423 cm^{-1} 'de gözlenmiştir (Basu ve Balakrishnan, 2017). Bu sonuçlar, ZIF-8 parçacıklarının PEI membranın yüzeyine gömülü olduğunu göstermiştir.

3.1.3. TGA

Sentezlenen membranların sıcaklıkla kütle kaybında meydana gelen değişim termal gravimetrik analiz (TGA) ile analiz edilmiştir. Saf PEI membran ve ZIF-8 katkılı PEI membranların termal dayanım eğrileri Şekil 3'te verilmiştir.



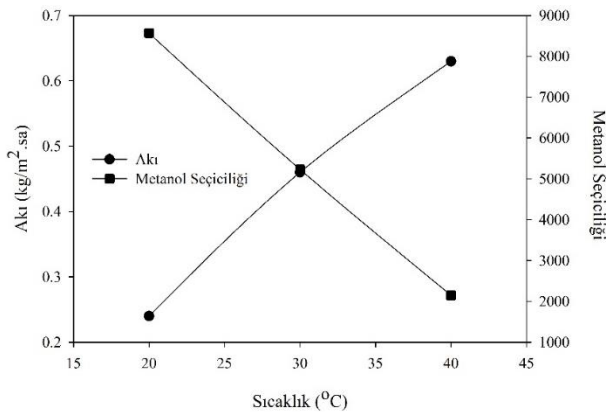
Şekil 3. Sentezlenen membranların TGA eğrisi

Katkısız ve ZIF-8 katkılı PEI membranda 100-200°C arasında görülen kütle kayıplarının ZIF-8 ve PEI yapısında bulunan solventlerin buharlaşmasından kaynaklandığı düşünülmektedir (Demirciyeva, 2006). 450 ve 500°C sıcaklıklarından sonra ise polimer zincirlerinin bozulması ile ilgili olarak temel kütle kaybı başlamıştır. Saf PEI membrana ilave edilen ZIF-8 katkısının membranın bozunma sıcaklığını yükselttiği görülmüştür. Saf PEI membranın kalıntı değeri %48.76 iken, ZIF-8 katkılı PEI membranın kalıntı değeri %50.80 olarak elde edilmiştir.

3.2. Pervaporasyon Prosesi ile Saflaştırma Sonuçları

3.2.1. Sıcaklığın etkisi

Sıcaklığın ağırlıkça %6 metanol içeren besleme çözeltisini ayırma performansına etkisi 20, 30 ve 40°C sıcaklıklarda, ağırlıkça %0.5 ZIF-8 katkılı PEI membran kullanılarak incelenmiştir. Sıcaklıkla toplam akı ve metanolün değişimi Şekil 4'te verilmiştir.



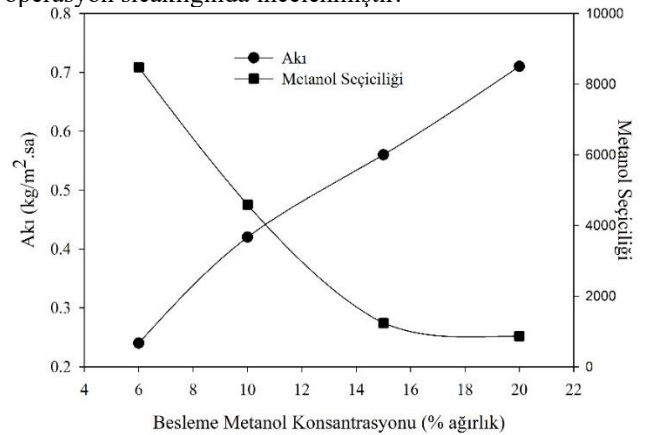
Şekil 4. Operasyon sıcaklığının ayırma performansına etkisi (Çalışma koşulları: %6 metanol içeren besleme, ağırlıkça %0.5 ZIF-8 katkılı PEI membran)

Sıcaklık arttıkça, toplam akı değeri de artış göstermiştir. Operasyon sıcaklığının ayırma performansını etkisi iki şekilde olmaktadır: itici güç ve membranın geçirgenliği. Sıcaklık arttıkça karışımdaki metanol ve metilalin doymuş buhar basınçları artış gösterir. Artan doymuş buhar basıncı, alt akım ve üst akım arasında bir itici güç oluşturmuş ve bu

itici güç geçirgenlik akısında artış ile sonuçlanmıştır. Bunun yanı sıra, membranın geçirgenliği, besleme karışımındaki bileşenlerin membran yüzeyinde çözünürlüğü ve membran boyunca difüzyonu ile ilgilidir. Bileşenlerin difüzyonu da operasyon sıcaklığı ile artmakta ve buna bağlı olarak metanolünde membrandan difüzyonu artış göstermektedir. Ayrıca operasyon sıcaklığındaki artış polimer zincirlerinin hareketliliğini arttırmış ve difüzyon kanalları genişlemiştir. Böylece karışımdaki bileşenlerin difüzyonu hızlanmış, toplam akı değeri de artış göstermiştir. Metanolün seçicilik değeri ise düşüş göstermiştir. Bu durum, artan hareketlilik ile birlikte difüzyon kanallarının genişlemesi ve polimer zincirlerinin esnekliği ile ilgilidir. Geniş difüzyon kanalları, hedef bileşen metanol ile birlikte metilal moleküllerinde membrandan difüze olmasına neden olur ve toplam akı artarken metanol seçiciliği azalır (Guo ve ark., 2004; Zhang ve ark., 2017). 20°C'de 0.24 kg/m².sa akı değeri elde edilirken, 40°C'de bu değer 0.63 kg/m².sa'ye yükselmiştir. 20°C'de metanol seçiciliği 8569 iken 40°C'de 2147'ye düşmüştür.

3.2.2. Besleme metanol konsantrasyonunun etkisi

Besleme karışımındaki metanol konsantrasyonunun pervaporasyonun ayırma performansına etkisi ağırlıkça %0.5 ZIF-8 katkılı PEI membran kullanılarak, 20°C operasyon sıcaklığında incelenmiştir.



Şekil 5. Besleme metanol konsantrasyonunun ayırma performansına etkisi (Çalışma koşulları: 30°C, ağırlıkça %0.5 ZIF-8 katkılı PEI membran)

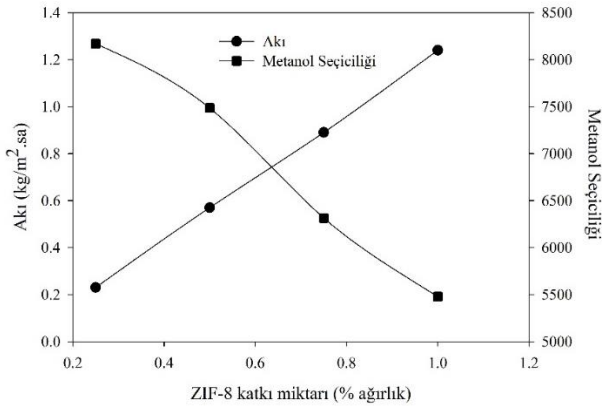
Şekil 5'te besleme karışımındaki metanol konsantrasyonundaki artış ile toplam akının arttığı görülmektedir. Pervaporasyonda membran boyunca taşınım, çözünme difüzyon mekanizmasına dayanmaktadır. Difüzyon konsantrasyona bağlı olduğu için konsantrasyonda meydana gelecek değişim difüzyonu kolaylaştırmaktadır. Besleme konsantrasyonu arttıkça beslemedeki hedef bileşen ile membran arasındaki etkileşim artarak, akı değeri de artmaktadır. Metanol konsantrasyonu arttıkça membranın şişme derecesi de artış göstermektedir. Şişme derecesi ile membranın artan serbest hacmi ve genişleyen difüzyon kanalları, metanol molekülleri ile birlikte metilal moleküllerinin de taşınımını kolaylaştırmaktadır. Beslemedeki metanol konsantrasyonu arttıkça seçicilik değeri ise azalmıştır. Bu durum artan serbest hacim ile birlikte metilalin de membrandan

difüzyonunu kolaylaştırır. Geçen akımdaki metilal konsantrasyonu arttıkça, metanol seçiciliği düşmüştür. Özetle beslemedeki metanol konsantrasyonundaki artış, membranın şişmesi ile sonuçlanmış ve metanol seçiciliği düşmüştür (Kittur ve ark., 2013; Jalal ve ark., 2015; Tsou ve ark., 2015).

Ağırlıkça %6 metanol içeren besleme karışımı ile yapılan deneylerde 0.24 kg/m².sa akı değeri elde edilirken, ağırlıkça %20 metanol içeren besleme karışımı ile yapılan deneylerde 0.71 kg/m².sa akı değeri elde edilmiştir. Metanol seçicilik değeri ise ağırlıkça %6 metanol içeren besleme karışımında 8478 iken ağırlıkça %20 metanol içeren besleme karışımında 864'e düşmüştür.

3.2.3. ZIF-8 katkı oranının etkisi

ZIF-8 miktarının (ağırlıkça %0.25, %0.5, %0.75 ve %1) toplam akı ve metanol seçiciliği üzerindeki etkisi Şekil 6'da gösterilmiştir.



Şekil 6. ZIF-8 katkı miktarının ayırma performansına etkisi (Çalışma koşulları: 20°C, ağırlıkça %6 metanol içeren besleme)

ZIF-8 miktarı arttıkça toplam akı değerinin arttığı gözlenmiştir. Bu durum, PEI membran içerisinde yer alan ZIF-8'in metanol için tercihli difüzyon kanallarına sahip olması ile açıklanabilir. ZIF-8 yükleme oranı arttıkça, membran matrisi içerisinde difüzyon kanallarının artması metanol transferini kolaylaştırdığı gibi metanol ile birlikte metilalinde membrandan transferini arttırır. Bu yüzden akı artarken, metanolün seçicilik değeri azalır. Ağırlıkça %0.25 ZIF-8 katkılı PEI membranda 0.23 kg/m².sa akı değeri elde edilirken ZIF-8 oranı %1'e arttırıldığında akı değeri 1.24 kg/m².sa'e yükselmiştir. Metanol seçiciliği değerleri ise ağırlıkça %0.25 ve %1 ZIF-8 katkılı PEI membranlarda sırasıyla 8169 ve 5478 olarak elde edilmiştir.

4. Sonuç

Bu çalışmada, yeşil çözücü ve yakıt biyokatki maddesi metilalin saflaştırılması için ZIF-8 katkılı PEI membranlar kullanılmıştır. Hazırlanan membranlar farklı karakterizasyon yöntemleri kullanılarak analiz edilmiştir. FTIR analizi ile membranların karakteristik pikleri ve bağ değişiklikleri belirlenmiştir. Membranların termal dayanımları TGA ile analiz edilmiştir. Membranların kesit

görüntüleri SEM analizi ile incelenmiştir. Karakterizasyon testleri sonucunda ZIF-8'in PEI membran ile uyumlu bir yapı sergilediği, ZIF-8 ilavesinin termal dayanımı artırdığı görülmüştür. Pervaporasyon ile metilal/metanol karışımlarının saflaştırılmasında ise operasyon sıcaklığının, besleme konsantrasyonunun ve ZIF-8 yükleme oranının ayırma performansı üzerindeki etkileri incelenmiştir. Optimum çalışma koşulları, 20°C operasyon sıcaklığı, ağırlıkça %6 metanol besleme konsantrasyonu ve ağırlıkça %0.5 ZIF-8 yükleme oranı olarak belirlenmiştir. Bu şartlar altında en yüksek ayırma performansı 0.57 kg/m².h akı ve 8169 metanol seçiciliği olarak elde edilmiştir. Elde edilen sonuçlar sentezlenen ZIF-8 yüklü PEI membranın metilal/metanol karışımından metanolün saflaştırılması için yüksek ayırma performansı gösterdiği ve pervaporasyon prosesinin metilal/metanol karışımını ayırma için alternatif bir süreç olduğunu göstermektedir.

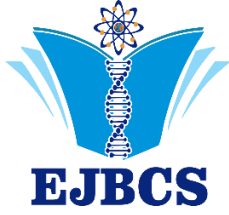
Teşekkür

Bu çalışma Bursa Teknik Üniversitesi Bilimsel Araştırma Projeleri birimi tarafından 210ÖAP03 numaralı proje kapsamında desteklenmiştir.

Kaynaklar

- Amirilargani M, Sadatnia B 2014. Poly(vinyl alcohol)/zeolitic imidazolate frameworks (ZIF-8) mixed matrix membranes for pervaporation dehydration of isopropanol. *J. Membr. Sci.* 469:1–10.
- Ahmed SF, Debnath JC, Mehejabin F, Islam N, Tripura R, Mofijur M, Hoang AT, Rasul MG, Vo DVN 2023. Utilization of nanomaterials in accelerating the production process of sustainable biofuels. *Sustain. Energy Technol. Assess.* 55:102894.
- Baker RW 2000. *Encyclopedia of Separation Science*. Germany: Academic Press, pp. 205.
- Barankova E 2017. *Synthesis of Thin Film Composite Metal-Organic Frameworks Membranes on Polymer Supports*, King Abdullah University of Science and Technology, Doctor of Philosophy, Kingdom of Saudi Arabia.
- Basile A, Figoli A, Khayet M. 2015. *Pervaporation, Vapour Permeation and Membrane Distillation: Principles and Applications* (1. Basım). UK:Woodhead Publishing.
- Basile A, Marcello De Falco MD, Centi G, Iaquaniello G. 2016. *Membrane Reactor Engineering: Applications for a Greener Process Industry*, United Kingdom:Wiley.
- Basu S, Balakrishnan M. 2017. Polyamide thin film composite membranes containing ZIF-8 for the separation of pharmaceutical compounds from aqueous streams. *Sep. Purif. Technol.* 179:118–125.
- Carretier E, Moulin P, Beaujean M, Charbit F. 2003. Purification and dehydration of methylal by pervaporation. *J. Membr. Sci.* 217:159–171.
- Chen BK, Su C, Tseng T, Tsay MC 2006. Preparation of Polyetherimide Nanocomposites with Improved Thermal, Mechanical and Dielectric Properties. *Polym. Bull.* 57:671–68.
- Das S, Banthia AK, Adhikari B. 2007. Improved conversion to ethyl acetate through removal of water of esterification by membrane pervaporation. *Indian J. Chem. Technol.* 14:552–559.

- Demirciyeva F 2006. Membran Yöntemi Kullanarak Metan-Karbon dioksit Gaz Karışımından Metanın Ayrıştırılması. Ondokuz Mayıs Üniversitesi Fen Bilimleri Enstitüsü, Samsun.
- Dong Y, Dai C, Lei Z 2018. Extractive distillation of methylal/methanol mixture using the mixture of dimethylformamide (DMF) and ionic liquid as entrainers. *Fuel* 216:503–512.
- Gao R, Zhang Q, Lv R, Soyekwo F, Zhu A, Liu Q. 2017. Highly efficient polymer-MOF nanocomposite membrane for pervaporation separation of water/methanol/MTBE ternary mixture. *Chem. Eng. Res. Des.* 117: 688-697.
- Gonçalves VLC, Pinto BP, Silva JC, Mota CJA 2008. Acetylation of glycerol catalyzed by different solid acids. *Catal. Today*, 133–135:673–677.
- Guo WF, Chung TS, Matsuura T 2004. Pervaporation study on the dehydration of aqueous butanol solutions: a comparison of flux vs. permeance, separation factor vs. selectivity. *J. Membr. Sci.* 245:199–210.
- Jalal TA, Bettahalli NMS, Le NL, Nunes SP 2015. Hydrophobic Hyflon AD/Poly(vinylidene fluoride) Membranes for Butanol Dehydration via Pervaporation. *Ind. Eng. Chem. Res.* 54:11180–11187.
- Kittur AA, Jeevankumar BK, Kariduraganavar MY, College SDM 2013. Pervaporation separation of water-dioxane mixtures through poly (vinyl alcohol)-silicone based hybrid membranes. *Int. J. Curr. Eng. Technol.* 1:148–156.
- Li J, Si X, Li X, Wang N, An Q, Ji S 2018. Preparation of acid-resistant PEI/SA composite membranes for the pervaporation dehydration of ethanol at low pH. *Sep. Purif. Technol.* 192:205–212.
- Lu X, Ma J, Ji L, Huang Z 2007. Experimental Study on the Combustion Characteristics and Emissions of Biodiesel Fueled Compression Ignition Engines with Premixed Dimethoxymethane. *Energ. Fuel.* 21:3144–3150.
- Mensitieri G, Scherillo G, Manna PL, Musto P 2019. Sorption Thermodynamics of CO₂, H₂O, and CH₃OH in a Glassy Polyetherimide: A Molecular Perspective. *Membranes.* 9: 1-30.
- Park KS, Ni Z, Cote AP, Choi JY, Huang R, Uribe-Romo FJ, Chae HK, O'Keeffe M, Yaghi OM 2006. Exceptional chemical and thermal stability of zeolitic imidazolate frameworks. *PNAS.* 103:10186–10191.
- Shi GM, Yang T, Chung TS 2012. Polybenzimidazole (PBI)/zeolitic imidazolate frameworks (ZIF-8) mixed matrix membranes for pervaporation dehydration of alcohols. *J. Membr. Sci.* 415–416:577-586.
- Song Q, Nataraj SK, Roussanova MV, Tan JC, Hughes DJ, Li W, Bourgoin P, Alam MA, Cheetham AK, Muhtaseb SAA, Sivaniah E. 2012. Zeolitic imidazolate framework (ZIF-8) based polymer nanocomposite membranes for gas separation. *Energy Environ. Sci.* 8: 8359-8369.
- Tsou CH, An QF, Lo SC, Guzman MD, Hung WS, Hu CC, Lai JY 2015. Effect of microstructure of graphene oxide fabricated through different self-assembly techniques on 1-butanol dehydration. *J. Membr. Sci.* 477:93–100.
- Wasewar K, Patidar S, Agarwal VK 2009. Esterification of lactic acid with ethanol in a pervaporation reactor: modeling and performance study. *Desalination* 243:305–313.
- Zhang S, Zou Y, Wei T, Mu C, Liu X, Tong Z 2017. Pervaporation dehydration of binary and ternary mixtures of n-butyl acetate, n-butanol and water using PVA-CS blended membranes. *Sep. Purif. Technol.* 173: 314–322.



Moringa oleifera bitki yaprağının mineral ve yağ asidi bileşenlerinin belirlenmesi

¹*Serpil Kılıç , ²Murat Kılıç 

^{*1} Isparta Uygulamalı Bilimler Üniversitesi, Teknik Bilimler MYO, Isparta, Türkiye

² Isparta Uygulamalı Bilimler Üniversitesi, Merkezi Araştırma Laboratuvarı Uygulama ve Araştırma Merkezi, Isparta, Türkiye

*Corresponding author : serpilkilic@isparta.edu.tr
Orcid No: <https://orcid.org/0000-0002-4940-1839>

Received : 01/01/2023
Accepted : 11/05/2023

Özet: Son yıllarda bitkilerin besinsel bileşenleri, sağlık üzerindeki etkileri nedeniyle pek çok çalışmalara konu olmuştur. Bu çalışmada Moringa oleifera yaprak tozunda mineral ve yağ asidi içeriği belirlenmiştir. Element analizi için numuneler, bir mikrodalga fırında HNO₃ ve HCl ile sindirildi. Numunelerde mineral konsantrasyonları İndüktif Eşleşmiş Plazma Kütle Spektrometresi (ICP-MS) ile belirlendi. Numunelerde magnezyum 6393 µg g⁻¹, demir 927 µg g⁻¹, çinko 138 µg g⁻¹ ve bakır ise 6 µg g⁻¹ olarak tespit edilmiştir. Yağ asidi ekstraksiyonu sonrası, yağ asidi ve ester profilleri için Gaz Kromatografisi Alev İyonlaşmalı Dedektörü (GC-FID) kullanılarak tanımlanmıştır. Moringa oleifera yaprağında yağ asitlerinin ana bileşenleri olarak lauric asit (C12:0), tridekanoik asit (C13:0), miristik asit (C14:0), palmitik asit (C16:0), stearik asit (C18:0), oleik asit (C18:1), linoleik asit (C18:2), gama-linolenik asit (C18:3) tayin edilmiştir.

Anahtar Kelimeler: Moringa oleifera, mineral tayini, yağ asidi analizi

Determination of minerals and fatty acid components in leaf powder of Moringa oleifera plant

Abstract: In recent years, the nutritional components of plants have been the subject of many studies due to their effects on health. In this study, mineral and fatty acid content of Moringa oleifera leaf powder was determined. Samples were digested with HNO₃ and HCl in a microwave oven for element analysis. In samples, mineral concentrations were determined by Inductively Coupled Plasma Mass Spectrometry (ICP-MS). The mineral content was determined as magnesium 6393 µg g⁻¹, iron 927 µg g⁻¹, zinc 138 µg g⁻¹, and copper 6 µg g⁻¹ by Inductively Coupled Plasma Mass Spectrometry in samples. After fatty acid extraction, fatty acid and ester profiles were verified using Gas Chromatography Flame Ionization Detection (GC-FID). The main components of fatty acids in Moringa oleifera leaf were determined as lauric acid (C12:0), tridecanoic acid (C13:0), myristic acid (C14:0), palmitic acid (C16:0), stearic acid (C18:0), oleic acid (C18:1), linoleic acid (C18:2), gamma-linolenic acid (C18:3).

Keywords: Moringa oleifera, mineral determination, fatty acid analysis

© EJBCS. All rights reserved.

1. Giriş

Bitkiler tarih boyunca uzakdoğuda insanları hastalıklardan korumak için şifa amacıyla kullanılmıştır. Bu bitkiler hastalıkları önleyici (kalp ve damar hastalıkları gibi), sağlığı koruyan, hastalıkları tedavi eden ilaç olarak kullanılan bitkiler olarak tanımlanmaktadır. Son yıllarda, hastalıkları önleme veya tedavi etmede sentetik ilaçlardan daha etkili olabileceği inancı nedeniyle diğer doğal bitkiler artmıştır (Martín-Domingo ve ark. 2017). Bundan yola çıkarak çalışmada kullanılan Moringa oleifera, Güney Himalaya eteklerinde ortaya çıkan ve şu anda dünyanın neredeyse her tropikal, subtropikal ve yarı kurak bölgesinde bulunan Moringaceae familyasının bir ağacıdır (Bhosale ve ark., 2021). Moringa oleifera bitkisinin besin

bileşenleri ve değerleri son zamanda birçok çalışmada yer almaktadır (Magat ve ark. 2009; Gyamfi ve ark. 2011; Mbailao ve ark. 2014; Ananias ve ark. 2016). Dışarıdan alınan, sağlıklı beslenmede önemli olan bu tür takviyelerin besin değeri konusunda farkındalık oluşmuş ve bu ürünlere talep artmıştır.

M. oleifera'nın yaprakları için yapılan çalışmada; ateş, yüksek tansiyon, cilt, sindirim ve romatizma hastalıklarının tedavisinde kullanılan ilaçların içeriğinde olduğu bildirilmektedir (Islam ve ark. 2005). Yine bitki yaprağının, β-karoten, C vitamini, E vitamini ve polifenollerin zengin kaynakları içerdiği tespit edilmiştir (Nambiar ve Seshadri 2001; Ross 1999). Bazı temel elementler ise büyüme fonksiyonuna katılırken, bazıları ise

kemik yapısında rol oynar (Gyamfi ve ark. 2011). Bunların eksikliğinde veya aşırılıkları vücudun biyokimyasal fonksiyonlarının kesintiye uğratabilir (Akhter ve ark. 2004). Yağlar, proteinler, karbonhidratlar önemli yapı taşı ve enerji kaynaklarıdır. Özellikle yağlar, diyetlerde önemli yere sahip olan temel bileşenlerdir. Bu nedenle, sağlık üzerinde kötü etkileri olan farklı türdeki yağ asitlerinin içeriği, günlük tüketiciler için oldukça önemlidir. Uzmanlara göre beslenmede yer alması gereken yağların yağ asit içeriğinin bilinmesi ve ona göre kullanılması önem arz etmektedir (Karaca ve Aytac 2007). Bu durum, etiketleme doğruluğunun kontrolü için gıdaların yağ asit profilini belirlemenin önemini vurgulamaktadır.

Bu amaçla çalışmada, ticari olarak yetiştirilen Güney Afrika menşei *M. oleifera* yaprak tozu örneği üretici firmadan temin edilerek; majör element ve yağ asitleri bileşenleri belirlenmiştir. Bu elde edilen veriler, fonksiyonel gıda formülasyonu için besin bileşenleri ve miktarları açısından zengin içeriklerinin belirlenmesinde faydalı olacağı düşünülmektedir. Bt tkinin yaprak kısmına ait mineral ve yağ asidi miktarlarının Moringa bazlı geleneksel gıda ürünlerinin besinsel önemini ortaya çıkardığı düşünülmektedir.

2. Materyal ve Metot

2.1. Kimyasallar ve Cihazlar

Element analizi için kalibrasyon standardı olarak 10 mg L⁻¹ multi element standart çözeltisi kullanıldı. Nitrik asit (HNO₃, Suprapure® %65) ve hidrojen klorür (HCl, Suprapure®, % 30), distile su için Millipore Elix 10 UV, Milli-Q Syntesis marka saf su sistemi, numune parçalama işlemi için ise Berghof Speedwave® Four Microwave Digestion System marka mikrodalga cihazı, element tayini için Perkin Elmer elan DRC-e marka İndüktif Eşleşmiş Plazma Kütle Spektrometresi (ICP-MS) kullanıldı. Yağ asidi standardı olarak Supelco FAME mix 4, yağ asidi profili için ise Shimadzu marka Gaz Kromatografisi Alev İyonlaşma Dedektörü (GC-FID) cihazı kullanıldı.

2.2. Element Tayini İçin Numunenin Hazırlanması

Ticari olarak satın alınan homojen hale getirilmiş 0.1 g olarak tartılan numune mikrodalga ünitesi teflon kaplarına konularak, 3 mL HNO₃ (suprapure) ve 0.2 mL HCl ilave edildi. Mikrodalga ünitesinin sıcaklık programı birbirini takip eden üç adımda gerçekleştirildi. İlk adımda sıcaklık 5 dakika içinde 80°C'den 150°C'ye, ikinci adımda 15 dakika içinde 225°C'ye yükseltildi. Son adımda ise 10 dakika içinde 70°C'ye düşürüldükten sonra numune çözünür hale getirildi. Örnekler distile su ile 25 mL'ye tamamlandı. Hazırlanan numuneler, ICP-MS cihazında analiz edilmiştir (Kilic 2018). Cihaz çalışma koşulları ise Tablo 1'de verildi.

Tablo 1. ICP-MS çalışma koşulları

Spektrometre	Elan DRC-e (Perkin Elmer SCIEX, Norwalk, CT, USA)
Örnek girişi	Scott Spray Chamber
RF gücü	1000
Skimmer/ Sample cone	Nikel
Gaz akış oranı (L min ⁻¹)	Nebulizer gaz akışı: 0.91, Auxiliary gaz akışı: 1.20, Plazma gaz akışı: 19
Nebulizer	Meinhard TQ plus Quartz 0.5 ml
Tarama modu	Pik sekmesi
Analitik kütleler	Standart mod ⁶³ Cu, ⁵⁷ Fe, ²⁴ Mg, ⁶⁶ Zn
Tarama okuma sayısı	20
Okuma tekrar sayısı	1
Tekrar sayısı	3
Oto örnekleme	CETAX ASX-520
Bekleme süresi	50
Örnek yıkama	Zaman (50), hız (+/- rpm)-48
Erteleme	Zaman (15), hız (+/- rpm)-20

2.3. Yağ Asidi Metil Esterlerinin Hazırlanması

0.25 g NaOMe üzerine 40 mL metanol (MeOH) ve 10 mL hekzan eklenerek, çalkalandı. Hazırlanan türevlendirici kullanılmak üzere 4°C'de bekletildi.

2.4. Yağ Asidi Tayini İçin Numunenin Ekstraksiyonu

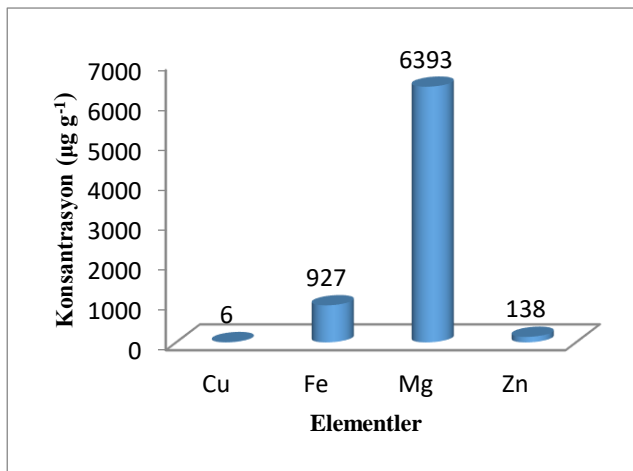
Homojen hale getirilen yaprak tozu örneği kullanılarak yağ asit kompozisyonunun belirlenmesi için 25 mg tartıldı. Üzerine hazırlanan türevlendiriciden 750 µL eklendi. Karıştırıcı kullanılarak örneğin karışması sağlandı. 1 gece oda sıcaklığında bekletildi. Örnek üzerine 1 mL hekzan eklenerek, faz ayırımı oluşması sağlandı. Oluşan faz viyale alınarak, Shimadzu marka GC-FID cihazı ile analiz edildi. Bunun için CP-Wax 52-CB (60 m x 0.32 mm) kapiler kolon kullanıldı. Enjektör bloğu sıcaklığı 250°C, dedektör sıcaklığı 265°C'ye ayarlandı. Başlangıçta kolon sıcaklığı 80°C'de tutuldu, ardından 20 dakikada 175°C'ye yükseltildi, 4 dakika 21°C ve 2 dakika 250°C'de tutuldu. Kolon akış hızı ise 3 mL dk⁻¹, toplam süre ise 83.25 dakika olarak belirlendi.

2.5. Metot Doğrulama

Metot doğrulama, kullanılan analiz yöntemin amaca doğru uygulanabilirliğinin ölçümü için geçerlilik durumunu ortaya koymak için yapılmaktadır (Taverniers ve ark. 2004). Bu amaçla cihaz performansı için kalite kontrol (QC) takibi yapıldı.

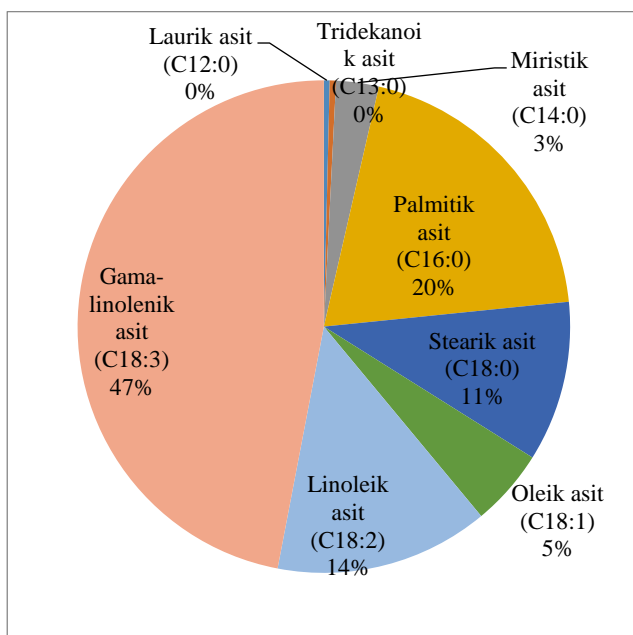
3. Tartışma ve Sonuç

Çalışmada *M. Oleifera* yaprak tozunun elementel analiz sonuçları Şekil 1'de verildi. Elde edilen verilere göre *M. Oleifera* yaprak tozunun elementel bileşim analizinde magnezyum $6393 \mu\text{g g}^{-1}$, demir $927 \mu\text{g g}^{-1}$, çinko $138 \mu\text{g g}^{-1}$ ve bakır $6 \mu\text{g g}^{-1}$ olarak tespit edildi. Mineral sonuçları literatür çalışmaları ile karşılaştırıldı. Yapılan çalışma sonuçları incelendiğinde magnezyum konsantrasyonunun yüksek (15450 mg kg^{-1}), çinko (51 mg kg^{-1}) ve demir (43 mg kg^{-1}) konsantrasyonlarının ise daha düşük tespit edildiği görüldü (Ngigi ve Muraguri 2019). Sonuçlar arasındaki fark bitkinin farklı coğrafi ve toprak yapısında yetiştirilmesi ile açıklanabilir.



Şekil 1. *Moringa oleifera* yaprağına ait mineral kompozisyonu ($\mu\text{g g}^{-1}$).

Minerel çalışmasının dışında *M. oleifera* yaprak tozuna ait 8 adet yağ asit profili tanımlandı. Yağ asit % miktarları ise Şekil 2'de verildi.



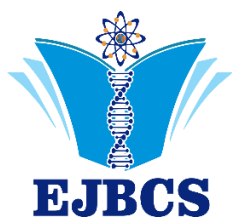
Şekil 2. *Moringa oleifera* yaprağına ait yağ asidi kompozisyonu(%).

Elde edilen sonuçlara göre; gama-linolenik asit (C18:3) %46.99 olarak en yüksek miktarda tespit edildi. Sırası ile palmitik (C16:0) %19.80, Linoleik (C18:2) %14.04, Stearik (C18:0) %10.53 ve Oleik asit (C18:1) miktarları %5.05 tespit edildi. Tridekanoik (C13:0) ve laurik (C12:0) asit konsantrasyonları ise %0.41-0.38'ini oluşturduğu görüldü. Yapılan çalışmalarda linolenik asit sonuçları, *M. oleifera*'nın yapraklarında, çiçeklerinde ve yumuşak kabuklarında sırasıyla %56.4, %23.0 ve %26.2 benzer bir içeriği kaydedilmiştir. Yine başka bir çalışmada Moringa tohumu yağı, çok yüksek oleik asit (%65-75), palmitik asit (%5-10) ve stearik asit (%5-10) içeriği ile kapsamlı bir şekilde karakterize edilmiştir (Abdulkarim ve ark. 2005; Amaglo ve ark., 2010; Lalas ve Tsaknis 2002). Yapılan bir başka çalışmada ise *M. oleifera* yapraklarında, en yüksek miktarda (%49-59) olarak a-linolenik asit, bunu palmitik asit (%16-18), ve Linoleik asit ise (%6-13) oranda izledi. Palmitoleik, stearik, oleik ve erusik asit ise %1-5 aralığında tespit edilmiştir (Saini ve ark. 2014). Saini ve ark tarafından yapılan çalışmada *M. oleifera* yapraklarına ait yağ asit miktarları çalışmamıza göre daha düşük düzeyde olduğu gözlemlenmiştir. Sonuçlar, genotipik faktörlerin *M. oleifera*'nın yapraklarındaki yağ asidi bileşimini önemli ölçüde etkilediğini ve ayrıca bitkinin farklı yenilebilir kısımları arasında değişiklik olabildiğini göstermektedir. Tespit edilen yağ asitlerinden linolenik asit, dokosaheksaenoik asit (DHA) dahil olmak üzere uzun zincirli n-3 yağ asitlerinin öncüsü olduğu için insan diyetinde önemli bir rol oynar (Barcelo-Coblijn ve Murphy 2009). Linoleik asidin ise kalp damar hastalıkları riskini azaltıcı, immün direnci artırıcı, dokularda oksidasyonu önleyici ve kanser oluşumunu engelleyici gibi biyolojik özellikleri olduğu ortaya konulmuştur (Çelebi ve Kaya 2008). Palmitik asit LDL seviyelerinde artış, HDL düzeylerinde azalmaya sebep olmaktadır (Bodur ve Uçar 2021). Omega-3 ve omega-6 yağ asitlerinin yine kalp, eklem romatizması gibi hastalıkların önlenmesinde kullanıldığı, omega-6 kanamaları azaltıcı, omega-3 ise damar genişletici özelliklere sahip olduğu bildirilmektedir (Çelik ve Demirel 2004).

Moringa oleifera bitkisinin besin bileşenlerinin zengin bir içeriğe sahip olması nedeni ile son yıllarda yapılan çalışmalarda sıkça adından söz ettirmektedir. Yapılan çalışmalar incelendiğinde ise magnezyum, demir, bakır ve çinko gibi mineraller açısından zengin olması beslenme ve sağlık açısından *Moringa oleifera* bitkisinin oldukça önemli olduğu sonuçlarına varılmaktadır. Bu bitkinin içeriğinde insan sağlığı açısından önemli olan yağ asitlerinde yer almasıyla dikkat çekmektedir. Ayrıca linoleik, linolenik ve palmitik asit açısından zengin oluşu bu yönleri ile önemli ortaya çıkmaktadır. Sonuçlara bakıldığında, *M. oleifera*'nın yapraklarındaki mineral ve yağ asidi bileşimi genotipik faktörlerin önemli ölçüde etkilediğinden dolayı farklılık gösterdiği ve bu bitkinin sağlığa faydaları olan zengin gıda takviyesi olduğu düşünülmektedir. Bu tespit edilen miktarlara göre, günlük alım düzeylerinin tavsiye edilebilirliği açısından da önem arz etmektedir.

Kaynaklar

- Abdulkarim SM, Long K, Lai OM. 2005. Some physicochemical properties of *Moringa oleifera* seed oil extracted using solvent and aqueous enzymatic methods. *Food Chem* 93: 253–263.
- Akhter P, ur-Rehman K, Orfi SD, Ahmad N. 2004. Assessment of iodine levels in Pakistani diet. *Nutrition* 20: 783–787.
- Amaglo NK, Bennett RN, Lo Curto RB. 2010. Profiling selected phytochemicals and nutrients in different tissues of the multipurpose tree *Moringa oleifera* L. grown in Ghana. *Food Chem* 122:1047–1054.
- Ananias NK, Kandawa-Schulz M, Hedimbi M, Kwaambwa HM, Tutu H, Makita C, Chimuka L. 2016. Comparison of metal content in seeds of *Moringa ovalifolia* and *Moringa oleifera*. *Africal J Food Sci* 10(9): 172–177.
- Barcelo´-Coblijn,G, Murphy EJ. 2009. Alpha-linolenic acid and its conversion to longer chain n-3 fatty acids: benefits for human health and a role in maintaining tissue n-3 fatty acid levels. *Prog Lipid Res* 48:355–374.
- Bhosale TJ, Chavan,MK, Sabale,TD, Dr Lavar,VS. 2021. Proximate analysis of *Azadirachta indica* & *Moringa oleifera* L. leaves as feed additives for ruminants. *Pharm J Innova SP-10*(12): 1884-1886.
- Bodur M, Uçar A. 2021. Palmitoleik asidin aazı kronik hastalıklardaki rolü: Kısa derleme. *Düzce Üniversitesi Sağlık Bil Enst Der* 11(1): 103-107.
- Çelebi Ş, Kaya A. 2008. Konjuge linoleik asitin biyolojik özellikleri ve hayvansal ürünlerde miktarını artırmaya yönelik bazı çalışmalar. *Hayvansal Üretim* 49(1): 62-68.
- Çelik S, Demirel M. 2004. İnsan ve hayvan sağlığı bakımından yağ asitleri ve konjuge linoleik asidin önemi. *YYÜ Fen Bil Enst Der* 1: 25–35.
- Gyamfi ET, Yeboah,PO, Steiner-Asiedu,M, Fletcher JJ. 2011. Assessment of essential elements in *Moringa oleifera*. *Elix Food Sci* 36: 3222–3225.
- Islam S, Jahan MAA, Khatun R. 2005. In vitro regeneration and multiplication of year-round fruit bearing *Moringa oleifera* L. *J Biol Sci* 5(2): 145-148.
- Karaca E, Aytaç S. 2007. Yağ itkilerinde ağ asitleri kompozisyonu üzerine etki eden faktörler. *OMÜ Ziraat Fak Der* 22(1): 123-131.
- Kilic S. 2018. Aromatik bitki ve yağlarının mineral element miktarlarının karşılaştırılması. *Gıda* 43(4): 617-623.
- Lalas S, Tsaknis J. 2002. Characterization of *Moringa oleifera* seed oil variety ‘‘Periyakulam 1’’. *J Food Comp Anal* 15: 65–77.
- Magat SS, Raquepo CM, Pabustan CD. 2009. Mineral macro-nutrients, micro-nutrients and other elements in leaves of malunggay plant (*moringa oleifera*) sampled in some locations in the Philippines. *Crop Agronomy. Nutrition and Farming Systems Program, Technology Advisory Notes*.
- Martín-Domingo MC, Plaa A, Hernández AF, Olmedoa P, Navas-Acienc A, Lozano-Paniagua D, Gila F. 2017. Determination of metalloid, metallic and mineral elements in herbal teas. Risk assessment for the consumers. *J Food Comp and Anal* 60: 81-89.
- Mbailao M, Mianpereum T, Albert N. 2014. Proximal and elemental composition of *Moringa oleifera* (Lam) leaves from three regions of chad. *J Food Res Sci* 3(10): 12–20.
- Nambiar V, Seshadri S. 2001. Bioavailability trials of beta-carotene from fresh and dehydrated drumstick leaves (*Moringa oleifera*) in a rat model. *Plant Foods Hum Nutr* 56 (1): 83-95.
- Ngigi AN, Muraguri BM. 2019. ICP-OES determination of essential and non-essential elements in *Moringa oleifera*, *Salvia hispanica* and *Linum usitatissimum*. *Scie African* 6: e00165.
- Ross IA. 1999. Medicinal plants of the world; chemical constituents, traditional and modern medicinal uses. Humana Press. Totowa, New Jersey, 231-239p.
- Saini RK, Shetty NP, Giridhar P. 2014. GC-FID/MS Analysis of fatty acids in Indian Cultivars of *Moringa oleifera*: Potential sources of PUFA. *JAOCs* 91: 1029–1034.
- Taverniers I, De Loose M, Van Bockstaele E. 2004. Trends in quality in the analytical laboratory. II. Analytical method validation and quality assurance. *TrAC Trends Anal Chem* 23(8): 535-552.



Morphological and molecular identification of fungi isolated from various habitat in Kirkuk city – Iraq

Yawooz Hameed Mahmood^{1*}, Abdul-hameed M. Hamoody², Rushdi Sabah Abdulqader³

¹University of Samarra, College of Education, Biology Department, Samarra, Iraq.

²Al-Salam University College, Medical Laboratory Technologies Department, Baghdad, Iraq.

³University of Kirkuk, College of Pure Education, Biology Department, Kirkuk, Iraq.

*Corresponding author : yavuz.h86@uosamarra.edu.iq
Orcid No: <https://orcid.org/0000-0001-5997-6276>

Received : 04/04/2023
Accepted : 11/05/2023

Abstract: The aim of this study is isolate and identify fungi from different habitat in Kirkuk City - Iraq. The fungal species were isolated from soil and water in four season 2021-2022, collected the samples from various geographical habitat in Kirkuk City. The fungi isolation from soil and water done by inoculating (1ml) from serial dilutions on Potato Dextrose Agar (PDA) plates. The molecular identification of the isolated fungi at the species level, by PCR using specific internal transcribed spacer primer (ITS1/ITS4). The PCR products were sequenced and compared with the other related sequences in GenBank (NCBI). Seven fungal species were identified. The results showed that the (*Aspergillus flavus* 20.83%) was the most abundant fungus, while the (*Penicillium citrinum* 8.30%) was the less prevalent one in all resources and locations. The seven local fungal isolates were registered within NCBI, and this is the first record of these isolates in Iraq

Keywords: *Aspergillus flavus*, *Penicillium citrinum*, Kirkuk

© EJBCS. All rights reserved.

1. Introduction

Fungi are eukaryotic organisms is surrounded by a bilayer nuclear membrane and cytoplasm containing the endoplasmic reticulum, mitochondria, the Golgi apparatus, and other cytoplasmic organelles. Fungi lack plastids, and this is what distinguishes them from plant cells, so they are not self-feeding, but depend for their food on external sources, either decomposing organic materials or other organisms such as plants and animals, and on this basis, they are parasitic, Saprophytic or symbiotic (Gravesen *et al.*, 1994).

Fungi are one of the most widespread living organisms in nature, as the number of diagnosed species reached (100,000) species. It exists in humans, animals and plants Its can spread in the soil, air and waters, some factors affect the growth and distribution of fungi as temperature, pH, moisture, amount and type of nutrients (Pellon *et al.*, 2020). Fungi are importance in nature through their relationship to human life and work on recycle elements and break down organic matter (Webster & Weber, 2007). Pathogenic fungi

can cause harm to humans, animals and plants (Wang *et al.*, 2014).

Fungi are used to treatment different types of wastewater becauseit its ability to analyzes many organic pollutants by its enzymes that secrete it, such as estrase and cellulase an enzyme and return it to its original components therefore it has the ability to maintain ecological balance, especially in aquatic environments, freshwater (Bermingham *et al.*, 1996). The aimed of study to find out the geographical distribution of the fungi isolated from the soil and water from Different habitat in Kirkuk City - Iraq.

2. Materials and Method

2.1. Describing The Study Area

The study area is located within the borders of Kirkuk City and is 255 km away from the capital, Baghdad (Kamel, 2013). As shown in the figure (1) the distance between the first site and the second site was 5.2 km, while the distance between the second and third site was 8.1 km, meaning that the distance between the first and third site is 13.3 km. As for the distance between the fourth site and the fifth site, it

was 1.6 km, and between the fifth and sixth sites was 0.8 km, meaning that the distance between the fourth and sixth sites is 2.4 km. The first, second and third sites are located on Khasa River channels while the sites fourth, fifth and sixth sites are located on North Oil Company channel.

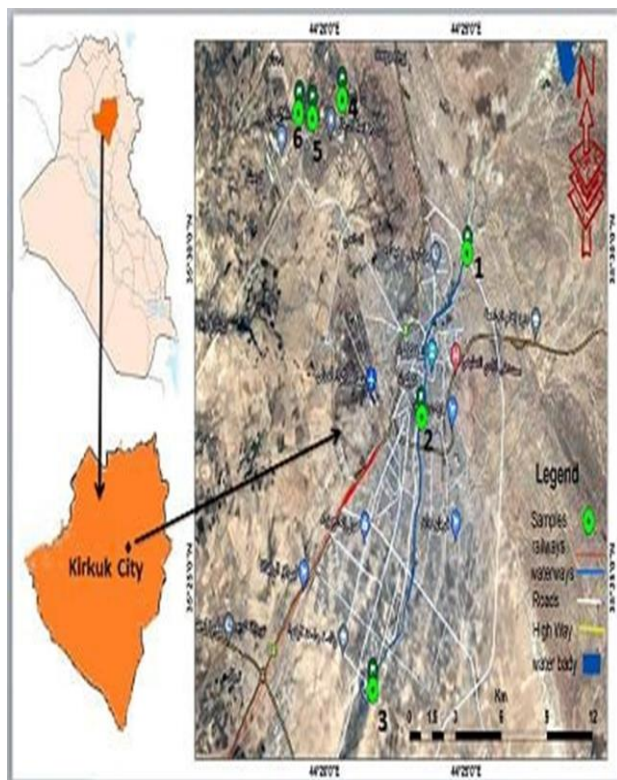


Fig. 1 Shows the locations of sampling collection

2.2. Samples Collected

The soil and water samples were collected from the North Oil Company and Khasa River channels in Kirkuk City - Iraq (September 2021 to September 2022). The samples of soil collected about 100g with sterilized bags from top soil layer (0-30 cm in depth) after that the samples of soil separated and labeled according to their location (Gaddeyya *et al.*, 2012). The samples of water collected by 5 liter polyethylene bottles and washed with 10% dilute hydrochloric acid and then rinsed with distilled water (Nollet, 2007).

2.3. Isolation and Examination of Fungi

The method of dilution was used to isolate the fungi from the soil and water samples by taken 1 gm of samples (soil or water) added to 100 ml sterile water, then the mixture was shaken for one minute and left to settle for a period of ten minutes. After preliminary experiments, the third dilution was chosen, 1ml of each dilution was with on Potato Dextrose Agar (PDA) supplemented with chloramphenicol move the plate to increase the spread of the sample. The plates were incubated at 28°C in the dark for 5-7 days (Reddy *et al.*, 2014). After that pure colonies of fungal observed and maintained for examination (Jasuja *et al.*, 2013).

Fungal morphology was studied microscopically by observing colony traits (colour, shape, size, and hyphae), and microscopically by compound microscope using a lactophenol blue-stained slide fixed with a small part of the mycelium (Cappuccino & Sherman, 1996).

2.4. DNA Extraction and PCR Amplification

Genomic DNA was isolated from Fungal growth according to the protocol of ABIopure Extraction (ABIopure™ Total DNA). The DNA purity was measured using a nano-spectrometer. For molecular identification of fungi species used the universal primers (ITS1 and ITS4). The sequences of primers were:

Primer Name	Seq.	Annealing temp. (°C)	Product size (bp)
ITS1	5'-TCCGTAGGTGAACCTGCGG-3'	55	≈600
ITS4	5'-TCCTCCGCTTATTGATATGC-3'		

The PCR products were resolved by horizontal electrophoresis in a 1% agarose gel using UV light after treatment with dye (safe red) and with a digital camera and the PCR products were sequenced and analyzed by comparison with all available sequences in the National Centre for Biotechnology Information (NCBI) (<http://www.ncbi.nlm.nih.gov>) using the Basic Alignment Sequence Tool (BLAST): (<http://blast.ncbi.nlm.nih.gov/Blast.cgi>), (Javadi *et al.*, 2012).

3. Results: The isolated and identified seven fungal species in this study were checked on the basis of cultural, microscopic, morphological and molecular features Figure



(2 – 8).

The *Aspergillus niger* shows as a black color in colony (Figure 2- A1) and the microscopic arrangement of conidia (Figure 2- A2).

Fig. 2 A1 *Aspergillus niger* colony and A2 conidia

The *Aspergillus terreus* shows as a brown color in colony (Figure 3- B1) and the microscopic arrangement of conidia (Figure 3- B2).

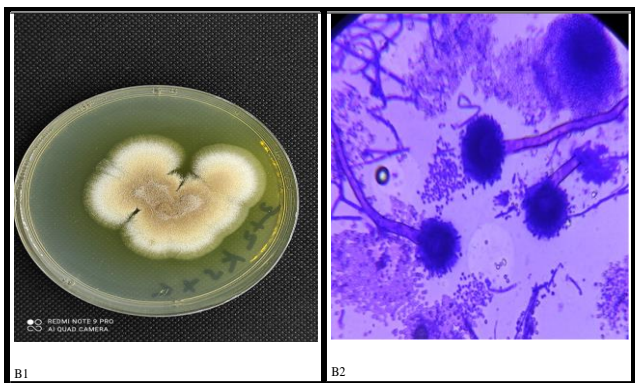


Fig. 3 B1 *Aspergillus terreus* colony and B2 conidia

The *Aspergillus flavus* shows as green color colony (Figure 4- C1) and the microscopic arrangement of conidia (Figure 4- C2).

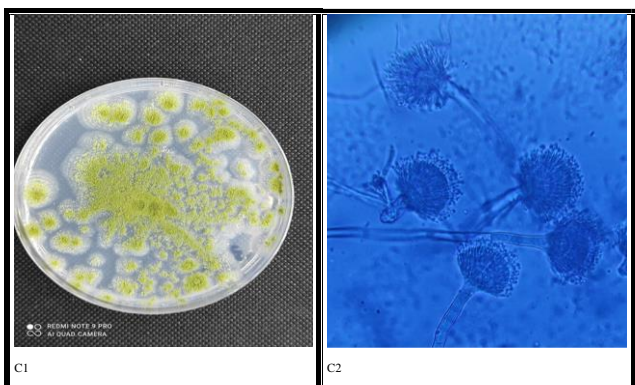


Fig. 4 C1 *Aspergillus flavus* colony and C2 conidia

The *Alternaria alternate* shows greenish-black surface colony (Figure 5- D1) and the microscopic observed macroconidia (Figure 5- D2).

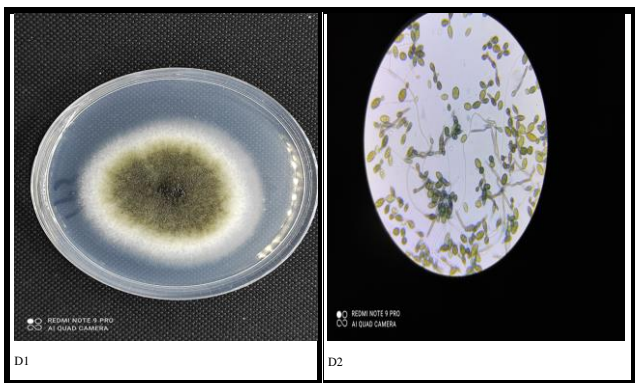


Fig. 5 D1 *Alternaria alternate* colony and D2 macroconidia

The *Penicillium citrinum* shows as a bluish-green colony (Figure 6-E1), and the brush arrangement of phialospores (Figure 6-E2).

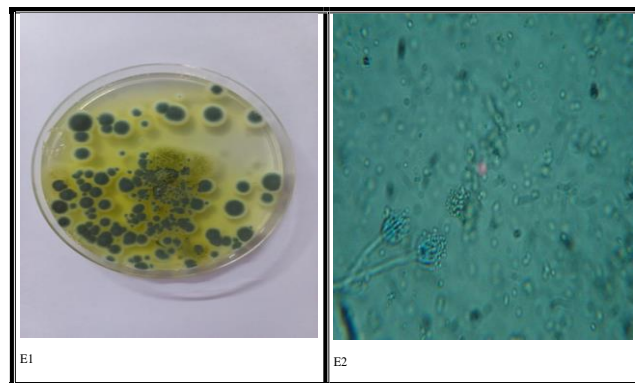


Fig. 6 E1 *Penicillium citrinum* colony and E2 phialospores

The revealed morphological features of *Trichoderma asperellum* are shown in (Figure 7- F1) include the mycelia were white and dark green, and arranged in concentric rings

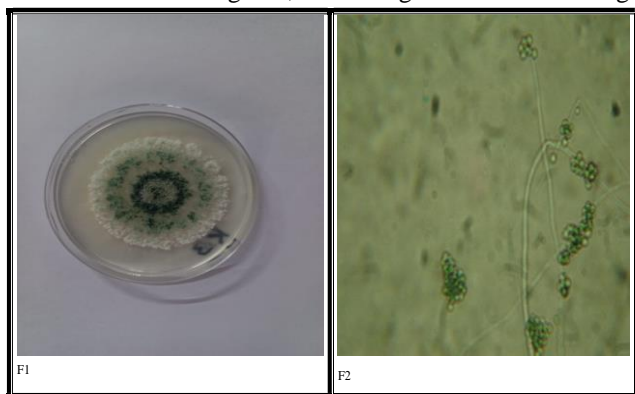


Fig. 7 F1 *Trichoderma asperellum* and F2 conidiogenous

and small green or white conidiophores of cells called conidi-ogenous located at the ends of the many branches of conidiophores (Figure 7- F2).

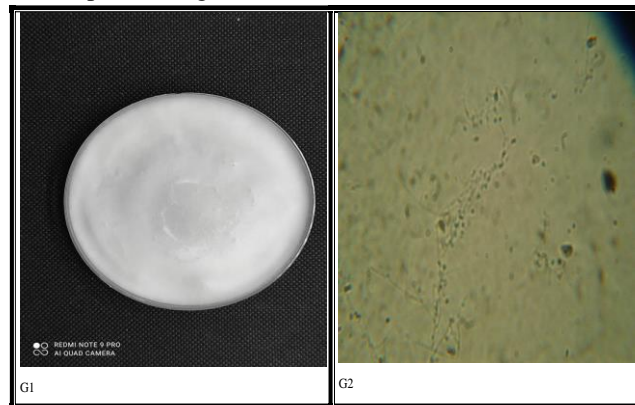


Fig. 8 G1 *Lecanicillium aphanocladii* and G2 aphanophilides

The *Lecanicillium aphanocladii* are distinguished by their white color and high on the surface of the mide PDA (Figure 8- G1) and Distinctive microscopic features such as aphanophilides that are arranged singly, in pairs, or in a group are shown in (Figure 8- G2) .

4. Discussion: In this study, used morphological and molecular (rDNA ITS sequences comparison and analysis) examination methods to isolated and identified the 7 species of fungi

from soil and water in Kirkuk City, Iraq. It is (*Aspergillus niger*, *Aspergillus terreus*, *Aspergillus flavus*, *Alternaria alternate*, *Penicillium citrinum*, *Trichoderma asperellum* and *Lecanicillium aphanocladii*). All of them identified species were isolated from the soil and water except (*A. terreus*) were isolated more from the soil and this match with soil is the basic source of the fungi (Chandrashekar *et al.*, 2014).

The distribution and growth of fungi affect with different factors as soil pH, moisture, salinity, temperature and organic matter and that lead to variation in ratio of growth fungi (Sharma & Raju, 2013).

For the identification of fungi to the genus level, can be dependence on morphological examination (Wang *et al.*,

Table 1 The Percentage of Fungal Species Isolates at Study Sites.

Scientific name of fungal isolate	Collection sites - Kirkuk City				The sum of fungal isolates	fungal isolate %
	The North Oil Company Channel		Khasa River Channel			
	soil	water	soil	water		
<i>Aspergillus flavus</i>	8	7	8	7	30	20.83
<i>Aspergillus niger</i>	8	5	7	6	26	18.06
<i>Alternaria alternate</i>	7	4	7	4	22	15.30
<i>Trichoderma asperellum</i>	5	4	6	5	20	13.90
<i>Lecanicillium aphanocladii</i>	5	3	6	4	18	12.50
<i>Aspergillus terreus</i>	7	1	6	2	16	11.11
<i>Penicillium citrinum</i>	5	1	4	2	12	8.30
The total sum of the isolates	43	27	43	31	144	100

2016). But for a more accurate identification we need to a molecular examination (Lutzoni *et al.*, 2004), that carried out by DNA barcoding using the ITS region sequencing (ITS1 – ITS4). The DNA sequences were compared to those in the databases using NCBI-BLAST. The seven local fungal isolates were registered at the National Center for Information Technology (NCBI) under No. OP268345.1 for *Aspergillus niger*, No. OP268344.1 for *Aspergillus flavus*, No. OP268334.1 for *Aspergillus terreus*, No. OP268285.1 for *Alternaria alternata*, No. OP268332.1 for *Trichoderma asperellum* No. ON908684.1 for *Penicillium citrinum* and the No. OP020444.1 for *Lecanicillium aphanocladii*, all the fungal first recorded of these isolates in Iraq.

According to the results of this study, (Table 1) that all species of fungi were present throughout the study period, and this indicates the high ability of these species to adapt to difficult environmental conditions. The results shown that *Aspergillus flavus* 20.83 (% was the most abundant

fungus, while (*Penicillium citrinum* 8.30%) was the less prevalent one in all resources and locations.

5. Conclusion: Fungi were isolated and identified from the Khasa River channel and North Oil Company channel in Kirkuk City showed the presence of different species of fungi in these environments and the presence of *Aspergillus* spp more than others. The study indicated that the molecular identification of fungi added the ability to accurately identify the species of fungi, and the result of this study was seven local fungal isolates were registered at the National Center for Information Technology (NCBI). So, this study recommends more work in the future to be done in this habitat to isolate and identify fungi.

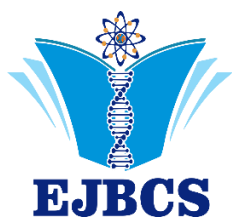
Acknowledgements

This research did not receive any specific grant from funding agencies in the public, commercial, or not-for-profit sectors.

References

- Anderson IC, Parkin PI. 2007. Detection of active soil fungi by RT-PCR amplification of precursor rRNA molecules. *Microbiol Methods*. 68:248–253.
- Bermingham S, Maltby L, Cooke RC. 1996. Effect of a coal mine effluent on aquatic hyphomycetes. *Field Study Appl Ecol*. 33: 1311-1321.
- Cappuccino JG, Sherman N. 1996. *Microbiology. laboratory manual*. 4th ed. Benjamin. Cummings pub.
- Chandrashekar MA, Soumya Pai K, Raju NS. 2014. Fungal Diversity of Rhizosphere Soils in Different Agricultural fields of Nanjangud Taluk of Mysore District. Karnataka. India. *Int.J.Curr.Microbiol.App.Sci*. 3:559-566.
- Gaddeyya G, Niharika PS, Bharathi P, Kumar PKR. 2012. Isolation and identification of soil mycoflora in different crop fields at Salur Mandal. *AdvAppl Sci Res*. 3:2020-2026.
- Gravesen S, Frisvad JC, Samson RA. 1994. *Microfungi*. Munksgaard Publishers. Copenhagen.
- Jasuja ND, Saxena R, Chandra S, Joshi SC. 2013. Isolation and identification of microorganism from polyhouse agriculture soil of Rajasthan. *African J Microbiol Res*. 7: 4886-4891.
- Javadi MA, Ghanbary MAT, Tazick Z. 2012. Isolation and molecular identification of soil inhabitant *Penicillia*. *Ann of Biol Res*. 3: 5758-5761.
- Kamel T. 2013. Mesopotamia in Mesopotamia. Iraqi Nation Studies Center. [www.mesopotamia4374.com/dose/Mesopotamia in Mesopotamia](http://www.mesopotamia4374.com/dose/Mesopotamia%20in%20Mesopotamia). Iraqi Nation Studies Center. Accessed 20 Oct 2013.
- Lutzoni F, Kauff F, Cox CJ, Laughlin D, Celio G. 2004. Assembling the fungal tree of life progress classification and evolution of the subcellular traits. *Am J Bot*. 91: 1446-1480.
- Nollet LM. 2007. *Handbook of water analysis*. 2nd ed. CRC Press. London.
- Pellon A, Sadeghi N, Moyes DL. 2020. New insights in *Candida albicans* innate immunity at the mucosa toxins epithelium metabolism and beyond. *Frontiers in cellular and infection microbiology*.10-81.
- Reddy PL, Babu BS, Radhaiah A, Sreeramulu A. 2014. Screening, identification and isolation of cellulolytic fungi from soils of

- Chittoor District. India. *Int J Curr Microbiol Appl Sci.* 3: 761-771.
- Sharma MS, Raju NS. 2013. Frequency and percentage occurrence of soil mycoflora in different crop fields at H D Kote of Mysore district. *Inter J Environ Sci.* 3: 1569-1576.
- Wang JH, Zhang HP, Gong S, Xue RS, Agboola Y, Liao C. 2014. Molecular identification mycotoxin production and comparative pathogenicity of *Fusarium temperatum* isolated from maize in China. *J. Phytopathol.* 162:147-157.
- Wang Z, Nilsson RH, James TY, Dai Y, Townsend JP. 2016. *Biology of Microfungi.* pp 25-46.
- Webster J, Weber RA. 2007. Introduction to fungi. In: Jack S. *Fungi*, 3rd edn. New York.



Molecular modeling and thermodynamics of the interaction between DNA base pairs and radon originated ionizing alpha radiation

Caglar Celik Bayar*^{ID}

*Zonguldak Bulent Ecevit University, Faculty of Engineering, Metallurgical and Materials Engineering Department, Zonguldak, Turkey

*Corresponding author : caglarbayar@gmail.com, caglarbayar@beun.edu.tr
Orcid No: <https://orcid.org/0000-0002-2293-2963>

Received : 27/12/2022
Accepted : 22/05/2023

Abstract: Ionizing alpha radiation (He^{2+}) is known to adversely affect human DNA, but the biochemical reasoning is not clear yet. Relatedly, the present computational study was conducted to investigate the effects of ionizing alpha radiation onto the Watson-Crick type DNA base pairs (nucleotides) Adenine-Thymine (AT') and Guanine-Cytosine (GC'). The long-range cation (He^{2+})- π interactions were modeled for this purpose. A hybrid DFT functional of M06-2X was used with 6-31G(d,p) and 6-311G(d) basis sets at unrestricted level. The results showed that alpha radiation severely changed the considered base pairs' hydrogen bond lengths and their interaction enthalpies and Gibbs free energies, however, the more drastic changes were observed in GC' when compared to those of AT'. This observation was also supported with performed frontier molecular orbital analyses. GC' was more favored to form He^{2+} complexes (oxidize) than AT' and consequently these complexes had more exothermic interaction energies (formed more spontaneously) than that of AT'. It could be highlighted that the molecular modeling proposed in this study would contribute to the enlightenment of the uncertainty in this field.

Keywords: DNA base pairs, alpha radiation, interaction enthalpy, interaction Gibbs free energy, M06-2X

© EJBCS. All rights reserved.

1. Introduction

Radon gas (^{222}Rn) is the radiation source that is naturally produced in the soil and has the most ionizing effect with its alpha (α) radiation. The radioactive property of radon atoms and their being in gaseous state at the same time cause adverse effects on human health by being inhaled into the lungs. The most important negative effect is lung cancer. For the first time, Bale (Bale 1980) and Harley (Harley 1952) suggested that lung cancer does not arise directly from radon atoms, but from product nuclei formed by the decay of the radon atom (Soğukpınar 2013). The International Agency for Research on Cancer (IARC) defined radon gas as a cancer-causing agent in 1988. The risk of developing lung cancer in smokers who are exposed to 1-800 Bq/m³ of radon gas has been reported 22-25 times higher than non-smokers. Both non-smokers and individuals who are not exposed to radon gas do not develop lung cancer (Soğukpınar 2013; Zeeb and Shannoun 2009).

Since radon gas is a member of the noble gas group, it is chemically passive and does not react. Since the half-life of radon gas is longer than the duration of inhalation (3,82 days), the radon gas that is inhaled is exhaled without decomposing again. Metal atoms (^{214}Po , ^{218}Po , ^{214}Pb and

^{214}Bi) are formed as a result of the decay of radon atoms. When these atoms adhere to airborne dust and aerosols and are inhaled into the lungs, they cling to the lung epithelium tissue surrounding the inner structure and are not expelled again during exhalation. The product formed by decomposition of radon, ^{214}Pb , which has the longest half-life, decays in less than 27 minutes. Short-lived product nuclei degrade before the normal cleansing period of the lung, and may cause damage to sensitive epithelial cells and mutation in the DNA structure. The ^{214}Po and ^{218}Po nuclei, which have the highest decay energy, cause the greatest damage to the lung cells with α radiation they make. The very short half-life (55,6 s) of the thoron (^{220}Rn) atom, which is a second isotope of the radon atom, caused its density to be low in the environment under normal conditions. Likewise, actinon (^{219}Rn), a third radon isotope, has a very short half-life (3,96 s) and the relative abundance of the actinon main nucleus in nature is very low. For this reason, thoron and actinon are often neglected in radon gas measurements, and the ^{222}Rn isotope is generally referred to (Durrani and Ilić 1997; Soğukpınar 2013). The ^{222}Rn isotope is continuously produced in the natural decay series of element uranium (^{238}U). Therefore, radon gas-related lung cancer has been reported mostly in uranium miners in

the world. As people learn about the health effects of radon gas, the radon level in the mines is constantly monitored, and it is tried to be kept at a certain level with ventilation (Soğukpınar 2013).

The α -Particle cannot pass through human skin (National Radiological Protection Board 1998). However, when radioactive nuclei are degraded within the body through nutrition or breathing, they produce ionizing α -particles and can trigger different types of cancer. It was reported that ionizing alpha particles could cause chromosomal aberrations (Chen et al. 1984; Robertson et al. 2013), double strand DNA breaks and generate reactive oxygen species (Narayanan et al. 1997; Robertson et al. 2013) resulting in cell cycle shortening, apoptosis and an increased potential of carcinogenesis. Accordingly, the tumor suppressor gene TP53 (previously named p53) mutations and deletions were frequently observed in various cancers (Robertson et al. 2013; Wazer et al. 1994) including those of the lung and investigations previously located unique mutations in regions referred to as biomarkers (hotspots) that could result from radon exposure (Robertson et al. 2013). The related study was conducted on radon exposed 52 Colorado uranium miners having large and squamous lung cell carcinomas (Taylor et al. 1994). It was reported that 31% of the workers possessed the AGG to ATG (Arg \rightarrow Met) transversions, at the TP53 gene, codon 249, exon 7. This result led the authors to highlight this region as a potential hotspot for radon associated lung cancer. However, no clear radon-induced TP53 hotspot mutations were identified in uranium miner cohorts in further studies (Hollstein et al. 1997; McDonald et al. 1995; Popp et al. 1999; Robertson et al. 2013; Wesch et al. 1999; Wiethage et al. 1999; Yang et al. 2000). Conclusively, it can be stated that the cellular and molecular carcinogenic effects of radon exposure are still complex and uncertain (Robertson et al. 2013).

The long-range interactions of electron-deficient alpha particle arising from radon decay and electron-rich DNA base pairs have not been enlightened in a molecular term up to now to the best of the knowledge. In the present study, possible long-range interactions were modelled between the alpha particle (He^{2+} ion) and each of the ring of Watson-Crick type DNA base pairs, Adenine-Thymine (AT) and Guanine-Cytosine (GT), including π -bonds, separately. The considered DNA base pairs were neutral and consisted of 2'-deoxyribose-5'-phosphate residues which resembled the real case. However, they were not interacted with alpha particle because of the lack of π -bonds. The molecular modeling was performed using a hybrid DFT functional M06-2X suggested for noncovalent long-range interactions of main-group elements (Zhao and Truhlar 2008). Finally, comparisons were done between the alpha particle bound and non-bound DNA base pairs to find out the possible changes in hydrogen bond lengths and interaction Gibbs free energies. It was considered that such changes may cause serious damages in DNA structure and impair its vital functions. Since such an approach and possible interactions were not investigated before in the literature, this contributed the originality of the study.

2. Methods of Calculation

The structure optimizations and single point energy calculations including interaction enthalpies, interaction Gibbs free energies and frontier molecular orbital (FMO) analyses were performed in gas phase using Spartan 18 program software (Spartan'18 Parallel Suite 2018). A starting distance of 2.5Å between the alpha particle (He^{2+} ion) and DNA base pair ring centres was used to aid in convergence and find the local minima on the potential energy surface. Initial interaction angles were chosen as 90° in all complexes. The structure optimizations were performed at DFT UM06-2X/6-31G(d,p) level of theory (Zhao and Truhlar 2008) after performing the pre-optimizations at semi-empirical and Hartree-Fock levels. This basis set was previously applied to cation- π type interactions in the literature (Davis and Dougherty 2015; Dhindhwal and Sathyamurthy 2016). The interaction enthalpies, interaction Gibbs free energies and FMO energies of all the complexes were computed at UM06-2X/6-311(d)//UM06-2X/6-31(d,p) level of theory. The interaction enthalpies and Gibbs free energies were corrected considering basis set superposition error (BSSE) contributions (Ebrahimi et al. 2014; Mudedla et al. 2014). BSSE corrections use the Boys and Bernardi counterpoise technique (Boys and Bernardi 1970; Ebrahimi et al. 2014) which are due to overlap of the wave functions of the moieties (Mottishaw and Sun 2013). The calculations of all the considered complexes contained zero point energy corrections and had no imaginary frequencies which indicated that they stood for no transition states or saddle points on the potential energy surfaces.

3. Results and Discussion

3.1. Verifying the Basis Set Used

Before interacting DNA base pairs with alpha particle, it was necessary to test the validity of DFT UM06-2X/6-31G(d,p) theoretical level for optimizations. For this purpose, X-ray experimental data for Watson-Crick type Adenine-Thymine (AT) and Guanine-Cytosine (GT) base pairs (without deoxyribose and phosphate rings) were used as reference values and data obtained from the theoretical calculations were compared with them. The optimized structures of the AT and GC base pairs were shown in Figure 1. The experimental and theoretical atomic distances involved in hydrogen bonding were listed in Table 1 for these base pairs. It was figured out that the calculated distance between N1-O1 atoms was the same as the experimental distance while N2-N3 distance was close to the experimental one for the AT base pair. On the other hand, the calculated O1-N4 distance was a bit shorter than the experimental value while N1-N3 distance was close to it for the GC base pair. The N2-O2 distance was obtained a bit longer but still close to the experimental distance for the same base pair. Experimental data existing in Table 1 were reported in the studies of Saenger (Saenger 1984) and Mo (Mo 2006), previously. AT base pair had two hydrogen bonds between H1-O1 and N2-H3 atoms while GC base pair had that of three between O1-H3, H1-N3 and H2-O2 atoms.

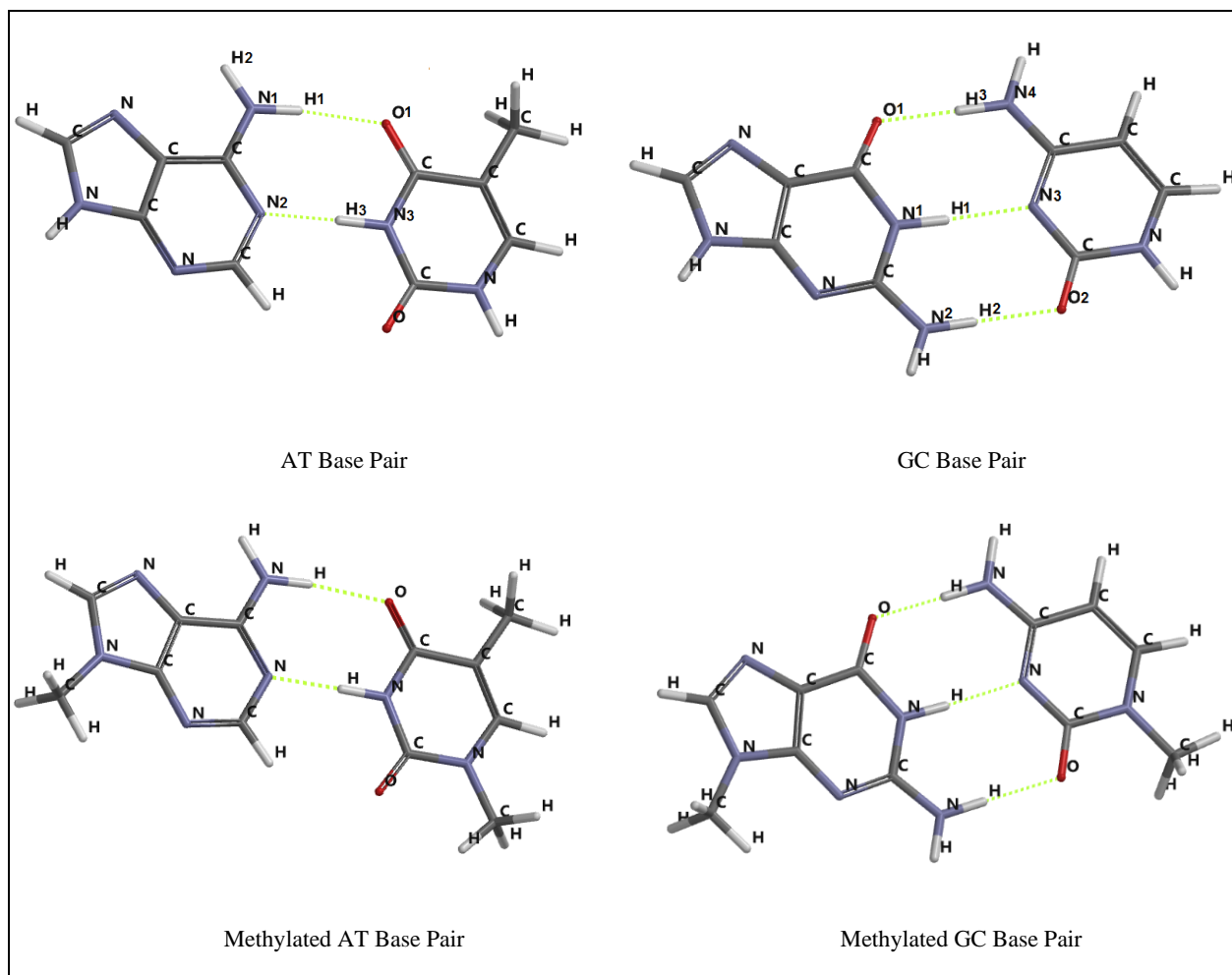


Fig. 1 The optimized structures of Watson-Crick type Adenine-Thymine (AT), Guanine-Cytosine (GC), 9-methyladenine and 1-methylthymine (methylated AT), 9-methylguanine and 1-methylcytosine (methylated GC) base pairs at DFT UM06-2X/6-31G(d,p) theoretical level.

These hydrogen bond lengths ranged from 1.74 Å to 2.04 Å in the considered base pairs.

The experimental interaction enthalpies of the Watson-Crick type methylated base pairs, 9-methyladenine and 1-methylthymine (methylated AT) and 9-methylguanine and 1-methylcytosine (methylated GC), were also used to check out the validity of the theoretical level used in the present study. The experimental values were calculated at room temperature and reported as -12.1 kcal/mol for the methylated AT and -21.0 kcal/mol for the methylated GC base pairs, respectively (Brameld et al. 1997; Guerra et al. 2000; Yanson et al. 1979). Relatedly, close interaction enthalpies were calculated as -12.4 kcal/mol and -25.2 kcal/mol for the methylated AT and GC base pairs, respectively, in the study. The optimized structures of the considered methylated base pairs were also presented in Figure 1. It was possible to conclude that the calculated atomic distances showed almost no change for the methylated and unmethylated AT and GC species (Table 1). As a result, the theoretical and experimental comparison of the atomic distances and interaction enthalpies showed that the theoretical method used in the study was reliable.

3.2. Structure Optimizations, Hydrogen Bonds and Interaction Distances

The optimized structures and aromatic ring numberings of Watson-Crick type AT and GC base pairs with 2'-deoxyribose-5'-phosphate residues (abbreviated as AT' and GC' throughout the study) were presented in Figure 2. These molecules were interacted with alpha particle and then optimized and thus formed the core of the study. Rings 1 and 2 belonged to the adenine side of AT' and guanine side of GC' whereas Ring 3 belonged to that of thymine and cytosine sides, respectively. The alpha particle had two possibilities to interact with these rings, from the upper and lower faces (Figure 2). The interactions from the upper faces were labeled as AT'-i and GC'-i (i=1-3), respectively, where i represented the aromatic ring numbers. Asterisk symbols (*) over i, AT'-i* and GC'-i*, were used to indicate the interactions from the lower face. In general, no significant shifts were observed at the end of the optimizations. However, there existed two exceptional optimized structures which were AT'-2* and AT'-(2-3)*. The initial structure of AT'-1* ended up with AT'-2* in which the He²⁺ ion shifted to the sterically less hindered side

Table 1. The atomic distances (Å) involved in hydrogen bonding of Watson-Crick type Adenine-Thymine (AT), 9-methyladenine and 1-methylthymine (methylated AT), Guanine-Cytosine (GC), 9-methylguanine and 1-methylcytosine (methylated GC) base pairs and AT' and GC' base pairs (with 2'-deoxyribose-5'-phosphate residues) and their He²⁺ exposed derivatives calculated at DFT UM06-2X/6-31G(d,p) theoretical level. The interactions of He²⁺ from the upper faces of the base pairs were denoted as AT'-i and GC'-i (i=1-3), respectively, where i represented the aromatic ring numbers. Asterisk symbols (*) over i, AT'-i* and GC'-i*, were used to indicate the interactions from the lower face (See Figure 2).

	N ₁ -O ₁	N ₂ -N ₃	H ₁ -O ₁	N ₁ -H ₁	N ₂ -H ₃	O ₁ -N ₄	N ₁ -N ₃	N ₂ -O ₂	O ₁ -H ₃	H ₁ -N ₃	H ₂ -O ₂	N ₂ -H ₂
AT	2.95 (2.95)	2.79 (2.82)	1.94		1.74							
Methylated AT	2.94	2.80	1.93		1.74							
AT'	2.94	2.79	1.92		1.74							
AT'-1	2.91	2.85		1.92	1.82							
AT'-2	2.92	2.85		1.93	1.82							
AT'-2*	2.95	2.86		1.96	1.83							
AT'-(2-3)*	2.91	2.84		1.92	1.81							
AT'-3	2.92	2.85		1.93	1.82							
AT'-3*	2.92	2.85		1.93	1.82							
GC						2.79 (2.91)	2.92 (2.95)	2.91 (2.86)	1.75	1.89	1.89	
Methylated GC						2.79	2.93	2.91	1.76	1.90	1.89	
GC'						2.81	2.92	2.91	1.78	1.89	1.89	
GC'-1						3.05	2.89	2.68	2.04	1.85		1.67
GC'-1*						3.03	2.89	2.68	2.01	1.85		1.67
GC'-2						3.05	2.89	2.68	2.04	1.85		1.67
GC'-2*						3.05	2.89	2.68	2.04	1.85		1.67
GC'-3						3.05	2.89	2.68	2.04	1.85		1.67
GC'-3*						3.05	2.89	2.68	2.04	1.85		1.67

Data in parentheses denote the experimental data (Mo 2006; Saenger 1984).

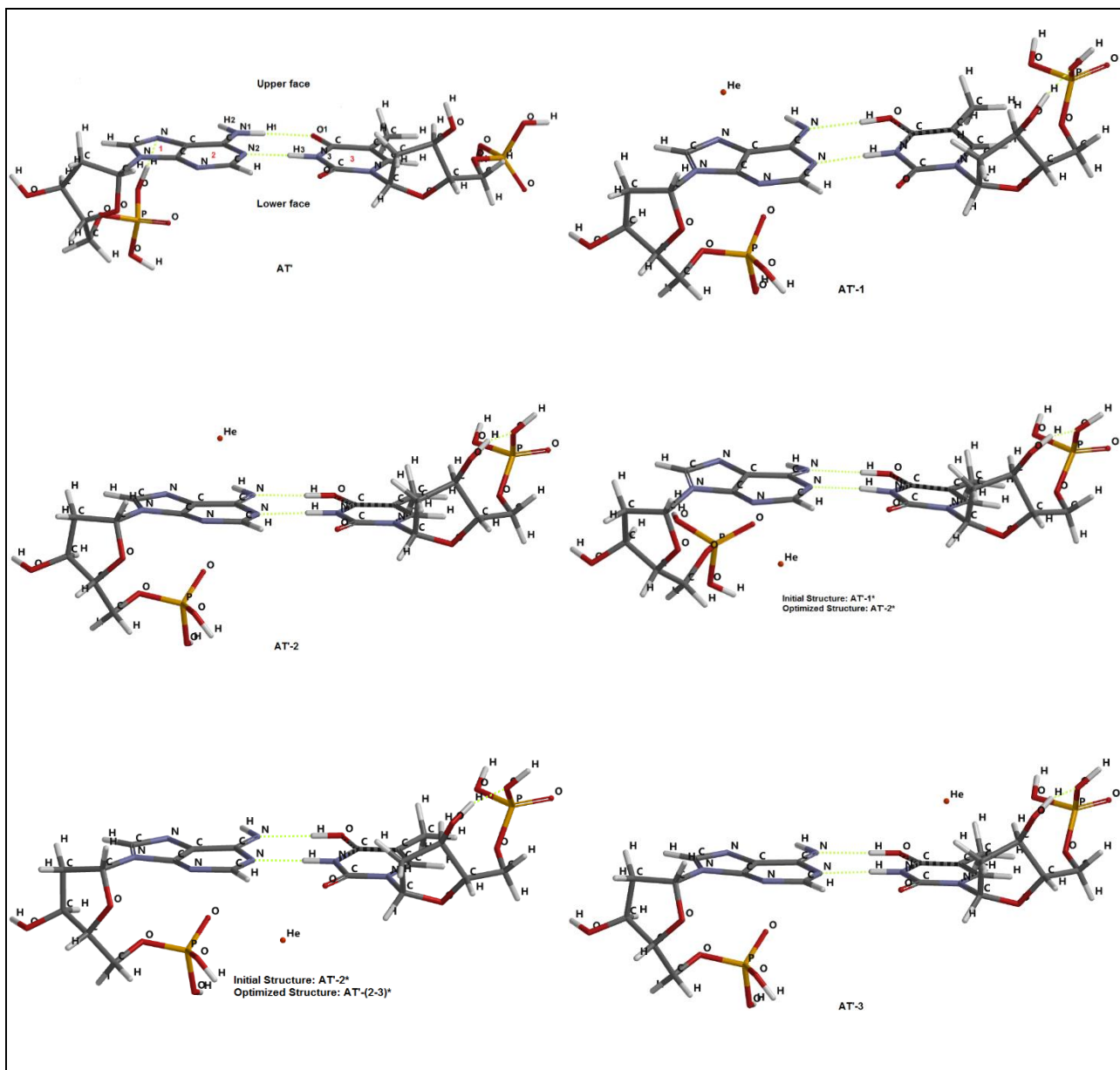


Fig. 2 The optimized structures of AT⁺ and GC⁺ base pairs (with 2'-deoxyribose-5'-phosphate residues) and their He²⁺ exposed derivatives at DFT UM06-2X/6-31G(d,p) theoretical level. The interactions of He²⁺ from the upper faces of the base pairs were denoted as AT⁺-i and GC⁺-i (i=1-3), respectively, where i represented the aromatic ring numbers. Asterisk symbols (*) over i, AT⁺-i* and GC⁺-i*, were used to indicate the interactions from the lower face.

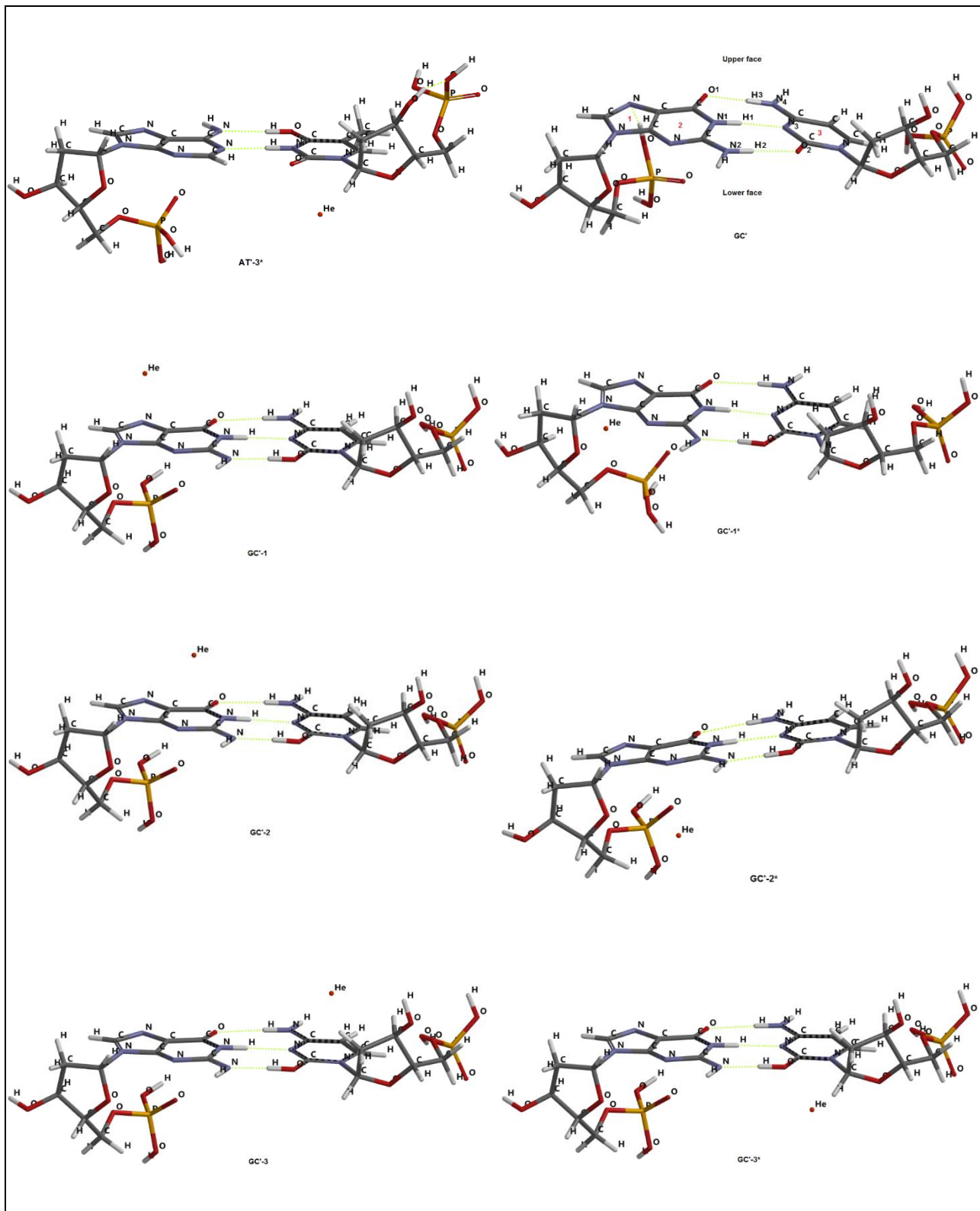


Fig. 2 Cont'd.

which was located under Ring 2. Similarly, the He^{2+} ion in AT'-2* initial structure shifted in between Rings 2 and 3 and formed the optimized structure of AT'-(2-3)*.

The hydrogen bonding atomic distances of the considered molecules were also demonstrated in Table 1. Compared to three molecules (AT, methylated AT and AT'), the $\text{N}_1\text{-O}_1$ distance slightly narrowed for most of the considered He^{2+} exposed structures. It almost stayed the same for AT'-2*. The $\text{H}_1\text{-O}_1$ hydrogen bond turned into $\text{N}_1\text{-H}_1$ hydrogen bond by shift of H_1 from N_1 to O_1 in alpha radiated derivatives with almost no change in their bond distances (except for AT'-2*). The $\text{N}_2\text{-N}_3$ and relatedly $\text{N}_2\text{-H}_3$ distances of these base pairs increased compared to AT, methylated AT and AT'. The average elongation at $\text{N}_2\text{-N}_3$ distance was 0.06 Å whereas it was 0.08 Å at $\text{N}_2\text{-H}_3$ distance. It was possible to deduce that the hydrogen bond distances were affected when the AT' molecule was exposed to alpha radiation, i.e. the distance above narrowed, while that of the below elongated. However, the trend was opposite for the $\text{GC}'\text{-i}$ and $\text{GC}'\text{-i}^*$ structures. The hydrogen bond distance above elongated whereas those of in the middle and below narrowed. This situation was explained as follows: The $\text{O}_1\text{-N}_4$ and corresponding $\text{O}_1\text{-H}_3$ distances increased significantly for alpha radiation exposed $\text{GC}'\text{-i}$ and $\text{GC}'\text{-i}^*$ structures compared to GC, methylated GC and GC'. The average elongation at the $\text{O}_1\text{-N}_4$ distance was 0.25 Å whereas it was 0.28 Å at the $\text{O}_1\text{-H}_3$ distance. Conversely, the $\text{N}_1\text{-N}_3$ and corresponding $\text{H}_1\text{-N}_3$ distances narrowed slightly, i.e. average decreases of 0.03 Å and 0.04 Å were observed in the former and latter, respectively. Finally, the $\text{N}_2\text{-O}_2$ distance was reduced by 0.23 Å, forming a new, shorter hydrogen bond between the N_2 and H_2 atoms (1.67 Å in all) by the shift of H_2 from N_2 to O_2 . Finally, it was figured out that more severe changes were observed in hydrogen bond distance in GC' rather than AT' when both of them were exposed to alpha radiation.

The interaction distance of He^{2+} from the ring centres of alpha radiation exposed AT' and GC' specie was demonstrated in Table 2. The corresponding distances were detected between 2.68-2.82 Å for AT'-i and AT'-i* base pairs. Exceptionally, He^{2+} lied somewhere in between adenine and thymine moieties of AT'-(2-3)* and located far away from the ring centres. Therefore, the larger distances were detected for it than for others (distances of 3.70 Å to Ring 2 and 4.10 Å to Ring 3). On the other hand, the related distances were obtained in between 2.69-3.56 Å for $\text{GC}'\text{-i}$ and $\text{GC}'\text{-i}^*$ base pairs.

Table 2. The interaction distance of He^{2+} (Å) from the ring centres of alpha radiation exposed AT' and GC' species optimized at DFT UM06-2X/6-31G(d,p) theoretical level.

Base Pair	Ring Number		
	1	2	3
AT'-1	2.76		
AT'-2		2.68	
AT'-2*		2.82	
AT'-(2-3)*		3.70	4.10
AT'-3			2.70
AT'-3*			2.69
$\text{GC}'\text{-1}$	2.77		
$\text{GC}'\text{-1}^*$	3.35		
$\text{GC}'\text{-2}$		2.71	
$\text{GC}'\text{-2}^*$		3.56	
$\text{GC}'\text{-3}$			2.76
$\text{GC}'\text{-3}^*$			2.69

3.3. Interaction Enthalpies and Gibbs Free Energies

The interaction enthalpies and Gibbs free energies of the AT, GC, their methylated forms, AT', GC' and their alpha radiated derivatives were listed in Table 3. All the values listed in the table were negative which indicated favored interactions. In general, the interaction enthalpies presented more exothermic character than interaction Gibbs free energies. The first observation was that no dramatic changes were observed in both energies for un-radiated specie. However, the values became drastically more exothermic when AT' and GC' were exposed to alpha radiation. The interaction enthalpies changed between (-48.8)-(-62.8) kcal/mol and (-64.5)-(-93.8) kcal/mol for radiated AT' and GC' derivatives, respectively. On the other hand, the interaction Gibbs free energies changed between (-36.0)-(-52.1) kcal/mol and (-49.8)-(-79.9) kcal/mol for radiated AT' and GC' specie, respectively. Additionally, the energies of GC and its derivatives existing in the table were more exothermic than that of AT. This condition could be explained in terms of hydrogen bond numbers; i.e. the GC and its derivatives having three hydrogen bonds would have greater stability than that of AT having two hydrogen bonds. Another striking observation was that the AT' derivatives radiated from the thymine moieties (AT'-3 and AT'-3*) and similarly the GC' derivatives radiated from the cytosine moieties (GC'-3 and GC'-3*) showed more exothermic character than the others.

Table 3. The interaction enthalpies and Gibbs free energies of the specie listed in Table 1 (UM06-2X/6-311G(d)//UM06-2X/6-31G(d,p)).

	ΔH_{298}° (kcal/mol)	ΔG_{298}° (kcal/mol)
AT	-14.1	-2.6
Methylated AT	-12.4 (-12.1)	-1.1
AT'	-12.4	-0.2
AT'-1	-51.0	-37.6
AT'-2	-51.2	-37.7
AT'-2*	-48.8	-36.0
AT'-(2-3)*	-51.0	-37.5
AT'-3	-62.8	-52.0
AT'-3*	-62.5	-52.1
GC	-27.4	-15.4
Methylated GC	-25.2 (-21.0)	-12.8
GC'	-23.8	-10.8
GC'-1	-65.1	-51.5
GC'-1*	-65.1	-50.9
GC'-2	-65.0	-51.4
GC'-2*	-64.5	-49.8
GC'-3	-93.8	-79.9
GC'-3*	-93.0	-79.8

Energies are BSSE corrected. Data in parentheses denote the experimental data (Brameld et al. 1997; Guerra et al. 2000; Yanson et al. 1979).

3.4. Frontier Molecular Orbital (FMO) Analyses

Mulliken electronegativity (χ_M), electronic chemical potential (μ), absolute hardness (η), global softness (S) and electrophilicity index (ω) are important properties to understand the chemical reactivity of the compounds. They are obtained according to the Equations (1) - (4) below.

$$\chi_M = -\mu = (I + A) / 2 \quad (1)$$

(Pearson 1997; Srivastava et al. 2009)

$$\eta = (I - A) / 2 \quad (2)$$

(Pearson 1997; Singh et al. 2004)

$$S = 1 / (2 \eta) \quad (3)$$

(Singh et al. 2004; Srivastava et al. 2009)

$$\omega = \mu^2 / (2 \eta) \quad (4)$$

(Parr et al. 1999; Srivastava et al. 2009)

I and A are the ionization potential and electron affinity, respectively (Pearson 1997). Note that $I = -\epsilon_{\text{HOMO}}$ and $A = -\epsilon_{\text{LUMO}}$ within the validity of the Koopmans' theorem (Koopmans 1934), where ϵ_{HOMO} and ϵ_{LUMO} are the energies of the highest occupied molecular orbitals and lowest unoccupied molecular orbitals, respectively.

Electrophilicity index (ω) defines the global electrophilic nature of a molecule within a relative scale (Raya et al. 2011). If we consider two reacting molecules, the one having higher ω acts as an electrophile whereas the other with lower ω acts as a nucleophile. As expected, the radiated AT' and GC' derivatives had more electrophilic character than their unirradiated forms (Table 4). The other point was that all the absolute hardness (η) and global softness (S) values were inversely proportional to each other for the considered species in the table. The unirradiated base pairs, AT' and GC', were both harder than their radiated forms.

Molecules with high HOMO energy can donate their electrons more easily compared to molecules with low HOMO energy, and hence are more reactive in oxidation reactions. Accordingly, molecules with low LUMO energy are more apt to accept electrons than molecules with high LUMO energy. Hence, they are more reactive in reduction reactions. This information is used in describing the reactivity (stability) of the molecules. The $f_{\text{H/L}}$ index is defined as a stability index of molecules through oxidation. It's the ratio between the HOMO and LUMO energies. Molecules with low values of $f_{\text{H/L}}$ show more persistent character to oxidation than the molecules having high values of $f_{\text{H/L}}$ (Rokhina and Suri 2012). Accordingly, the AT' had lower $f_{\text{H/L}}$ value than GC' which denoted its more resistance to oxidation (Table 4).

Note that there was a strong relationship between the considered AT' and GC' base pairs' oxidation tendency and their radiation interaction energies. The higher $f_{\text{H/L}}$ value of GC' indicated that it was more prone to oxidation and as a result the radiated derivatives of it showed more exothermic interaction energies than that of AT'. Additionally, the $f_{\text{H/L}}$ values of all the radiated specie lied in between that of AT' and GC'.

4. Conclusion

It is known that the theoretical method and basis set used in such computational studies act as limiting parameters for the obtained results. However, in the present study, the selection of these two was mainly based on comparison of the results with experimental data as much as possible. In the light of this, the major outcomes of the study were summarized as follows:

a. When the AT' and GC' base pairs (Adenine-Thymine and Guanine-Cytosine base pairs including 2'-deoxyribose-5'-phosphate residues) were exposed to alpha radiation, the hydrogen bond distances were severely affected. The distance above narrowed while that of the below elongated in all the radiated AT'

Table 4. The frontier molecular orbital energies, reactivities and stabilities of AT', GC' and their He²⁺ exposed derivatives (UM06-2X/6-311G(d)//UM06-2X/6-31G(d,p)).

	ϵ_{HOMO} (eV)	ϵ_{LUMO} (eV)	I (eV)	A (eV)	χ_{M} (eV)	η (eV)	S (eV ⁻¹)	ω (eV)	$f_{\text{H/L}}$
AT'	-0.27	0.0067	0.27	-0.0067	0.13	0.14	3.6	0.06	-40.3
AT'-1	-0.48	-0.37	0.48	0.37	0.43	0.06	9.1	1.6	1.3
AT'-2	-0.48	-0.37	0.48	0.37	0.43	0.06	9.1	1.6	1.3
AT'-2*	-0.48	-0.38	0.48	0.38	0.43	0.05	10.0	1.8	1.3
AT'-(2-3)*	-0.48	-0.37	0.48	0.37	0.43	0.06	9.1	1.6	1.3
AT'-3	-0.48	-0.37	0.48	0.37	0.43	0.06	9.1	1.6	1.3
AT'-3*	-0.48	-0.37	0.48	0.37	0.43	0.06	9.1	1.6	1.3
GC'	-0.24	-0.00021	0.24	0.00021	0.12	0.12	4.2	0.06	1142.9
GC'-1	-0.50	-0.36	0.50	0.36	0.43	0.07	7.1	1.3	1.4
GC'-1*	-0.50	-0.36	0.50	0.36	0.43	0.07	7.1	1.3	1.4
GC'-2	-0.50	-0.36	0.50	0.36	0.43	0.07	7.1	1.3	1.4
GC'-2*	-0.50	-0.36	0.50	0.36	0.43	0.07	7.1	1.3	1.4
GC'-3	-0.50	-0.36	0.50	0.36	0.43	0.07	7.1	1.3	1.4
GC'-3*	-0.50	-0.36	0.50	0.36	0.43	0.07	7.1	1.3	1.4

derivatives. However, the trend was opposite for the radiated GC' structures, i.e. the bond distances above elongated whereas those of in the middle and below narrowed. However, more drastic changes were observed in radiated GC' specie rather than AT' specie in terms of hydrogen bond distance.

b. The alpha radiation interaction energy values of AT' and GC' were negative (exothermic). Additionally, the interaction enthalpies presented more exothermic character than interaction Gibbs free energies. However, the AT' derivatives radiated from the thymine moieties and the GC' derivatives radiated from the cytosine moieties presented more exothermic character than the others.

c. The higher $f_{\text{H/L}}$ value of GC' revealed that it was more favoured to be oxidized by He²⁺ than AT' and consequently the He²⁺ complexes of GC' had more exothermic interaction energies (formed more spontaneously) than that of AT'.

Acknowledgements

Thanks to Zonguldak Bulent Ecevit University Scientific Research Projects Coordination Office for financial support (Project No. BAP-2020-77654622-03).

Authors' Contributions

The author contributed to each part of the study.

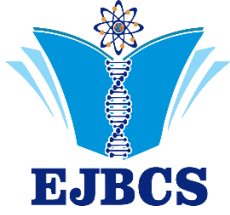
Conflict of Interest Disclosure

The author reports no conflicts of interest.

References

- Bale WF. 1980. Memorandum to the files, March 14, 1951: hazards associated with radon and thoron. Health Phys. 38(6):1062-1066.
- Boys SF, Bernardi F. 1970. The calculation of small molecular interactions by the differences of separate total energies. Some procedures with reduced errors. Mol. Phys. 19(4):553-566.
- Brameld K, Dasgupta S, Goddard WA. 1997. Distance dependent hydrogen bond potentials for nucleic acid base pairs from ab initio quantum mechanical calculations (LMP2/cc-pVTZ). J. Phys. Chem. B 101(24):4851-4859.
- Chen DJ, Strniste GF, Tokita N. 1984. The genotoxicity of alpha particles in human embryonic skin fibroblasts. Radiat. Res. 100(2):321-327.
- Davis MR, Dougherty DA. 2015. Cation- π interactions: computational analyses of the aromatic box motif and the fluorination strategy for experimental evaluation. Phys. Chem. Chem. Phys. 17(43):29262-29270.
- Dhindhwal V, Sathyamurthy N. 2016. The effect of hydration on the cation- π interaction between benzene and various cations. J. Chem. Sci. 128(10):1597-1606.

- Durrani SA, Ilić R. 1997. Radon measurements by etched track detectors: applications in radiation protection, earth sciences and the environment. World Scientific, Singapore, New Jersey, London, Hong Kong.
- Ebrahimi A, Karimi P, Akher FB, Behazin R, Mostafavi N. 2014. Investigation of the π - π stacking interactions without direct electrostatic effects of substituents: the aromatic||aromatic and aromatic||anti-aromatic complexes. *Mol. Phys.* 112(7):1047-1056.
- Guerra CF, Bickelhaupt FM, Snijders JG, Baerends EJ. 2000. Hydrogen bonding in DNA base pairs: reconciliation of theory and experiment. *J. Am. Chem. Soc.* 122(17):4117-4128.
- Harley JH. 1952. Sampling and measurement of airborne daughter products of radon [dissertation]. Rensselaer Polytechnic Institute, Troy (NY).
- Hollstein M, Bartsch H, Wesch H, Kure EH, Mustonen R, Mühlbauer KR, Spiethoff A, Wegener K, Wiethage T, Müller KM. 1997. p53 gene mutation analysis in tumors of patients exposed to alpha-particles. *Carcinogenesis* 18(3):511-516.
- Koopmans T. 1934. Über die zuordnung von wellenfunktionen und eigenwerten zu den einzelnen elektronen eines atoms. *Physica* 1(1-6):104-113.
- McDonald JW, Taylor JA, Watson MA, Saccomanno G, Devereux TR. 1995. p53 and K-ras in radon-associated lung adenocarcinoma. *Cancer Epidemiol., Biomarkers Prev.* 4(7):791-793.
- Mo, Y. 2006. Probing the nature of hydrogen bonds in DNA base pairs. *J. Mol. Model.* 12(5):665-672.
- Mottishaw JD, Sun H. 2013. Effects of aromatic trifluoromethylation, fluorination, and methylation on intermolecular π - π interactions. *J. Phys. Chem. A* 117(33):7970-7979.
- Mudedla SK, Balamurugan K, Subramanian V. 2014. Computational study on the interaction of modified nucleobases with graphene and doped graphenes. *J. Phys. Chem. C* 118(29):16165-16174.
- Narayanan PK, Goodwin EH, Lehnert BE. 1997. Alpha particles initiate biological production of superoxide anions and hydrogen peroxide in human cells. *Cancer Res.* 57(18):3963-3971.
- National Radiological Protection Board. 1998. Living with radiation. NRPB, London.
- Parr RG, Szentpály LV, Liu S. 1999. Electrophilicity index. *J. Am. Chem. Soc.* 121(9):1922-1924.
- Pearson RG. 1997. Chemical hardness. Wiley-VCH, Weinheim, New York (NY).
- Popp W, Vahrenholz C, Schuster H, Wiesner B, Bauer P, Täuscher F, Plogmann H, Morgenroth K, Konietzko N, Norporth K. 1999. p53 mutations and codon 213 polymorphism of p53 in lung cancers of former uranium miners. *J. Cancer Res. Clin. Oncol.* 125(5):309-312.
- Raya A, Barrientos-Salcedo C, Rubio-Póo C, Soriano-Correa C. 2011. Electronic structure evaluation through quantum chemical descriptors of 17 β -aminoestrogens with an anticoagulant effect. *Eur. J. Med. Chem.* 46(6):2463-2468.
- Robertson A, Allen J, Laney R, Curnow A. 2013. The cellular and molecular carcinogenic effects of radon exposure: a review. *Int. J. Mol. Sci.* 14(7):14024-14063.
- Rokhina EV, Suri RPS. 2012. Application of density functional theory (DFT) to study the properties and degradation of natural estrogen hormones with chemical oxidizers. *Sci. Total Environ.* 417-418:280-290.
- Saenger W. 1984. Principles of nucleic acid structure. Springer-Verlag, New York (NY).
- Singh PP, Srivastava HK, Pasha FA. 2004. DFT-based QSAR study of testosterone and its derivatives. *Bioorg. Med. Chem.* 12(1):171-177.
- Soğukpınar H. 2013. Determination of seasonal correction factors for indoor radon concentrations in Eskisehir [dissertation]. Eskişehir Osmangazi University, Eskişehir, Turkey.
- Spartan'18 Parallel Suite. 2018. Wavefunction, Inc., Irvine (CA).
- Srivastava HK, Pasha FA, Mishra SK, Singh PP. 2009. Novel applications of atomic softness and QSAR study of testosterone derivatives. *Med. Chem. Res.* 18(6):455-466.
- Taylor JA, Watson MA, Devereux TR, Michels RY, Saccomanno G, Anderson M. 1994. p53 mutation hotspot in radon-associated lung cancer. *Lancet* 343(8889):86-87.
- Wazer DE, Chu Q, Liu XL, Gao Q, Safaii H, Band V. 1994. Loss of p53 protein during radiation transformation of primary human mammary epithelial cells. *Mol. Cell. Biol.* 14(4):2468-2478.
- Wesch H, Wiethage T, Spiethoff A, Wegener K, Müller KM, Mehlhorn J. 1999. German uranium miner study: historical background and available histopathological material. *Radiat. Res.* 152(6s):S48-S51.
- Wiethage T, Wesch H, Wegener K, Müller KM, Mehlhorn J, Spiethoff A, Schömgig D, Hollstein M, Bartsch H. 1999. German uranium miner study: pathological and molecular genetic findings. *Radiat. Res.* 152(6s):S52-S55.
- Yang Q, Wesch H, Mueller KM, Bartsch H, Wegener K, Hollstein M. 2000. Analysis of radon-associated squamous cell carcinomas of the lung for a p53 gene hotspot mutation. *Br. J. Cancer* 82(4):763-766.
- Yanson IK, Teplitsky AB, Sukhodub LF. 1979. Experimental studies of molecular interactions between nitrogen bases of nucleic acids. *Biopolymers* 18(5):1149-1170.
- Zeeb H, Shannoun F. 2009. WHO handbook on indoor radon: a public health perspective. World Health Organization, France.
- Zhao Y, Truhlar DG. 2008. Density functionals with broad applicability in chemistry. *Acc. Chem. Res.* 41(2):157-167



Longevity toxicity after chronic α -endosulfan exposure in wild population of *Drosophila melanogaster* Oregon-R (Diptera: Drosophilidae)

Handan Uysal^{1*} 

¹Ataturk University, Science Faculty, Biology Department, Erzurum, Turkey

*Corresponding author : hauysal@atauni.edu.tr
Orcid No: <https://orcid.org/0000-0002-4290-8223>

Received : 26/03/2023
Accepted : 16/06/2023

Abstract: The rapid increase in the world population causes different problems such as nutrition and shelter. In this case, people brutally destroy arable land to shelter, and concretization is rapidly spreading. In addition, it is necessary to increase the amount of products to be taken from the limited agricultural areas for the food needs of the increasing population. The decrease in agricultural areas appears as a factor that reduces the amount of product taken from the unit area. In addition, weeds and especially insects reduce the yield, storage, and marketing quality of products obtained from restricted areas. This type of plant products can also be considered a disease carrier vector in the food chain. To increase the yield, various insecticides have been developed against target organisms such as insects and one of these insecticides is α -endosulfan. However, non-target organisms living in the same ecosystem can also be affected by all these insecticides. In the present study, it was researched whether the chronic α -endosulfan application has an effect on longevity in non-target organisms. According to the data obtained, α -endosulfan shortened the maximum and mean lifespan in both male and female populations of the Oregon-R wild strain of *Drosophila melanogaster* based on dose-time interaction. The shortening observed in life span for both populations was statistically significant ($p < 0.05$) compared to the control group. This situation can be considered as "population aging".

Keywords: Model organism, Insecticide, Lifespan, Aging

Drosophila melanogaster Oregon-R (Diptera: Drosophilidae) yabancı popülasyonunda kronik α -endosülfan maruziyetinden sonra in vivo ömür uzunluğu toksisitesi

Özet: Dünya nüfusundaki hızlı artış beslenme ve barınma gibi farklı problemlere de sebep olmaktadır. Bu durumda insanlar barınabilmek için öncelikle tarıma elverişli alanları hunharca tahrip etmekte ve betonlaşma hızla yaygınlaşmaktadır. Ayrıca, artan nüfusun besin ihtiyacı için kısıtlı olan tarım alanlarından alınacak ürün miktarının artırılması da gereklidir. Tarım alanlarındaki azalma, birim alandan alınan ürün miktarını azaltan bir etken olarak karşımıza çıkmaktadır. Ayrıca, yabancı otlar ve özellikle böcekler de kısıtlı alanlardan elde edilen ürünlerin verim, depolama ve pazarlama kalitesini düşürmektedir. Bu tip bitkisel ürünler, besin zincirinde hastalık taşıyıcı vektörler olarak da değerlendirilebilir. Ürün miktarını artırmak için böcekler gibi hedef organizmalara karşı çeşitli insektisitler geliştirilmiştir ve bu insektisitlerden birisi de α -endosülfandır. Ancak aynı ekosistemde yaşayan ve hedef olmayan organizmalar da tüm bu insektisitlerden etkilenebilmektedir. Sunulan bu çalışmada kronik α -endosülfan uygulamasının hedef olmayan organizmalarda ömür uzunluğu üzerine etkili olup olmadığı araştırılmıştır. Elde edilen verilere göre, α -endosülfan doz-süre etkileşimine dayalı olarak *Drosophila melanogaster*'in Oregon-R yabancı soyuna ait hem erkek hem de dişi popülasyonlarında maksimum ve ortalama ömür uzunluğunu kısaltmıştır. Her iki popülasyon için ömür uzunluğunda gözlenen kısalma kontrol grubuna göre istatistik olarak önemli ($p < 0.05$) bulunmuştur. Bu durum "popülasyon yaşlanması" olarak değerlendirilebilmektedir.

Anahtar Kelimeler: Model organizma, İnsektisit, Yaşam süresi, Yaşlanma

1. Introduction

The ecosystem is called the external environment in which organisms live. The physical elements of the ecosystem are soil, water, and air. On the other hand, the biological elements of the ecosystem are humans, animals, plants, and microorganisms. The inability to protect the initial state of the environment with unnatural conditions, especially by human hand, is defined as environmental pollution. Chemicals used in homes, industry, or for medical purposes cause air, water, and soil pollution. All the factors that pollute air and water also increase soil pollution further. The flora and fauna of the soil are affected by acid rainfall, dirty irrigation water, industrial wastes, and even piles of garbage. In particular, microorganisms found in the soil are organisms that are primarily exposed to pollution. Accordingly, the reduction of chemicals performed through soil bacteria may also be inhibited. All these reasons cause cumulative pollution in the soil. Different pollutants accumulated in the soil reach all consumer organisms through the food chain.

Plants, one of the most important rings of the food chain, are important for both animals and humans. For this reason, various pesticides are used to ensure the sustainability of herbal production and to increase the number of products that can be taken from the unit area. However, it is necessary not to ignore the risks to human health caused by pesticides and the preservation of natural balance.

Weeds and animal organisms that damage agricultural products are defined as a pesticide. The first information about the use of pesticides is found in the history of ancient Egypt and Greece. In 1882, French Botanist, Millardet, used the pesticide to prevent vineyard mildew. While the pesticides used in these years were of herbal origin, synthetic pesticides were produced since the 1930s. After 1990s, the usage of prohibitions and restrictions have begun to prevent risks to human health, the environment, or natural balance due to incorrect pesticides (Jayaraj et al. 2016; Affum et al. 2018; Sanlı and Tasdemir 2020). Because all types of pesticides can enter the human body through respiration, as well as passing from the soil to plant or spraying directly to the plant can switch to the human body (Altıkat et al. 2009). The pesticides used in the field of agriculture may remain in nature without disintegration and cause various diseases and even cancer in humans. Organochloric pesticides (OCPs), also defined as endocrine disruptive, are an extremely risky pesticide group (Şık et al. 2012; Zhang et al. 2016). Even low doses of OCPs accumulated in adipose tissue can cause many diseases such as eczema, dermatitis, chronic coronary insufficiency, and hypertonia (Altıkat et al. 2009). Some OCPs are banned by the Ministry of Food and Agriculture and Livestock because people also affect the central nervous system. In a study conducted by Jayaraj et al. (2016), although it was banned in 1987, the OCPs such as DDT, Heptachlor, and Endrin are still found in breast milk and fat tissue shows the dimensions of the danger. Because although they are banned, OCPs are detected in agricultural lands due to their permanent features and/or illegal use (Jiang et al. 2009; Satoh and Gupta 2011; Bozlaker et al. 2013; Yu et al. 2013;

Zhang et al. 2015; Sertaş et al. 2021). Although a legal restriction is imposed on the production and use of any pesticide, illegal uses cannot be prevented until existing stocks are consumed. For this reason, it is estimated that α -endosulfan ($C_9H_6Cl_6O_3S$), one of the last prohibited OCPs, can also be found in the soil or water as an environmental pollutant. (Tiryaki 2016; Türkyılmaz and Küçükçongar 2021). This insecticide and acaricide (IFCS 2003; Watts 2009) which is moderately toxic and lipophilic, affect organisms through the stomach and respiratory tract (Howland 1998; Kurutaş and Kılınç 2003; Arıkan et al. 2014). Compared to other organochlorine pesticides, α -endosulfan can still be found in threatening amounts in water due to its high solubility in water (Golfinopoulos et al. 2003). Although banned, endosulfan, which can be found in surface waters and underground waters, is potentially toxic to humans and especially aquatic organisms (Türkyılmaz and Küçükçongar 2021). In addition, different insecticides such as Thiodan and Thiothox, which are used today, contain endosulfan as an active ingredient (<https://grec.ifas.ufl.edu>). For this reason, although endosulfan is banned, it continues to exist in agriculture as an active ingredient. According to the EPA (U.S. Environmental Protection Agency), α -endosulfan concentrations above 0.22 μ g/L cause adverse effects for aquatic organisms (Mersie et al. 2003). The presence of endosulfan in water, which is one of the most important components of the ecosystem, makes us think that it can also be found in the food chain through plants.

Based on this idea, this study was conducted to determine the effects of α -endosulfan, which has a long half-life and can survive in the ecosystem because it is not used correctly on non-target organisms. For this purpose, it was researched whether chronic α -endosulfan application affects lifespan depending on dose-time interaction in male and female populations of wild type (wt.) of *Drosophila melanogaster* Oregon-R.

2. Materials and Method

2.1. Experimental organism and living conditions

The *D.melanogaster* Oregon-R Meigen (Diptera; Drosophilidae), a model organism in genetics, was used for longevity testing. This strain, which has been inbred for many years at Atatürk University, Faculty of Science, Department of Biology, Genetics Research Laboratory, has no mutant features, long wings, brown body, and round-red eyes. *Drosophila* stock cultures are kept in 250 mL glass bottles in heated-cooled temperature cabinets with 40-60% relative humidity, 25 ± 1 °C temperature, and constant dark conditions. Both main stock cultures and experimental groups are fed with Standard *Drosophila* Medium (SDM) containing granulated sugar, yeast, agar, cornmeal, and propionic acid to prevent contamination (Uysal et al. 2006). While the media of the main cultures are renewed every ten days, the media of the experimental groups are changed twice a week.

2.2. Insecticide used and lifespan assay

The open formula of α -endosulfan used in the study is given in Figure 1 (Zacharia, 2011). To determine the effects of α -endosulfan on longevity, ♀♀ and ♂♂ populations of the same age (72 ± 4 hours) belonging to the Oregon-R wild strain of *D. melanogaster* were studied separately. First of all, the crosses were made between individuals belonging to this strain and preliminary stocks were prepared and the parents in each culture bottle in which the pupal stage were removed from the medium. The individuals to be used in the experimental groups were collected in different culture bottles, male and female, in every four to five hours for three days, as soon as they emerged from the pupa and before mating.

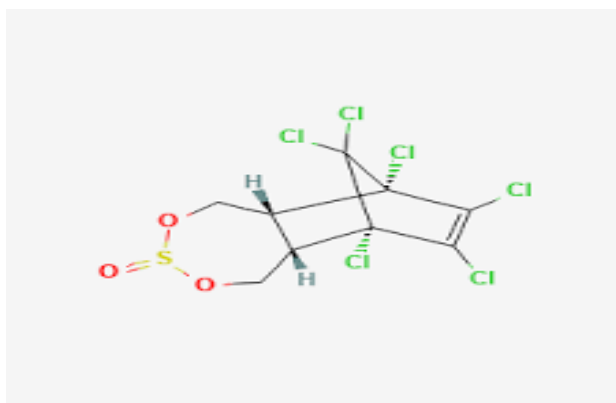


Figure 1. Chemical structure of α -endosulfan.

Then, two separate study setups, control and experimental groups were prepared simultaneously. SDM containing only distilled water and 1% acetone+SDM, the solvent of α -endosulfan (CAS numarası: 959-98-8, Fluka), were used as negative control groups. For the experimental groups containing α -endosulfan+SDM, preliminary trials were carried out and four different application doses (1, 2, 3, and 4 ppm) were determined. It was made in applications of less than 1 ppm, but no change was observed compared to the control groups. Mass deaths within 24 hours were also observed at higher applications than 4 ppm. To determine the longevity, all adult flies belonging to the control and experimental groups were first left to starve for 2 hours in culture bottles. Then, 100 individuals to be used in each application were divided into four groups of 25 individuals for convenience during counting. In the experimental groups, α -endosulfan was applied chronically and media containing different doses of α -endosulfan was renewed twice a week. All control and treatment groups were kept in heated-cooled incubators. Individuals were checked at each transfer and the deceased individuals were recorded by continuing the counts until the last individual died. Ambient conditions were kept stable for both control and experimental groups. The only variable was α -endosulfan, which was added to SDB at different doses.

2.3. Statistical analyses

The experiments were repeated three times for each group. The obtained data were analyzed with SPSS version 16.0 (Statistical Package for the Social Sciences Software, SPSS, Chicago, IL). The mean longevity of the control and experimental groups was compared using Duncan's one-way range test on the probability levels of 0.05.

The materials and methods section should contain sufficient detail so that all procedures can be repeated. Any modifications to existing methods should also be described.

3. Results

In this study, both maximum and mean lifespan were calculated to determine the effects of different doses of α -endosulfan on the ♀♀ and ♂♂ population of *D. melanogaster* (Table 1). While the maximum life span of *D. melanogaster* for the ♀♀ and ♂♂ populations was 78 and 76 days in the distilled water control group (no 1) respectively, this period was 72 days for both populations in the acetone control group (no 2). According to the data obtained, there was no difference at $p > 0.05$ level in terms of maximum lifespan between the distilled water and acetone control groups of both populations.

However, as a result of the chronic application of α -endosulfan at different doses (1, 2, 3, 4 ppm, no 3-6) in the ♀♀ population, the maximum lifespan was shortened to 42, 42, 36, 33 days, respectively (Figure 2b). A similar situation was also observed in the ♂♂ population as a result of α -endosulfan application at the same doses. In the ♂♂ population, the maximum lifespan was shortened with increasing dose of α -endosulfan (Figure 2a), and the observed maximum lifespan decreased to 42, 39, 33, and 30 days (Table 1). The difference between the acetone control group and the application groups was statistically significant for both populations ($p < 0.05$).

According to the data obtained, the average lifespan for the ♀♀ and ♂♂ populations was also calculated. The mean lifespan in the ♀♀ and ♂♂ populations was 47.49 ± 2.03 (no 1), 47.80 ± 2.14 (no 1), days for the distilled water control group and 46.65 ± 2.03 (no 2), and 46.05 ± 2.14 (no 2), days for the acetone control group, respectively ($p > 0.05$). However, these values decreased significantly depending on the dose increase in the α -endosulfan application groups. The mean lifespan for the ♀♀ population was calculated as 24.96 ± 2.03 and 17.43 ± 2.03 days in the lowest (1 ppm, no 3) and highest (4 ppm, no 6) application groups. These values decreased from 23.88 ± 2.14 (no 3) to 15.54 ± 2.14 (no 6) days in the ♂♂ population ($p < 0.05$). Negative correlation values for the decline in life span due to the increasing concentration of α -endosulfan were also found as $R: -611$ and $R: -612$ for the ♀♀ and ♂♂ populations, respectively (Table 1).

Table 1. Maximum and mean lifespan of male and female populations of *D. melanogaster* and the probability levels between groups.

Chronic α -Endosulfan Application								
Application groups (no)	Female population				Female population			
	No	ML1	ML2 \pm SE	$p <$	No	ML1	ML2 \pm SE	$p <$
Control (1)	100	78	47.49 \pm 2.03		100	76	47.80 \pm 2.14	
Acetone (2)	100	72	46.65 \pm 2.03		100	72	46.05 \pm 2.14	
1 ppm (3)	100	42	24.96 \pm 2.03	1-3,4,5,6*	100	42	23.88 \pm 2.14	1-3,4,5,6*
2 ppm (4)	100	42	21.60 \pm 2.03	2-3,4,5,6*	100	39	19.05 \pm 2.14	2-3,4,5,6*
3 ppm (5)	100	36	17.73 \pm 2.03	3-4,5,6*	100	33	16.80 \pm 2.14	3-4,5,6*
4 ppm (6)	100	33	17.43 \pm 2.03	4-5,6*	100	30	15.54 \pm 2.14	4-5,6*
Regression Level			R: -611			R: -612		

SE: Standard error, *: The difference between the groups is significant at the $p < 0.05$ level, R: Regression level.

No: Number of individuals, ML1: Maximum lifespan, ML 2: Mean lifespan

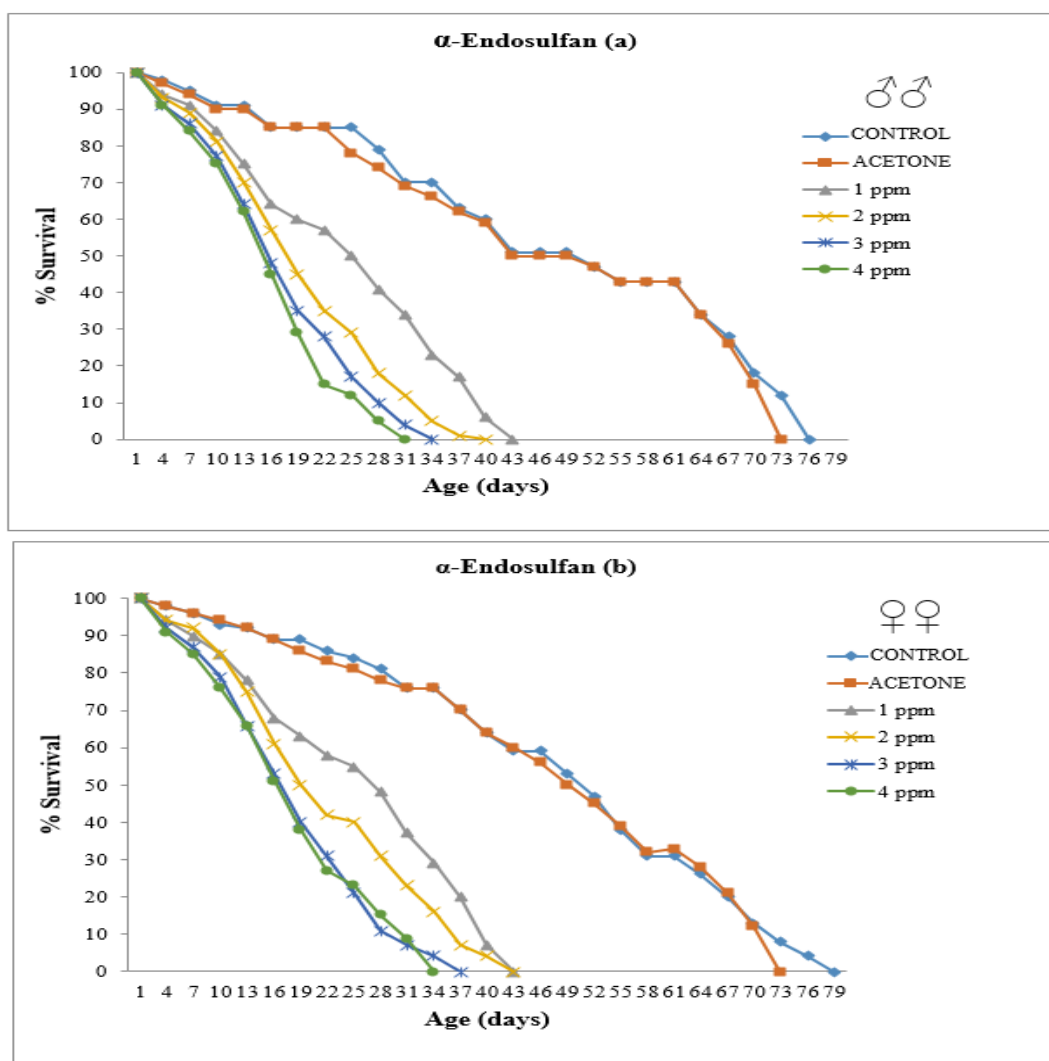


Figure 2. The survival curves of male (a) and female (b) individuals of *D. melanogaster* living medium applied with different concentrations of α -endosulfan during adult stages.

4. Discussion

Insecticides are synthetic or organic chemicals that both increase production in limited agricultural areas and are important for home and public health. Insects reduce the yield, storage, and quality of agricultural products and also act as disease vectors for humans and animals. However, insecticides developed against insects, which are the target organisms, are used unlimitedly and uncontrollably today. α -Endosulfan is a chlorinated hydrocarbon insecticide and acaricide belonging to the cyclodiene subgroup applied to a wide variety of insects and mites in plants, including tea, coffee, cotton, fruit, vegetables, rice, and grain. It has also been used in agriculture to control pests such as white flies, aphids, leafhoppers, Colorado potato beetles, and cabbage worms (Berntssen et al. 2017).

From 1954 to 2000, when α -endosulfan was registered, cumulative use in agriculture is 308,000 tons. Global consumption of insecticide rose from around 9000 tons/year in the early 1980s to 12800 tons in the 1990s. This shows that α -endosulfan is used very widely in different countries. Until 2010, when it was banned globally, it is stated that the worldwide α -endosulfan production was 18000-20000 tons/year (Cone 2010). This semi-volatile insecticide was added to the list of permanent organic pollutants in 2011 with the Stockholm Convention due to its long-range atmospheric transport, especially its accumulation in adipose tissue, and its endocrine disruptor in mammals (Mathew 2011).

In a study by Kristy (2008), this insecticide was even detected in dust from the Sahara desert collected from the Caribbean after being dispersed into the Atlantic Ocean. Therefore, they can be found in air, water, soil, rain, snow, ice, and even fog. Thus, they can affect very wide geographies and the creatures living there. Due to all these negative effects, its production and use have been banned worldwide since mid-2012. Although the legal use of α -endosulfan and its metabolites has been stopped due to the reasons such as high resistance to degradation in nature, bioaccumulation, and environmental transport, they can still be detected in environmental samples and pose a risk to the environment and public health (Kurutaş and Kılınç 2003; Türkyılmaz and Küçükçongar 2021). Although banned according to Türkyılmaz and Küçükçongar (2021), this insecticide can still be found in groundwater. The main concern for human health is that α -endosulfan shows xenoestrogenic (xenohormone) properties. Because xenoestrogens can mimic the effects of endogenous estrogen, they cause early puberty and reproductive system disorders in young people (Herman-Giddens et al. 1997; Aksglaede et al. 2006; Massart et al. 2008). Xenoestrogens found in wastewater treatment plants caused impaired ovarian and testicular histopathology, gonadal intersex, reduced gonadal size, induction of vitellogenin, and altered sex ratios in fish living in these areas (Vajda et al. 2008). Precocious puberty and rapid bone development have also been observed in humans fed contaminated milk or fed fish containing xenoestrogens due to bioaccumulation (Hotchkiss et al. 2008). According to different researchers, early puberty also increases the risk of breast cancer and

prostate cancer. Similar effects have been observed not only in humans but also in rats (Darbre 2006; Della Seta et al. 2008; Xu et al. 2010).

Non-target organisms as well as target organisms are affected by the use of α -Endosulfan as an insecticide (Güven and Koç 2020). This causes serious problems in terms of biodiversity (Mossler et al. 2006). The shortening of life span in fruit flies, which is one of the non-target organisms in this study, can be attributed to α -endosulfan. Because the only variable in the optimum living conditions of *D. melanogaster* is α -endosulfan (Material and Method). According to our data, there is a positive correlation between dose increase of α -endosulfan and the shortening of life span (Table 1, Figure 2). It has been shown in previous studies that α -endosulfan concentration and exposure time stimulate the formation of reactive oxygen species (ROS), which in turn causes double-strand breaks in DNA (Bajpayee et al. 2006; Robin and Raghavan 2016). Again, in previous studies, it was determined that different insecticides cause genomic instability by causing genotoxic changes. Chlordane, one of the organochlorine insecticides, also shortened the life span of *D. melanogaster*, just like α -endosulfan. In addition, it was observed that chlordane significantly increased the micronucleus frequency and decreased the nuclear division index in human lymphocyte cells (Özyurt et al. 2018). Again, chlorfenson, one of the organochlorine insecticides, was determined to induce somatic mutations in *D. melanogaster* by somatic mutation and recombination test (Kızılet and Uysal 2019). Similar genotoxic effects were seen after bifenthrin application, and this insecticide caused both micronucleus and sister chromatid exchanges in human lymphocytes (Kızılet and Uysal 2022). According to the same researchers, dimethoate (organophosphorus compounds, sub-group of insecticides) caused similar genotoxic effects (Kızılet et al. 2019). Breaks in DNA can also occur in the telomere regions of chromosomes. When the telomere reaches its critical length, cell division stops. This is called "aging at the cellular level". Cellular aging also accelerates the biological aging of the organism.

Hydroxyl radical, superoxide radical, and hydrogen peroxide are the most well-known ROS. Under normal conditions, organisms are protected from the destructive effect of ROS with the enzymes superoxide dismutase (SOD), glutathione peroxidase (GPx), glutathione reductase (GR), and catalase (CAT) and radical scavengers such as β -carotene, ascorbic acid and α -tocopherol taken with food. However, due to oxidative stress, ROS cause destruction in biomolecules and molecular damage begins in the cell. This accelerates normal biological aging.

There are many different definitions of aging. However, we can define aging in general as the loss of function of tissues and organs necessary for life over time. Intrinsic physiological losses may occur in tissues and organs due to age, and exogenic factors may accelerate the aging process. Biological aging does not depend on a single cause and cannot be explained by a single mechanism. Free radicals

theory, somatic mutation, telomere shortening, immunological theory, neuroendocrine theory, the theory of alteration of proteins, and antagonistic pleiotropy theory are some of the theories of aging. In our opinion, *D.melanogaster's* shortening of lifespan and accordingly, population aging can be explained by the "Theory of Free Radicals". Because *D.melanogaster* Oregon-R is a wild strain in terms of all genotypic properties. In our opinion, "the significant shortening of lifespan observed in adult individuals belonging to experimental groups ($p<0.05$) indicates the aging of the population".

5. Conclusion

Insecticides applied against various pests in agricultural areas may directly affect cumulatively influenced non-target organisms at any stage of their development (eggs, larvae, or adults). Sometimes insecticides such as α -endosulfan can be found in soil and underground waters, they can affect organisms through the food chain. As a result, insecticides, no matter what purpose it is used, also affect biodiversity. This situation should not be ignored and in our opinion, "organic insecticide use in agriculture should be spread and encouraged by the state".

Acknowledgements

This research did not receive any specific grant from funding agencies in the public, commercial, or not-for-profit sectors"

Authors' contributions: All stages of the study were carried out by the author.

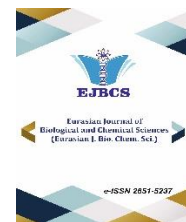
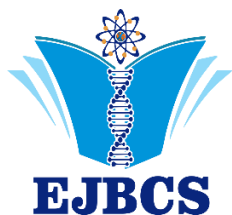
Conflict of interest disclosure:

None

References

- Affum AO, Acquah SO, Osa SD. 2018. Kwaansa-Ansah EE. Distribution and risk assessment of banned and other current-use pesticides in surface and groundwaters consumed in an agricultural catchment dominated by cocoa crops in the Ankobra Basin, Ghana. *Sci Total Environ.* 15(633): 630-640
- Aksglaede L, Juul A, Leffers H, Skakkebaek NE, Andersson A M. 2006. The sensitivity of the child to sex steroids: possible impact of exogenous estrogens. *Hum Reprod Update.* 12(4): 341-9
- Altıkat A, Turan T, Torun FE. 2009. Türkiye'de pestisit kullanımı ve çevreye olan etkileri. *Atatürk Üniv Ziraat Fak Derg.* 40(2): 87-92
- Arıkan Fİ, Özkan F, Dallar BY. 2014. Fark edilemeyen zehir: endosulfan. *Bakırköy Tıp Derg.* 10: 179-181
- Bajpayee M, Pandey AK, Zaidi S, Musarrat J, Parmar D, Mathur N. 2006. DNA damage and mutagenicity induced by endosulfan and its metabolites. *Environ Mol Mutagen* 47(9): 682-692
- Berntssen MHG, Maage A, Lundebye A. 2017. Chemical contaminants and residues in food (Second Edn) Woodhead Publishing Series in Food Science, Technology and Nutrition U.S.A. pp. 517-551
- Bozlaker A, Müezzinoğlu A, Odabaşı M. 2013. Processes affecting the movement of organochlorine pesticides (OCPs) between soil and air in an industrial site in Turkey. *Chemosphere.* 77(9): 1168-1176
- Cone M. 2010. EPA bans pesticide found on cucumbers, zucchini, green beans and other vegetables. *The Daily Green.*
- Darbre PD. 2006. Environmental oestrogens, cosmetics and breast cancer. *Best Pract Res Clin Endocrinol Metab.* 20(1): 121-43
- Della Seta D, Farabollini F, Dessi-Fulgheri F, Fusani L. 2008. Environmental-like exposure to low levels of estrogen affects sexual behavior and physiology of female rats. *Endocrinol.* 149(11): 5592-8
- Golfinoopoulos SK, Nikolaou AD, Kostopoulou MN, Xilourgidis NK, Vagi MC, Lekkas DT. 2003. Organochlorine pesticides in the surface waters of Northern Greece. *Chemosphere.* 50: 507-516
- Güven E, Koç I. 2020. Diversity of non-targeted nematode, bacteria and microfungi populations in soil after some pesticide treatment. *Yuzuncu Yil Univ Journal of Agric Sci.* 30(2): 252-65
- Herman-Giddens ME, Slora EJ, Wasserman RC, Bourdony CJ, Bhapkar MV, Koch GG, Hasemeier CM. 1997. Secondary sexual characteristics and menses in young girls seen in office practice: a study from the pediatric research in office settings network. *Pediatr.* 99(4): 505-12
- Hotchkiss AK, Rider CV, Blystone CR, Wilson VS, Hartig PC, Ankley GT, Foster PM, Gray CL, Gray LE. 2008. Fifteen years after "wingspread"-environmental endocrine disrupters and human and wildlife health: where we are today and where we need to go. *Toxicol Sci.* 105(2): 235-259
- Howland MA. 1998. Insecticides: chlorinated, hydrocarbons, pyrethrins, and DEET. In: Goldfrank LR, Flomenbaum NE, Lewin NA, Weissman RS, Howland MA (eds). *Goldfrank's Toxicologic Emergencies*, 6th edn. McGraw-Hill, New York, NY, 1451-8
- IFCS, 2003. Acutely toxic pesticides: initial input on extent of problem and guidance for risk management, intergovernmental forum on chemical safety. Forum IV, Bangkok, Thailand, 1-5
- Jayaraj R, Megha P, Sreedev P. 2016. Organochlorine pesticides, their toxic effects on living organisms and their fate in the environment. *Interdiscip Toxicol.* 9(3-4): 90-100. doi: 10.1515/intox-2016-0012
- Jiang YF, Wang XT, Jia Y, Wang F, Wu MH, Sheng GY, Fu JM. 2009. Occurrence, distribution and possible sources of organochlorine pesticides in agricultural soil of Shanghai. *J Hazard Mater.* 170(2-3): 989-97
- Özyurt E, Kızılet H, Uysal H. 2018. Hedef olmayan organizmalarda klordanın biyo-etkileşimi. *Commagene J Biol.* 2(1): 48-54
- Kızılet H, Uysal H. 2019. Induced somatic mutation during chronic exposure of chlorfenson on *Drosophila melanogaster* Oregon-R (wild type). *Drosoph Inf Serv.* 102: 4-8
- Kızılet H, Uysal H. 2022. Genoprotective role of purslane methanol extract against somatic mutations induced by bifenthrin, a third generation prethroid insecticide. *J Agric Sci.* 28(4): 583-591.
- Kızılet H, Yılmaz B, Uysal H. 2019. Herbal medicine against genotoxicity of dimethoate, an insecticide, in mammalian somatic cells. *Heliyon,* 5(3): e01337. doi:10.1016/j.heliyon. e01337
- Kristy R. 2008. Harmful elements in Sahara dust. *Trinidad and Tobago Express.* Retrieved, 05-14

- Kurutaş BE, Kılınc M. 2003. Pestisitlerin biyolojik sistemler üzerine etkisi. Arşiv. 12: 215-228
- Massart F, Meucci V, Saggese G, Soldani G. 2008. High growth rate of girls with precocious puberty exposed to estrogenic mycotoxins. J Pediatr. 152(5): 690-5
- Mathew R. 2011. Stockholm Convention approves recommendation for ban on endosulfan
- Mersie W, Seybold CA, Mcnamee C, Lawson MA. 2003. Abating endosulfan from run off using vegetative filter strips: the importance of plant species and flow rate. Agric Ecosyst Environ. 97: 215-223
- Mossler M, Aerts MJ, Nesheim ON. 2006. Florida Crop/Pest Management Profiles: Tomatoes: CIR 1238/PI039, Rev. 3/2006. EDIS
- Robin S, Raghavan SC. 2016. Induction of DNA damage and erroneous repair can explain genomic instability caused by endosulfan. Carcinogenesis. 37(10): 929-940
- Sanlı G, Taşdemir Y. 2020. Seasonal variations of organochlorine pesticides (OCPs) in air samples during day and night periods in Bursa, Turkey. Atmos Pollut Res. 11: 2142-2153
- Satoh T, Gupta C. 2011. Anticholinesterase pesticides: metabolism, neurotoxicity, and epidemiology. 1st Edition, Kindle Edition pp.1-9
- Serttaş A, Ayaz T, Yurdakul S, Doğan G, Göktaş RK, Civan M. 2021. Sera zirai toprağında toplam pestisit seviyeleri ve sera özellikleri ile pestisit seviyeleri arasındaki ilişkinin değerlendirilmesi. J Engr Sci Desig. 9(3): 900-910
- Şık B, Küçükçetin İÖ, ErKaymaz T, Yıldız G. 2012. Gıda güvenliği açısından endokrin sistem bozucu pestisitler. Akademik Gıda. 10(2): 89-95
- Tiryaki O. 2016. Türkiye’de yapılan pestisit kalıntı analiz ve çalışmaları. Erciyes Univ J Inst Sci Technol. 32(1): 72-82
- Türkyılmaz M, Küçükçongar S. 2021. Endosulfan ve metabolitlerinin su örneklerinde vorteks destekli sıvı-sıvı mikro ekstraksiyon ve yüksek performanslı sıvı kromatografi kullanılarak analizi. Bitlis Eren Univ J Sci. 10(4): 1404-1415
- Uysal H, Şişman T, Aşkın H. 2006. *Drosophila* Biology and Crossover Methods (Extended 2nd Edition). Atatürk University Publications, ISBN: 975-442-111-0, Erzurum, Türkiye
- Vajda AM, Barber LB, Gray JL, Lopez EM, Woodling JD, Norris DO. 2008. Reproductive disruption in fish downstream from an estrogenic wastewater effluent. Environ Sci Technol. 42(9): 3407-3414
- Watts M. 2009. Endosulfan 2nd Edition, PANAP (Pesticide Action Network Asia and the Pacific), Germany, 1-43
- Xu X, Dailey AB, Talbott EO, Ilacqua VA, Kearney G, Asal AR. 2010. Associations of serum concentrations of organochlorine pesticides with breast cancer and prostate cancer in U.S. adults. Environ Health Perspect. 118: 60–66
- Yu HY, Li FB, Yu WM, Li YT, Yang GY, Zhou SG, Zhang TB, Gao YX, Wan HF, 2013. Assessment of organochlorine pesticide contamination in relation to soil properties in the Pearl River Delta, China. Sci Total Environ. 447:160-68
- Zacharia JT. 2011. Identity, Pesticides In The Modern World-Trends In Pesticides Analysis, Margarita Stoytcheva, In Tech, Croatia, 3-10. ISBN 978-953-307-437-5
- Zhang A, Luo W, Sun J, Xiao H, Liu W. 2015. Supplementary material for distribution and uptake pathways of organochlorine pesticides in greenhouse and conventional vegetables. Environ Sci Eng. 505: 1142-1147
- Zhang J, Zhang J, Liu R, Gan J, Liu J, Liu W. 2016. Endocrine-disrupting effects of pesticides through interference with human glucocorticoid receptor. Environ Sci Technol. 50(1): 435-443



Computed Tomography Imaging, Macroanatomical and Morphometric Analysis of Os penis in Brown Bear (*Ursus arctos*)

Semine Dalga^{1*}, Gülseren Kırbaş Doğan¹, Yalçın Akbulut², Türkhun Çetin³, Volkan Kızılgöz³

¹University of Kafkas, Faculty of Veterinary, Department of Anatomy, Kars, Türkiye

²University of Kafkas, Faculty of Medicine, Department of Anatomy, Kars, Türkiye

³University of Erzincan, Faculty of Medicine, Department of Radiology, Erzincan, Türkiye

*Corresponding author : sdalga91@gmail.com
Orcid No: <https://orcid.org/0000-0001-7227-2513>

Received : 03/03/2022
Accepted : 23/06/2023

Abstract: The aim of this study is to reveal the macroscopic features of the brown bear (*Ursus arctos*) os penis (baculum), as well as its morphometric measurements with the help of computerized tomography and digital electronic caliper. The study material was obtained from an adult male brown bear weighing approximately 400 kg, which was brought to the Wildlife Protection and Rehabilitation Unit of Kafkas University and died as a result of a traffic accident in the Sarıkamış district of Kars. After the skin and soft tissues around the baculum were removed, they were kept in hydrogen peroxide for 2-3 hours. In the macroscopic examination, it was determined that the baculum was straight, close to the pen, except for a slight curve in the distal part, and ended with a small tubercle at the distal end. A small notch was found in the proximal part. In addition to the prominent sulcus urethralis in the ventral of the baculum, a short groove was also detected in its lateral. A cartilage tissue of 11.08 mm in length and 4.67 mm in thickness was determined in the distal of the bone. In the morphometric measurements made with a digital electronic caliper, the length of the baculum was 148.95 mm, while the diameters were measured as 4.58 mm in the distal and 13.72 mm in the proximal, respectively. In computed tomography, baculum length was 148.84 mm, distal diameter length was 5.63 mm, and proximal diameter length was 13.12 mm. In addition, computed tomography measured the length of the cortex as 0.76 mm, the length of the medulla as 5.74 mm in the distal, the cortex length of 0.77 mm and the medulla length of 5.32 mm in the proximal region. As a result, in this study, the macro anatomical and morphometric features of the brown bear baculum, which live in high altitude and cold climate conditions, were revealed.

Keywords: Brown bear, baculum, os penis, macroanatomy, morphometry, computed tomography

© EJBCS. All rights reserved.

1. Introduction

The brown bear (*Ursus arctos*) is a large bear with the widest distribution of any living ursid (Serhveen et al. 1999). The brown bear's principal range includes parts of Russia, Central Asia, China, Canada, the United States, Scandinavia, the Carpathian region, Anatolia, and Caucasus (McLellan et al. 2008; Zedrosser et al. 2001) The normal range of physical dimensions for a brown bear is a head-and-body length of 1.4 to 2.8 m and a shoulder height of 70 to 153 cm. The tail is relatively short, as in all bears, ranging from 6 to 22 cm in length (Parker 1990; Nowak 1999).

The os penis is a bony structure located in the corpus cavernosus penis in the distal part of the penis. There is a groove called sulcus urethralis in the ventral of the bone. This groove loses its width and depth as it goes from proximal to distal. The proximal end of the os penis is thick,

while the distal end is thin. The distal end ends with cartilage. (Dursun 2000; Nickel et al. 1981; Getty 1975; Gültekin et al. 2004). Several investigators have described the anatomy of the penis of both Carnivora and wild animals, the anatomy and bacula growth are well described for that, but no report on that of the brown bear. (Getty 1975; Gültekin et al. 2004; Miller 1979; Miller et al. 2000; Abella et al. 2013, Münzel et al. 2021). On the other hand, morphological of the penis bone in the brown bear has not been investigated so far. Therefore, the present study contributes to the knowledge of quantitative characteristics of the size of the penis bone in the brown bear. This first study of the brown bear baculum will contribute to the literature by providing very important information.

2. Materials and Method

The study material, os penis, was obtained from an adult male brown bear, weighing approximately 400 kg, who died as a result of a traffic accident in the Sarıkamış district of Kars. The procedures of classic maceration were applied to the example and the penis bone was brought out by cleaning. After the penis bone was macerated for 2-3 hours with hydrogen peroxide, measurements were by using digital caliper (0.001, BTS, UK) from the penis bone. Surfaces of the penis bone were examined for macroanatomical observations. Nomina Anatomica Veterinaria (NAV, 2017) was used in the spelling of anatomic terminology.

3. Results

In the brown bear, the length of the os penis was 148.95 mm, its proximal width was 13.72 mm, and its distal width was 4.58 mm. Its weight was determined as 5.73 g. In computed tomography, the length was measured as 148.84 mm, the distal diameter was 5.63 mm, and the proximal diameter was 13.12 mm. In addition, computed tomography measured the length of the cortex as 0.76 mm, the length of the medulla as 5.74 mm in the distal, the cortex length of 0.77 mm and the medulla length of 5.32 mm in the proximal region.

It was determined that the thickness of the os penis decreased from proximal to distal. Except for a slight curve in the distal part of the os penis, it was found to be almost straight and almost quadrangular in shape. It was determined that the distal end ended with a small tubercle. On the proximal part, there was a small notch. In addition to the prominent sulcus urethralis in the ventral aspect of the os penis, a short groove was also detected in its lateral aspect. A fibrous cartilage tissue with a length of 11.08 mm and a thickness of 4.67 mm was detected distal to the bone.



Figure 1. Points measured on the os penis with the help of digital caliper



Figure 2. Measuring points measured by CT over the os penis

Table 1. Findings measured on the baculum by classical morphometry and computed tomography

Parameters	Morphometric measurement	CT Measurement
Length of the os penis	148.95 mm	148.84 mm
Distal diameter	4.85 mm	5.63 mm
Proximal diameter	13.72 mm	13.12 mm
Cortex length of Distal		0.76 mm
Medulla length of Distal		5.74 mm
Cortex length of Proximal		0.77 mm
Medulla length of Proximal		5.32 mm

4. Discussion

In this study, the length, proximal width, distal width, and weights of the brown bear's os penis were determined as 148.95 mm, 13.72 mm, 4.85 mm, and 5.73 g, respectively. According to the analysis made with CT, the length of the os penis was 148.84 mm, the distal diameter length was 5.63 mm, and the proximal diameter length was 13.12 mm. Similarly, the proximal length of the cortex was 0.77 mm, the proximal length of the medulla was 5.32 mm, the distal length of the cortex was 0.76 mm, and the distal length of the medulla was 5.74 mm.

Dyck et al. (2004) reported the os penis dimensions of a 3-year-old polar bear (*Ursus maritimus*) living in the Canadian Arctic as 140 mm in length, 9.12 mm in width and 5.92 g in weight, respectively. According to Abella et al. (2013), lengths of fossil os penises are 151 mm in Sloth bear (*Melursus ursinus*), 104.7 mm in Andean bear (*Tremarctos ornatus*), 137 mm in American black bear (*Ursus americanus*), Asiatic Black Bear (*Ursus thibetanus*) length 118.25 mm, Grizzly bear (*Ursus arctos*) 133.8 mm, the bear *indarctos* (*Indarctos arctoides*) 238.6 mm and the polar bear (*Ursus maritimus*) They stated that the length was 186.5 mm.

Lønø (1970) stated that the os penis length of the adult polar bear (*Ursus maritimus phipps*) living in the Svalbard region was 155 mm, and its weight was 8.10 g. Didier (1950) stated the penis length as 135.4 mm in Grizzly bear (*Ursus arctos*) and 168 mm in the polar bear (*Thalarctos maritimosus*). Miller et al. (2000) stated that adult the Steller Sea Lion (*Eumetopias jubatus*) os penis averaged 180.1 mm in length, its weight was 36.7 g. According to the literature information given, it was seen that the os penis length of an adult living in Sarıkamış, weighing 400 kg, had higher values than many ursus breeds.

According to Abella et al. (2013) os penis's shape is slightly more sigmoidal and its distal tip is relatively better developed; only the baculum of Malayan sun bear (*Helarctos malayanus*) has developed an ossified tip at its distal end. Evans and Delahunta (2010) stated that is cartilaginous and not completely ossified throughout its life cycle in canidae. In our study, apart from a slight inclination in the distal part of the os penis, it was almost straight to the pen, and a fibrous cartilage tissue of 11.08 mm in length and 4.67 mm in thickness was detected in the distal part of the os penis.

The brown bear's os penis has sulcus urethralis at its ventral edge, similar to that of red fox and dog, and is gradually tapering from proximal to distal. Gültekin et al., (2004) reported that the os penis is triangular and has a crista at its distal end in Red Fox, whereas in brown bears the os penis is quadrilateral and has a tubercle at the distal end. Miller (1979) and Gültekin et al. (2004) mentioned in dogs and Red Foxes respectively, it was determined that the dorsoventral diameter of the entire os penis was larger than the laterolateral diameter.

5. Conclusion

As a result, in this study, the morphological features of the Brown bear os penis, which live in high altitude and cold

climate conditions, were revealed and compared with some wild species. It is thought that the data obtained in the study can be used in future morphometric, zoo-archaeological and taxonomic studies.

Acknowledgements

Authors' contributions: SD, GKD, YA, analyzed morphometrically and macroanatomically. TÇ and VK examined by CT. All authors edited and wrote the article.

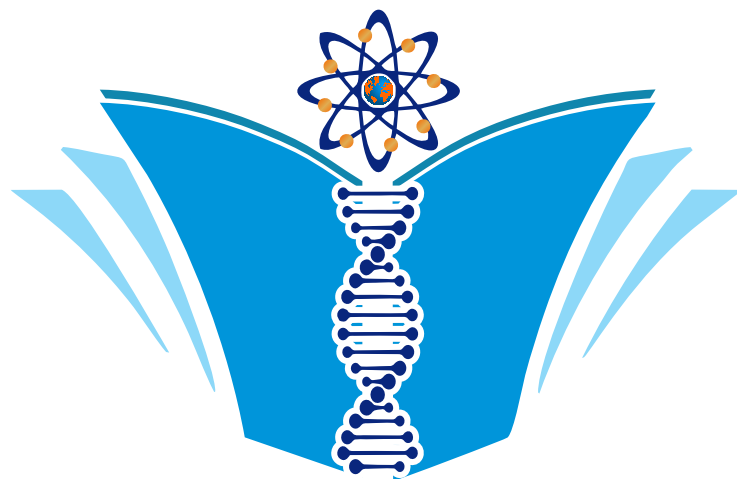
Conflict of interest disclosure: The authors declare that there were no conflicts of interest in the realisation of this research.

References

- Servheen C, Herrero S, Peyton B, Pelletier K, Moll K and Moll J. 1999. Bears: status survey and conservation action plan (Vol. 44) . IUCN.
- McLellan BN, Servheen C, Huber D. 2008. "Ursus arctos". IUCN Red List of Threatened Species. 1. International Union for Conservation of Nature. Retrieved 2013-10-05.
- Zedrosser A, Dahle B, Swenson JE and Gerstl N. 2001. Status and management of the brown bear in Europe. *Ursus*, 9-20.
- Parker SP. 1990. Grzimek's encyclopedia of mammals. McGraw-Hill, New York. ISBN 0-07-909508-9.
- Nowak RM. 1999. Walker's mammals of the world (Vol. 1). JHU Press.
- Dursun N. 2000. Veteriner Anatomi. Medisan Yayınevi, Ankara.
- Nickel R, Schummer A, Seiferle E. 1981. The Anatomy of the Domestic Animals. Vol 3. First Edition. Verlag Paul Parey, Berlin.
- Getty R. 1975. The Anatomy of Domestic Animals. Fifth Edition. WB Saunders Company, Philadelphia.
- Gültiken M, Yıldız D, Bolat D. 2004. The anatomy of os penis in red fox (*Vulpes vulpes*). *Ankara Üniv Yet Fak Derg*, 51, 71-73.
- Miller ME. 1979. Miller's Anatomy of the Dog. WB Saunders Company, Philadelphia.
- Miller EH, Pitcher KW, Loughlin TR. 2000. Bacular size, growth, and allometry in the largest extant otariid, the Steller sea lion (*Eumetopias jubatus*). *J Mammal*. 81(1):134-144.
- Abella J, Valenciano A, Perez-Ramos A, Montoya P and Morales J. 2013. On the Socio-Sexual Behaviour of the Extinct Ursid *Indarctos arctoides*: An Approach Based on Its Baculum Size and Morphology. *Plos One*. 8;8(9):e73711.
- Susanne C. Münzel, Giemisch L, Schmitz RW 2021. Sexual Symbol or Domestic Tool? The Use of Bear Bacula, an Assessment of the Archaeological and Ethnographical Record. Chapter
- Didier R. 1950. E'tude syste ´matique de l'os pe ´nien des mammife `res. *Mammalia* 14: 78-94.
- Evans HE, Delahunta A. 2010. Miller's Guide to the Dissection of the Dog. WB Saunders Company, Philadelphia. 303 p.

Lønø O. 1970. The polar bear (*Ursus maritimus* Phipps) in the Svalbard area. Norsk Polarinstitutt Skrifter 149:1—115.

Nomina Anatomica Veterinaria: International Committee on Veterinary Gross Anatomical Nomenclature: General Assembly of the World Association of Veterinary Anatomists. 6th edition, Gent, 2017.



EJBCS